Idaho
National
Engineering
Laboratory

Managed
by the U.S.
Department
of Energy

EGG-TMI-7955
June 1987

INFORMAL REPORT

ANALYSIS OF THE TMI-2 SOURCE RANGE MONITOR DURING THE TMI ACCIDENT

Horng-Yu Wu
Anthony J. Baratta
Ming-Yuan Hsiao
Bernard R. Bandini

EG&G Idaho

Work performed under
DOE Contract
No. DE-AC07-76ID01570

EGG-TMI-7955

ANALYSIS OF THE TMI-2 SOURCE RANGE MONITOR DURING THE TMI ACCIDENT

June 1987

Horng-Yu Wu
Anthony J. Baratta
Ming-Yuan Hsiao
Bernard R. Bandini

Prepared for:
EG&G Idaho, Inc.
Under Subcontract No. C85-130880

Work supported by the U. S. Department of Energy
Assistant Secretary for Nuclear Energy
Office of LWR Safety and Technology
Under DOE Contract No. DE-AC07-76ID01570

ABSTRACT

The source range monitor (SRM) data recorded during the first 4 hours of the Three Mile Island Unit No. 2 (TMI-2) accident following reactor shutdown were analyzed. An effort to simulate the actual SRM response was made by performing a series of neutron transport calculations. Primary emphasis was placed on simulating the changes in SRM response to various system events during the accident, so as to obtain useful information about core conditions at the various stages. Based on the known end-state reactor conditions, the major system events, and the actual SRM readings, self-consistent estimates were made of core liquid level, void fraction in the coolant, and locations of core materials. This analysis expands the possible interpretation of the SRM data relative to core damage progression. The results appear to be consistent with other studies of the TMI-2 Accident Evaluation Program, and provide information useful for the development and determination of the TMI-2 accident scenario.

ACKNOWLEDGMENTS

The authors wish to express their sincere appreciation to Dr. E. L. Tolman of EG&G Idaho, Inc. for his assistance and helpful discussions throughout this study. As part of the effort of the TMI-2 Accident Evaluation Program of the U.S. Department of Energy, special thanks are due for the financial support provided by EG&G Idaho, Inc., without which this study would not have been possible.

TABLE OF CONTENTS

1. INTRODUCTION 1

2. PREVIOUS WORK 11

3. CALCULATIONAL METHOD 21

3.1 Source Term Calculation 22

3.2 LOFT Reactor Model and Cross Section Preparation 28

3.2.1 Reactor Model 28
3.2.2 Cross Section Preparation 32

3.3 TMI-2 Reactor Model and Cross Section Generation 42

3.3.1 Reactor Model 42
3.3.2 Cross Section Preparation 45

3.4 LOFT Experiment LP-SB-2 54

3.5 LOFT Experiment LP-SB-3 58

4. RESULTS OF ANALYSIS 69

4.1 Homogeneous Voiding Model (t < 100 minutes) 73

4.2 Initial Core Heat-Up Response (100 < t < 174 min) 79

4.3 Core Relocation Analysis (t = 227 minutes) 86

4.4 Pump Transient and HPIS Injection (174 < t < 202 minutes) 89

4.5 Uncertainties 102

4.5.1 Void Fraction Uncertainty 102
4.5.2 Level Uncertainty 106
4.5.3 Fuel Relocation Analysis 107

5. CONCLUSIONS AND RECOMMENDATIONS 109

5.1 Conclusions 109

5.2 Recommendations 111

REFERENCES 115

1. INTRODUCTION

The accident at the Three Mile Island Nuclear Generating Station Unit-2 (TMI-2) resulted in extensive damage to the reactor core of this pressurized water reactor (PWR). This damage included fuel melting and the relocation of 10-20 tonnes of the fuel into the lower plenum. A number of groups[1-12] have studied the accident in an effort to understand the various events that resulted in the existing final core configuration shown in Figure 1.1.

The accident is the most severe to have occurred at a commercial PWR reactor to date. A better understanding of its progression as well as quantification of a number of unknown parameters will provide insight regarding degraded core accidents and their mitigation. This work examines the response of the source range monitor (SRM) during the accident in an attempt to resolve a number of outstanding issues including the following:

a. What was the coolant inventory as a function of time?

b. How can the relocation of the core into the lower plenum and the formation of a coolable configuration be understood?

c. What was the precise sequence of events that led to the core relocation?

d. What happened to the control rod material during the core heat-up and subsequent degradation?

The study was conducted as part of the TMI-2 Accident Evaluation Program.[*] This program is sponsored by the U.S. Department of Energy and is directed towards understanding what happened during the accident and resolving the outstanding technical issues relating to

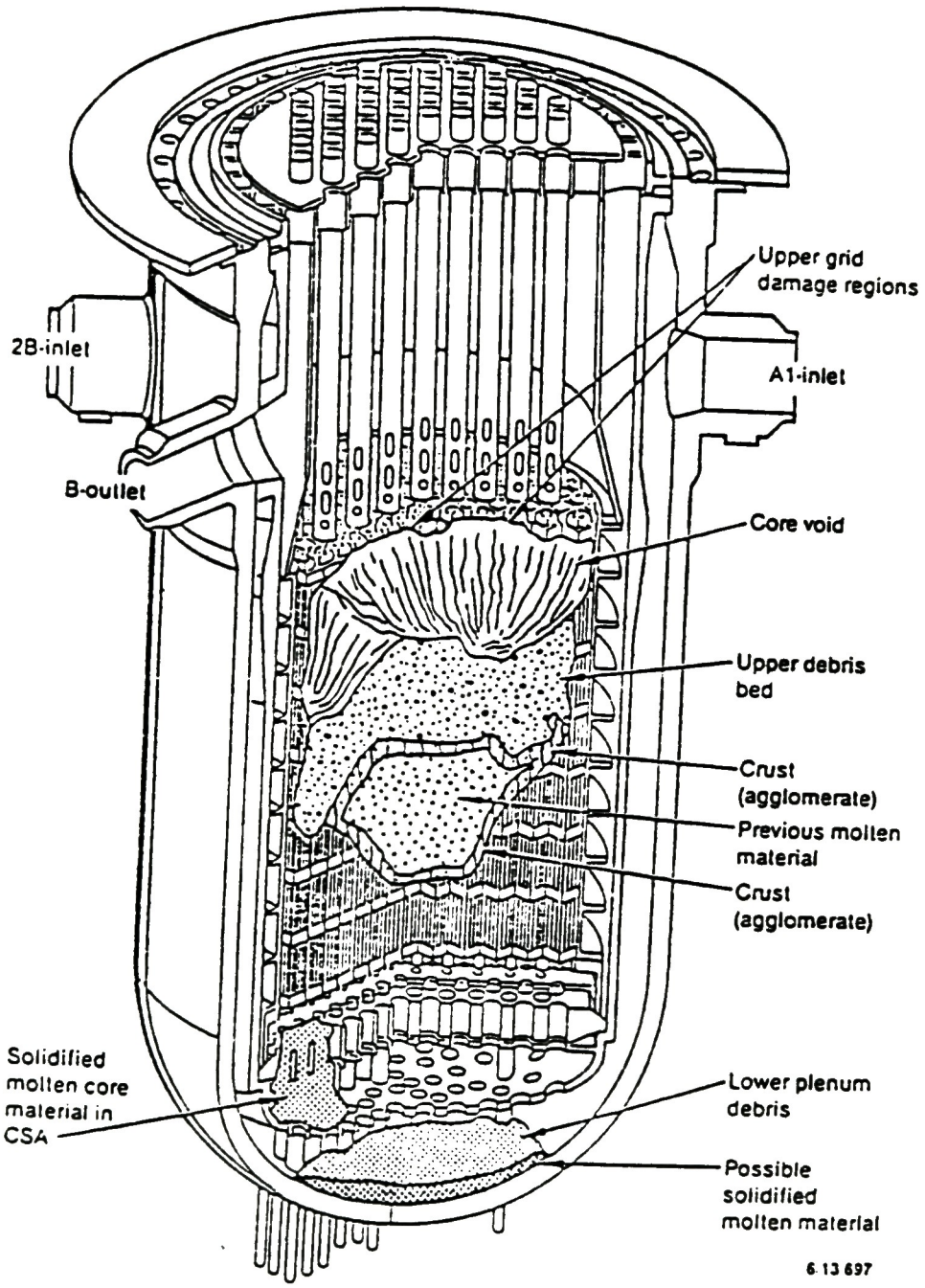

Figure 1.1 TMI-2 known end-state core configuration.[6]

the accident. The analysis reported here complements this effort providing additional insight into the progression of the accident.

The analysis examines the SRM data recorded during the first four hours of the accident. Normally these detectors provide a measure of the neutron level in the reactor when the reactor is shut down or at very low power levels. The response of the detector is determined by the neutron flux at the detector location. This flux is in turn a function of the core power history, fuel distribution, moderator density and distribution, and the distribution of control rod material in the reactor. Previous work has shown that these ex-core detectors provide a measure of the global status of the core and contain useful information on a variety of parameters relating to the fuel, moderator and control elements.[13,14] Since the detector response during the accident deviated significantly from that of a normal shutdown for an undamaged core (see Fig. 1.2),[15] an analysis of the SRM response should provide additional insight into and details of the accident. As part of the TMI Accident Evaluation Program, the information gained in this way will be a benchmark in the development and verification of a best-estimate accident scenario.

Figure 1.3 depicts the accident progression[5,6] as determined from known end-state conditions of the core and reactor vessel, data from plant instrumentation recorded during the accident, and the results from best-estimate analyses of the accident employing the severe core damage accident progression code SCDAP.[16] Part of this work was directed towards determining if the SRM response was consistent with this scenario. The remainder of this section describes the scenario[6] and the uncertainties relating to it.

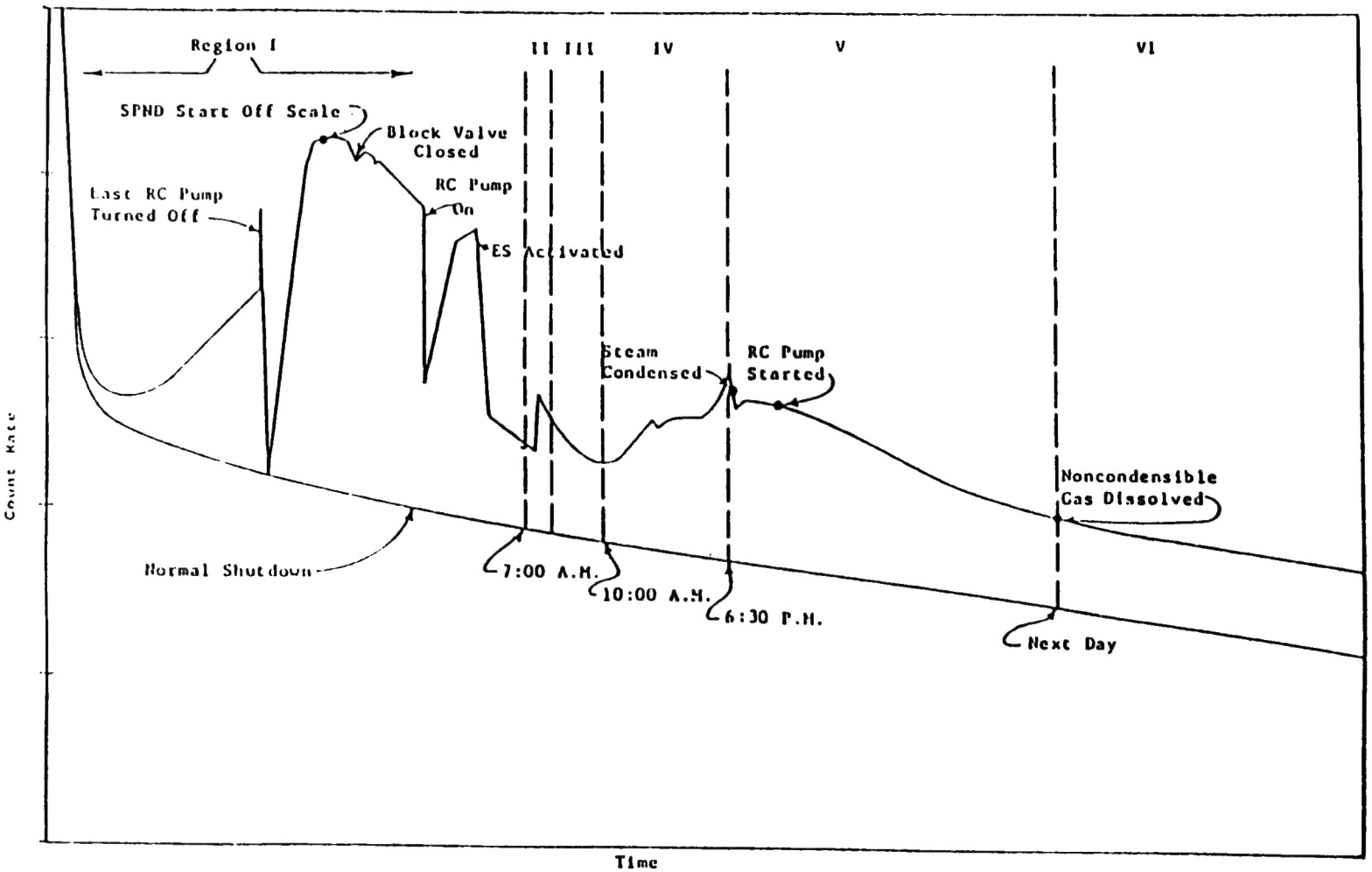

Figure 1.2 An illustration of SRM response (not to scale).[15]

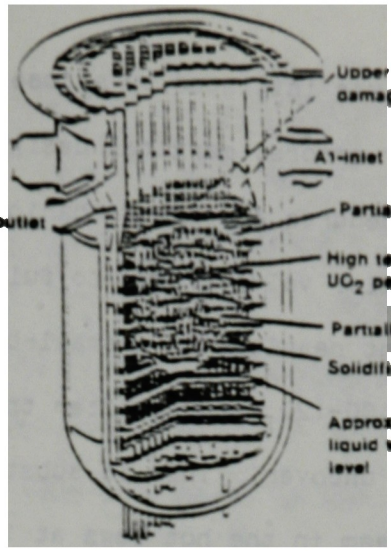

(a) Core condition just prior to pump transient at 174 minutes

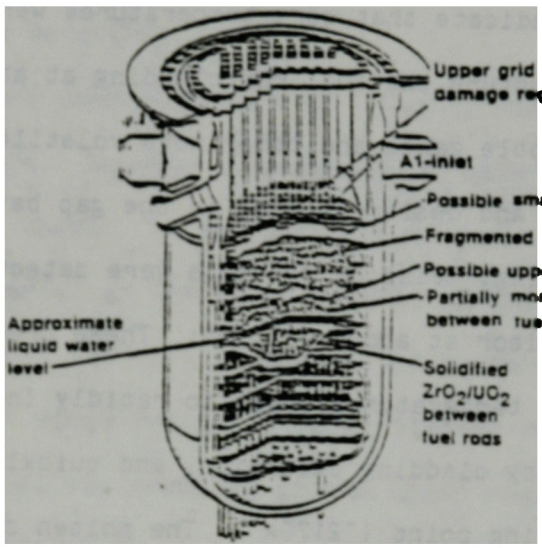

(b) Core condition just after pump transient—175 to 180 minutes

(c) End state core conditions—after 224 minutes

Figure ..3. Hypothesized States of the TMI-2 Accident Progression[6]

The accident was initiated by a loss of feedwater. Through a series of operator errors, marginal design, inadequacies in training and emergency procedures and the mechanical failure of the power-operated relief valve (PORV) to fully close, this loss of feedwater transient resulted in a small-break loss of coolant accident (LOCA). Between 100-120 minutes after the initial loss of feedwater, the core began to uncover. This is substantiated by the measurement of superheated steam in the hot legs at 113 min. Best-estimate predictions indicate that core temperatures were high enough to balloon and rupture the fuel rod cladding at about 140 min, releasing some of the noble gases and other more volatile fission products, such as the iodine and cesium located in the gap between the fuel pellets and the cladding. Fission products were detected by the containment radiation monitor at about 143 min. These predictions also suggested that cladding temperatures began to rapidly increase at about 150 min, due to zircaloy cladding oxidation, and quickly exceeded the zircaloy cladding melting point (~2170k). The molten zircaloy is thought to have dissolved some of the UO_2 fuel. The liquefied mixture probably flowed down and solidified in the lower, cooler regions of the core. The lowest level to which the molten material flowed was probably coincident with the coolant liquid level, which is estimated to have been in the lower one-third of the core.

By 174 min (just prior to the primary coolant pump transient, as discussed later), local core temperatures had probably reached fuel melting, particularly in the central, highest-temperature regions of the core. Between one-quarter and one-half of the core probably attained cladding melting temperatures and some subsequent fuel

dissolution and relocation. During the time period between 150 and 174 min, a relatively solid region of core materials composed of previously molten and intact fuel rods could have formed, as illustrated in Figure 1.3.a. The top of the core probably consisted of highly oxidized fuel rod remnants. High-temperature molten material probably had not yet penetrated below 0.75 m above the bottom of the core, since the Self Powered Neutron Detectors (SPNDs) at Level 1 and 2 (0.25 and 0.75 m above the core bottom, respectively) did not indicate any anomalous behavior.

The primary coolant pump transient at 174 min. rapidly injected some water into the core. However, the amount of water and the extent of core cooling is not known. Furthermore, flow blockage, resulting from the relocated material in the lower regions of the core probably limited coolant flow into the core. Thermal and mechanical shock due to the injected coolant would result in embrittlement and fragmentation of the fuel rod remnants in the upper regions of the core. These fuel rod fragments could have collapsed downward towards the molten and relocated core material, forming the rubble bed shown in Figure 1.3.b.

Thermal calculations and flow estimates suggest that the zone of relocated core materials continued to heat up even after injection of this water into the core at 174 minutes. These calculations are consistent with recent analysis of the in-core thermocouple alarms. The peripheral thermocouples responded to coolant injection into the core by falling back from a high-temperature alarm state, while the central thermocouples remained in their high-temperature alarm state when the core was flooded with coolant, indicating the presence of a

temporarily noncoolable mass in the central part of the core even before the pump transient.

Most, if not all, of the core materials found in the lower plenum probably relocated at approximately 225 min in a molten form. This relocation was indicated by anomalous output from the Level 1 and 2 SPNDs and by a very rapid increase of approximately 2 MPa in the primary system pressure. The increase in system pressure was apparently caused by the generation of substantial quantities of steam as the hot core material flowed into water in the lower plenum. The steam and water probably fragmented the molten material as it relocated into the lower plenum. This fragmentation may have resulted in the formation of a coolable configuration in the lower plenum. Core heatup and further core degradation were probably halted at this time by the presence of water in the lower plenum and the continued injection of water into the RCS by the high pressure injection system. The postulated final damage configuration of the reactor core and its support structures is illustrated in Figure 1.3.c.

As discussed by reference 6, a number of basic issues remain to be resolved. These issues are given in Table 1.1. The objective of this work was to analyze the SRM response, particularly during those times corresponding to when the dramatic changes in core geometry or coolant conditions were thought to have occurred, to allow benchmarking the accident scenario discussed here as well as to resolve a number of the outstanding technical issues identified in Table 1.1.

To accomplish this objective, a series of neutronics calculations were performed using the DOT 4.3 computer code. These simulated the

TABLE 1.1

Unresolved Technical Issues
Related to the Accident Scenario[4]

RCS Thermal-Hydraulics

1. What was the coolant inventory as a function of time?
2. What were the flow patterns within the reactor vessel?
3. How was the core reflooded?

Core Damage Progression

1. What was the peak temperature?
2. How did the control and burnable poison rods interact with the fuel rods?
3. What was the extent of flow blockage, and how did it affect the hydrogen production?
4. How can the relocation of the core into lower plenum and the subsequent formation of a coolable configuration be understood?
5. What was the degree of damage to the core support assembly, instrument structures, and RV lower head?

Fission Product Behavior

1. What were the releases from the fuel of the less volatile fission products?
2. What were the chemical forms of the fission products?
3. What were the physical and chemical interactions that affected fission product transport?
4. How did the long-term exposure to an aqueous environment affect fission product behavior?

material conditions in the reactor during the accident in an effort to reproduce the SRM response.

In the sections that follow, the analytical approach as well as prior work are described. Specifically, section 2 describes prior and related work. In section 3, the calculational method used in this analysis is presented along with benchmark calculations. Section 4 presents the results of the analysis as well as the uncertainties. Section 5 provides a summary of the conclusions of this work.

2. PREVIOUS WORK

A number of previous works have analyzed the TMI accident in an attempt to understand its progression. These studies include analysis of the SRM response as well as analyses of the response of other incore and ex-core instrumentation. This section describes a number of these studies relating to the present work.

The SRM response during the first 240 minutes of the accident is shown in Fig. 2.1.[1] A number of groups including NSAC,[1-5] Malloy and Chang,[6] and ORNL[7] have examined the response.

The NSAC study analyzed the response during the accident in an effort to correlate the structure with various system events and a postulated scenario. They explained the structure as follows.

The increase in count rate from point B to point E of Fig. 2.1[1] was due to homogeneous voiding in the core and downcomer (caused by water flashing to steam as the system pressure decreased) which resulted in decreased attenuation of the neutrons. The B- and A-loop coolant pumps were turned off at point D and point E respectively. Turning off the A-loop coolant pumps is believed to have caused phase separation, with the steam voids moving up and the liquid water settling downward in the vessel and primary system. This would have resulted in liquid water filling the core and downcomer causing the count rate to drop at point F. It is believed that at that time the coolant mass inventory was still sufficient to cover the core and to fill the downcomer. Filling of these regions with coolant of near normal density would cause the count rate to drop to nearly the normal value for an unvoided core as occurred at point F. The normal decay

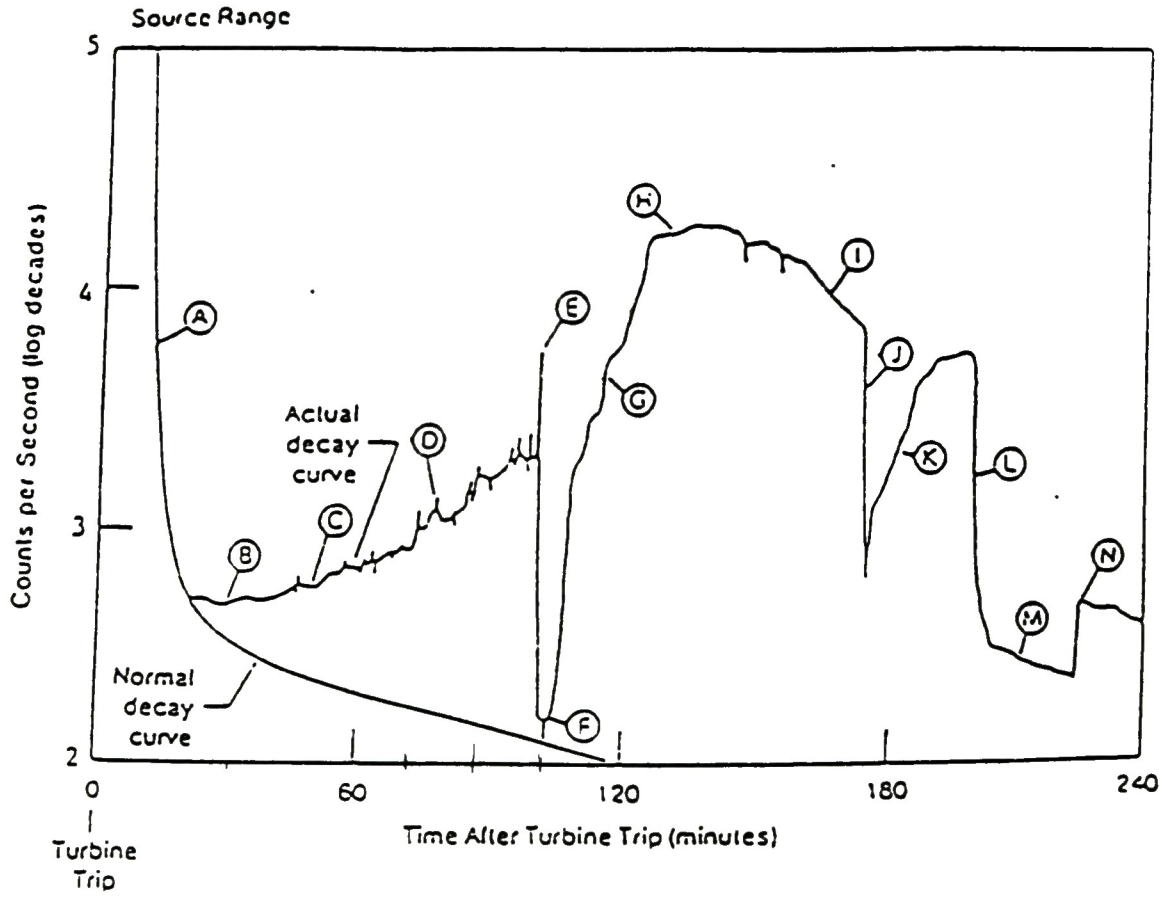

Figure 2.1 TMI-2 Accident Source Range Monitor Response.

curve shown in Figure 2.1 is that resulting from an actual TMI-2 scram that occurred at TMI about one week before the accident.

As the core heatup continued, the coolant boiled off, the core began to uncover, and the downcomer water level began to drop. The decreasing levels caused the count rate to increase from points F to point H. It should be noted that the downcomer water level should be lower than the corresponding two-phase mixture level in the core due to the hydro-static pressure equilibrium.

The leveling off and decrease of the count rate from point H to point I could be accounted for either by the overfilling or continuing to empty. In emptying, two counterbalancing effects interact to produce a decreasing count rate. As the water level decreases, the amount of neutron shielding decreases. This decrease increases the leakage of neutrons from the core, tending to raise the count rate. At the same time, the loss of coolant decreases both the photoneutron source strength and the effective neutron multiplication factor of the core, causing a decrease in source strength. The decreasing source strength tends to decrease the detector count rate. Based on water flow rates and other evidence, the vessel is thought to have continued to empty. At point J, the short-term flow from the operation of the number 2B pump probably filled the downcomer and caused the rapid drop in SRM count rate. From point J to L, the water injected by the 2B pump is boiled off, decreasing shielding and increasing neutron levels at the SRM. At point L, the High Pressure Injection System (HPIS) filled the downcomer and the core regions, thus returning the count rate to near but higher than normal values.

The interpretation discussed above showed that the response of neutron detectors located outside the reactor vessel could be correlated with the coolant conditions in the TMI vessel during the accident.

To understand the effects of the vessel coolant status on the ex-core detector's response, a detailed neutronics analysis is required. For large-break LOCA's, Gundy[16] has analyzed several LOFT experiments using such an approach. NSAC[1,3] and Malloy and Chang[9] performed similar analyses for the TMI accident.

These analyses focused on the coolant status during the first 174 minutes of the TMI accident. Because the extent of the core damage was unknown at the time these studies were conducted, an intact core configuration was assumed. Video and sonar data,[10,12] have shown that the core was severely damaged in the accident. Furthermore, thermal hydraulic data recorded during the accident suggests that this damage began as early as 140 minutes into the accident. As a result, the work by NSAC and Malloy and Chang are suspect beyond the onset of core damage. It is necessary to analyze the SRM signal beyond this time in light of this new information.

Estimates of coolant inventory have also been done using available thermal hydraulic data, system operation characteristics, and the initial conditions prior to the accident.[2] The core liquid level based on the analysis in Reference 2 is given in Fig. 2.2. It should be noted that the data shown in Fig. 2.2 is based only on thermal hydraulic considerations and do not take into account the SRM data or analyses.

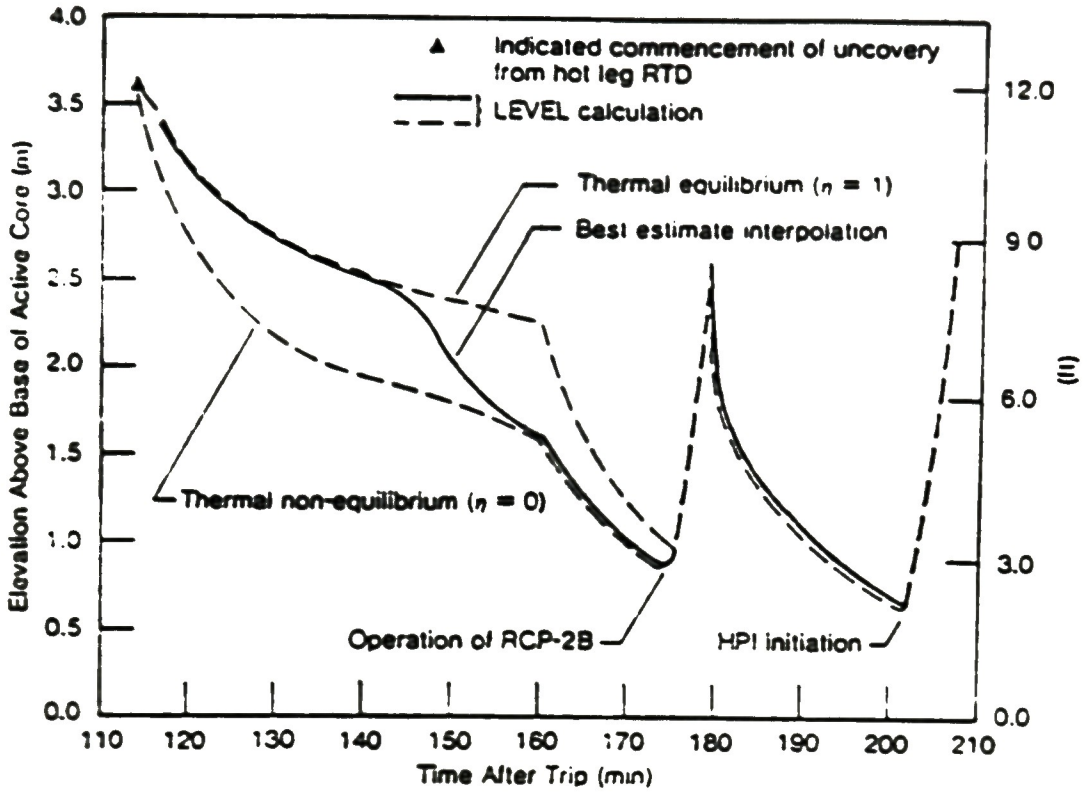

Figure 2.2 Calculated level path during uncovery of TMI-2 core. Solid curve is best estimate calculation.

In Reference 3, a comprehensive analysis of core instrumentation and other instrumentation responsive to fuel degradation during the TMI accident is reported. The purpose of that analysis was to try to understand and assess the core damage at TMI. The instrumentation examined included core exit thermocouples, self powered neutron detectors, ex-core neutron detectors, and containment radiation monitors. The ex-core detector work included a detailed neutronics study which updated the earlier unpublished work of Reference 18. Based on the analyses of the various instrument responses during the accident, the study concluded that:

a. The response of the containment area radiation monitors at 142 minutes suggests that fuel damage had occurred.

b. The neutron transport analysis of the ex-core neutron detectors showed that the reactor vessel water level continuously decreased from the time the last coolant pump was shut off (at 100 minutes) until the restart of the 2B pump at 174 minutes.

c. The sudden rise in the SRM at 225 minutes along with sudden changes in other instruments suggests that major core disruption may have occurred at that time. The report speculates that this may have been the time at which the upper core region collapsed and formed the rubble bed.

The revised SRM analysis of Reference 3 included a neutronics-based prediction of core water level, the results of which are shown in Fig. 2.3.

It should be noted that none of the works discussed above used models of the core which were consistent with the core damage scenario

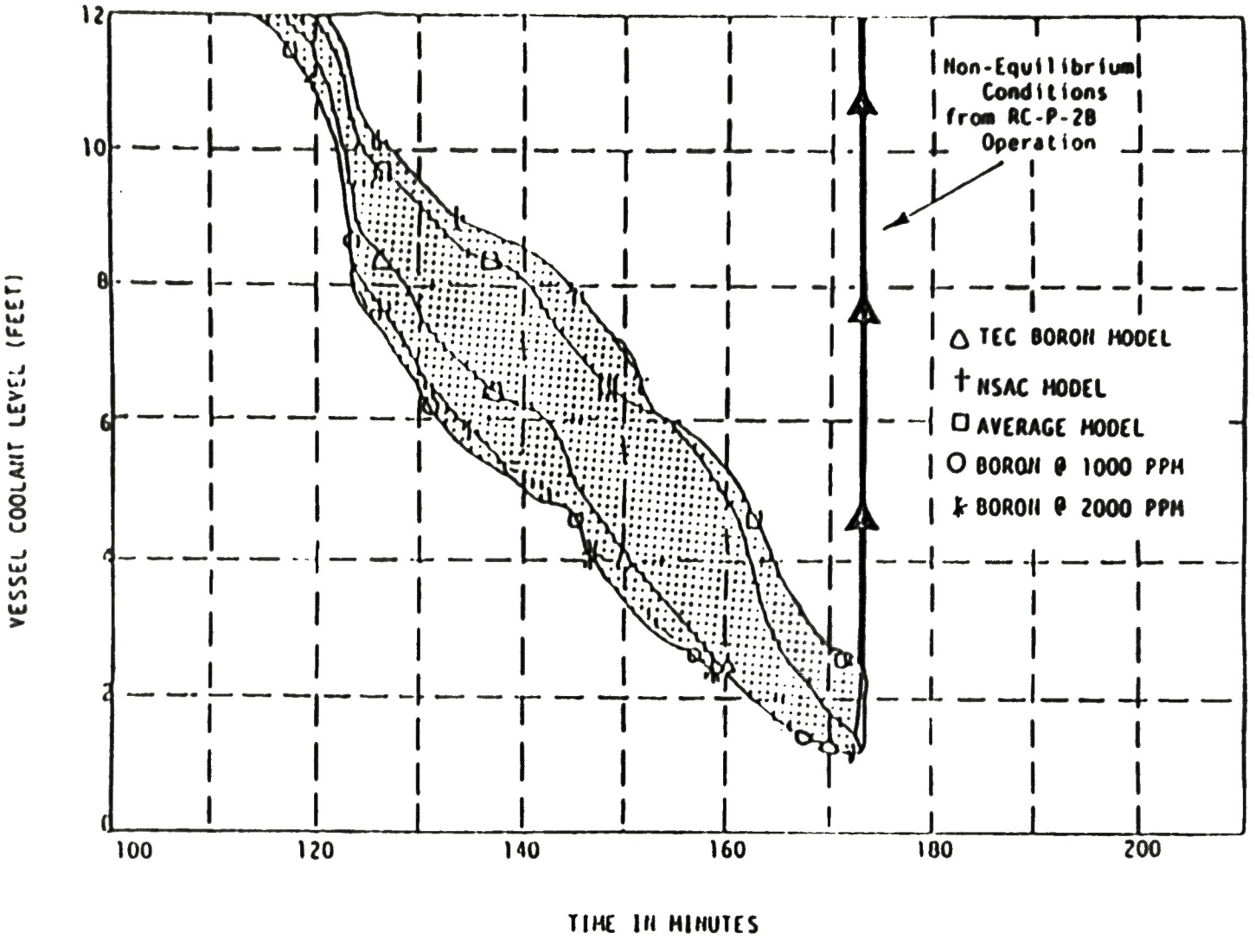

Figure 2.3 Calculated core uncovery history from source range detector response.[3]

envisioned by the TMI-2 Accident Evaluation Program.[6] As a result, the various neutronics analyses of the SRM response are in need of reexamination. Since it is now known that the damage to the TMI core is much more extensive than originally envisioned in any of these studies, an updated analysis is needed. For example, the previous analyses did not consider the core reconfiguration that is now thought to have occurred when the 2B pump was restarted at 174 minutes or the presence of fuel in the lower plenum.

Finally, several simplifying assumptions were included in the NSAC transport analyses of the ex-core detectors which have the potential to significantly alter the results. It was, for example, assumed that an analysis of the effects of core water level and moderator density done to explain the SRM behavior prior to 174 minutes could be extrapolated to times beyond 174 minutes. This extrapolation assumed an intact core, which is inconsistent with the current scenario. As a result, no analysis of the SRM response beyond the start-up of the 2B pump at 174 minutes was done. Also, the changing energy content of the neutron flux at the SRM location and its effect on SRM response was neglected.

Since core damage is known to influence the SRM response as shown by Baratta et al,[19] any analysis must take this into account. Furthermore, as the core voids, the neutron flux at the detector changes significantly in its energy content, causing an alteration in SRM sensitivity which must also be accounted for.

A related analysis worth mentioning concerns the fuel distribution in the TMI-2 damaged core. This analysis is based on thermal neutron flux measurements obtained from two strings of solid

state track recorders (SSTR).[19,20] The SSTR's were installed in the annular gap between the TMI-2 reactor vessel and the biological shield. Readings obtained from the SSTR's were then used to estimate the thermal neutron flux in the gap.[20] The resulting axial flux profile differed significantly from what would be expected for a normal core, and suggested that there might be some fuel relocated to the lower head, although the amount was not quantified in the initial study.[20]

The flux profile obtained from the SSTR readings was further analyzed using the discrete ordinate transport code, DOT 4.3, and associated neutronics models of the damaged core.[19] A total of eleven different models were tried. The various models examined differed in the way the fuel was distributed in the core and in the source strength used for the fixed sources.

The SSTR analysis[19] showed that the thermal flux profile was dominated by neutrons streaming in the annular gap from fuel in the lower vessel head. The SSTR readings were also found to be relatively insensitive to the arrangement of the fuel inside the normal core region. Satisfactory agreement between the calculated and measured thermal flux profile was obtained with 10 tonnes of UO_2 in the lower plenum. Allowing for uncertainties in the calculations and in the measurements it was estimated that there were between 5 to as many as 20 tonnes of UO_2 in the lower plenum. This SSTR analysis[19] for the first time quantified the amount of fuel relocation in the lower head. This was done prior to the visual examination of the lower head, which confirmed the presence of core material there. Together with the work of the Accident Evaluation Program, this suggests that the SRM data have the potential to substantially improve our understanding of the

core material relocation and the core liquid level uncertainties during the accident. Indeed, this inspires the present work and the approach used herein.

3. CALCULATIONAL METHOD

The source range monitor response depends on two factors: neutron source distribution and the shielding effect of materials between the core and the detector. To analyze the SRM response during the TMI-2 accident, both need to be modeled properly. In this section, the calculational method used in the present analysis is described and its adequacy is justified. First, the calculation of neutron source strength for the period of interest is described in subsection 3.1. This establishes the neutron source distribution for the analysis of the SRM response. Second, reactor models are constructed for computer code simulations. In this work, the two-dimensional, neutron transport code DOT 4.3[21] was used. The method used by the DOT code in calculating the spatial and energy distribution of the neutron flux in a two-dimensional geometry is known as the method of discrete ordinates. In this method, the Boltzmann transport equation for neutral particles is approximated numerically by a finite spatial mesh, a finite energy mesh, and a feature unique to discrete ordinates codes, a finite angular mesh at each spatial mesh. Thus, given a source of neutral particles (neutrons or photons) and a tabulation of microscopic interaction cross sections (which may include anisotropic scattering), DOT can provide an accurate approximation of the energy, angular, and spatial distribution of the neutron flux anywhere within the system being modeled. In addition, the DOT code has the capability to model symmetric systems in one of three two-dimensional coordinate systems: X-Y Cartesian geometry, R-Z cylindrical geometry and R-θ cylindrical geometry.

In this analysis, the R-Z cylindrical geometry was used. The reactor models include core, internals, vessel and shielding. The DOT symmetry axis was taken to correspond to the axial axis through the centerline of the reactor vessel. The models were divided into a multitude of homogeneous zones representing several core sections, reactor upper internals, lower internals, vessel, shielding, etc.

To assure the adequacy of the calculational method, including the source term, the reactor modeling technique and the computational procedure, the method was first applied to two loss-of-coolant experiments of the Loss of Fluid Test (LOFT) Facility.[22] Since LOFT was well instrumented, more complete measurements of pertinent parameters were available for comparison with calculations. This comparison allowed verification of the methodology prior to its use in analyzing the TMI-2 SRM response during the accident. The reactor model and the procedure for cross section preparation for the LOFT facility are described in subsection 3.2, while those for TMI-2 are given in subsection 3.3. Subsections 3.4 and 3.5 describe the bench-mark calculation of LOFT experiments LP-SB-2 and LP-SB-3, respectively.

3.1 Source Term Calculation

There are several possible neutron sources in a recently shutdown reactor core. The major source for the first few minutes after shutdown is the delayed neutron source, which is strongly time dependent. By using a point kinetics code[23] with six delayed neutron groups, it was determined that the delayed neutron source for the LOFT

facility during the experiments fell to 1.97×10^{8} n/sec in 1000 seconds. A second neutron source arises from spontaneous fission which occurs due to the buildup of Pu-240 and Cm-242. The inventory is quite small in these experiments. This source, as calculated by the ORIGEN code[24] is only 1.4×10^{3} n/sec. A third neutron source results from the inventory of the alpha emitters. For example, an alpha-n neutron source is produced through the reaction

$$O^{18} + \alpha \text{ ------} \rightarrow Ne^{21} + n.$$

The total neutron source from alpha-n reactions, as calculated by the ORIGEN code is 4.38×10^{3} n/sec. The start-up source is from the spontaneous fission of Cf-252 with a source strength of 3.38×10^{7} n/sec. The last major neutron source is from photoneutrons. Fission products emit high energy gammas which result in photoneutron production through reactions such as

$$D^{2} + \gamma \text{ ------} \rightarrow H^{1} + n.$$

This reaction has a threshold energy of 2.226 Mev, so that only the higher energy gammas can cause this reaction.

Figure 3.1 shows the procedures used to calculate the photoneutron source. The time dependent gamma source from fission product decays was calculated by the ORIGEN code.[24] To convert this gamma source to a neutron source, a shielding calculation was performed to determine the spatial distribution of the gamma flux. A space and energy dependent photoneutron source was calculated assuming 0.015% D_2O in H_2O.

A comparison of the strengths of the different neutron sources at LOFT is provided in Table 3.1. It appears that all sources are negligible with respect to the photoneutron and delayed neutron

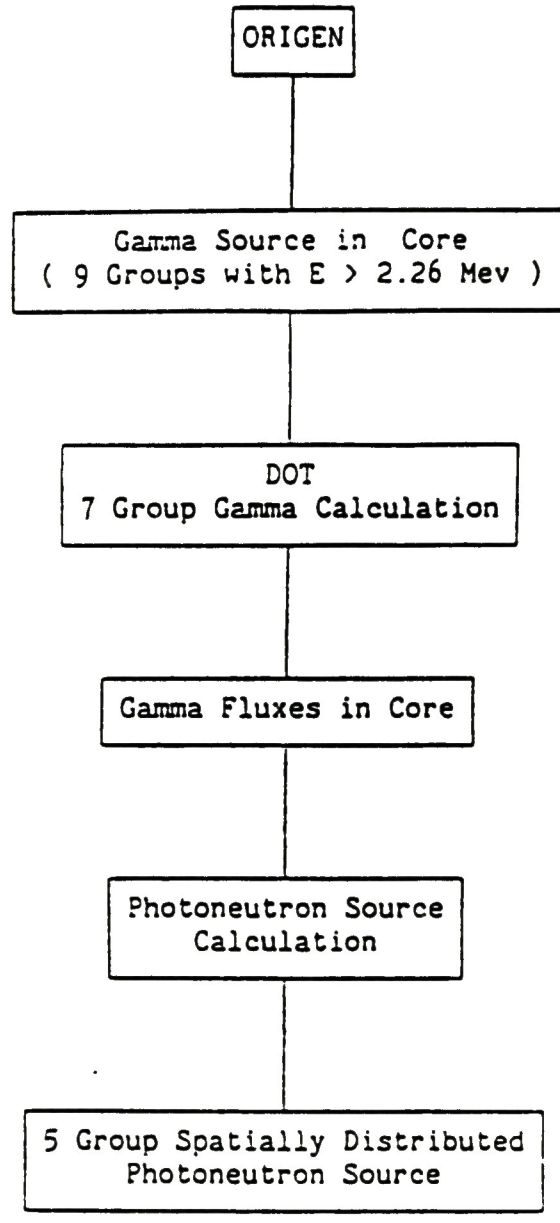

Figure 3.1 Procedure for calculation of photoneutron source.

TABLE 3.1

Neutron Sources in the LOFT Core After Shutdown

Source	n/sec	Comments
Delayed neutron	3.70×10^{13} - 1.97×10^{8}	(100 to 1000 sec)
Photoneutron	2.74×10^{10} - 1.22×10^{10}	(100 to 1000 sec)
Alpha-N source	4.38×10^{5}	(~ Constant)
Spontaneous fiss.	1.40×10^{5}	(~ Constant)
Start-up source	3.38×10^{7}	(~ Constant)

sources. The time-dependent photoneutron and delayed neutron sources are shown in Fig. 3.2. This figure shows that the delayed neutron source dominates during the first 400 seconds after a shutdown. The photoneutron source then begins to become significant at about 400 seconds, and it becomes the dominant neutron source at about 900 seconds.

Since the coolant inventory in the primary system changes very slowly during a small-break loss of coolant accident (LOCA), it can be assumed that the neutron flux shape does not change significantly in the first few minutes. The detector response then follows the delayed neutron decay curve. At 1000 seconds after the reactor shutdown, the photoneutrons are the dominant neutron source. The photoneutron source plays the role of the external source and causes the fission chain reactions in a subcritical shutdown reactor. The neutronics behavior of the core in this time period depends on the core coolant status and the strength of the photoneutron source. By assuming that the flux shape changes very slowly in a small-break LOCA, the neutronics analysis can then be performed by a series of static calculations with the estimated core void and source strength distribution at each time point. Therefore, a shielding type calculation with a distributed fixed source plus fission, was determined to be the best approach for this analysis.

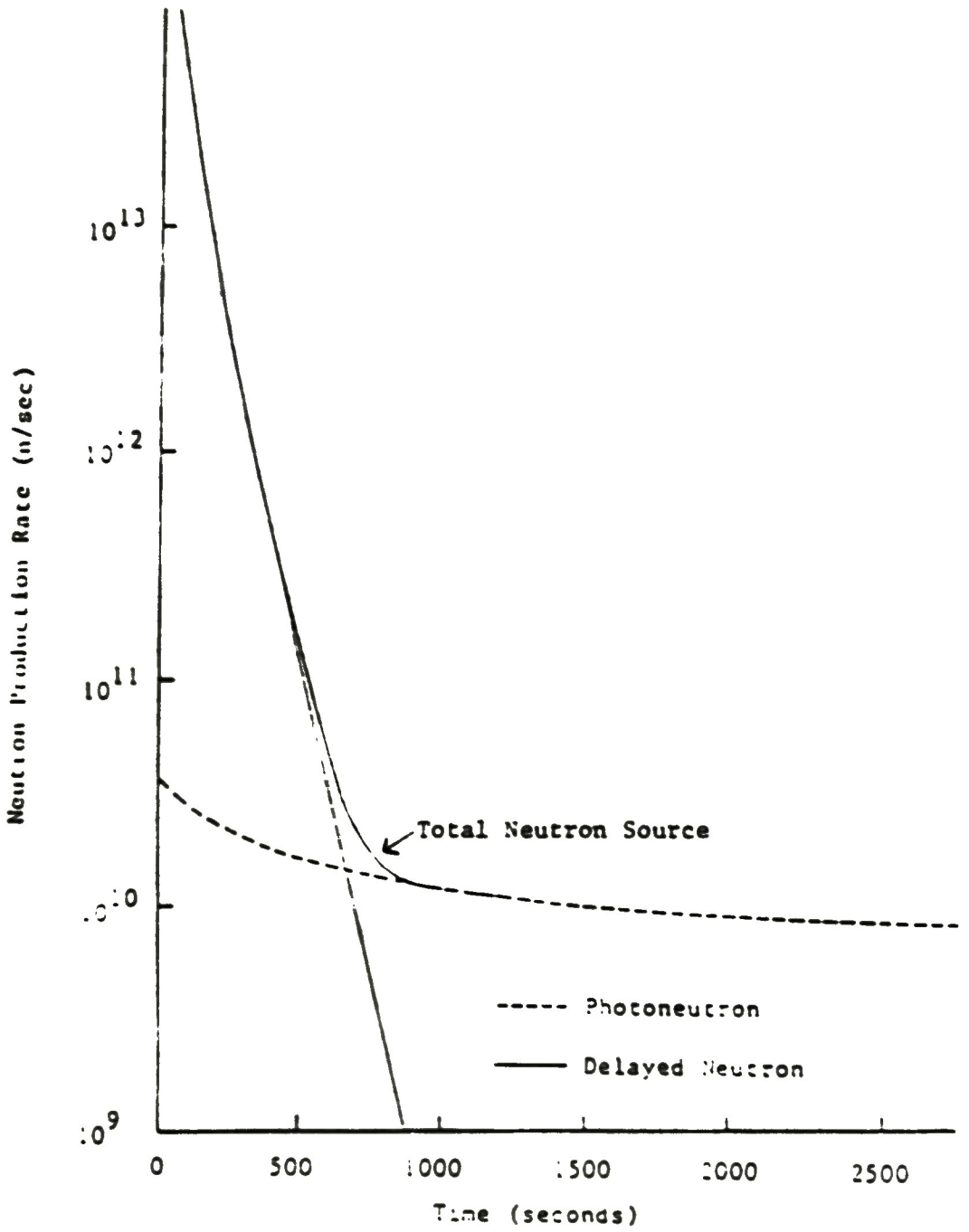

Figure 3.2. Estimate of photoneutron emission rate, delayed neutron production rate, and total neutron production rate following scram.

3.2 LOFT Reactor Model and Gross Section Preparation

3.2.1 Reactor Model

The LOFT facility,[22] a 50 MWth PWR, is designed to simulate the major responses of the components and systems in a commercial PWR to a LOCA. The facility includes the reactor vessel, the intact loop, the broken loop, the blow down suppression system, and the Emergency Core Cooling System (ECCS). The major components of the LOFT facility are shown in Fig. 3.3, and the reactor is shown in cross section in Fig. 3.4.

The neutron detectors are located outside the reactor vessel on a water filled shield tank. As a result, the neutronic model of the LOFT reactor covers a large number of regions. The models contain the core regions, the upper internal regions, the lower internal regions, the downcomer regions, the reactor vessel, the vessel gap region, and the biological shielding. Because of the large number of regions to be modeled, with the corresponding large physical dimensions in each direction, the mesh spacing size is kept fairly large and the number of neutron energy groups is kept small to save computation time.

The neutronics model for the LOFT facility was developed from the geometry given in Reference 17. The R-Z geometry for the model used in this work is shown in Fig. 3.5. Also shown are the locations of the source range monitor (SRM) and the detectors A, B, C and D which are part of a specially installed Penn State Non-Invasive Liquid Level/Density Gauge System (SRM, A, B, C and D are located in the shield tank water region in the figure, respectively). The model

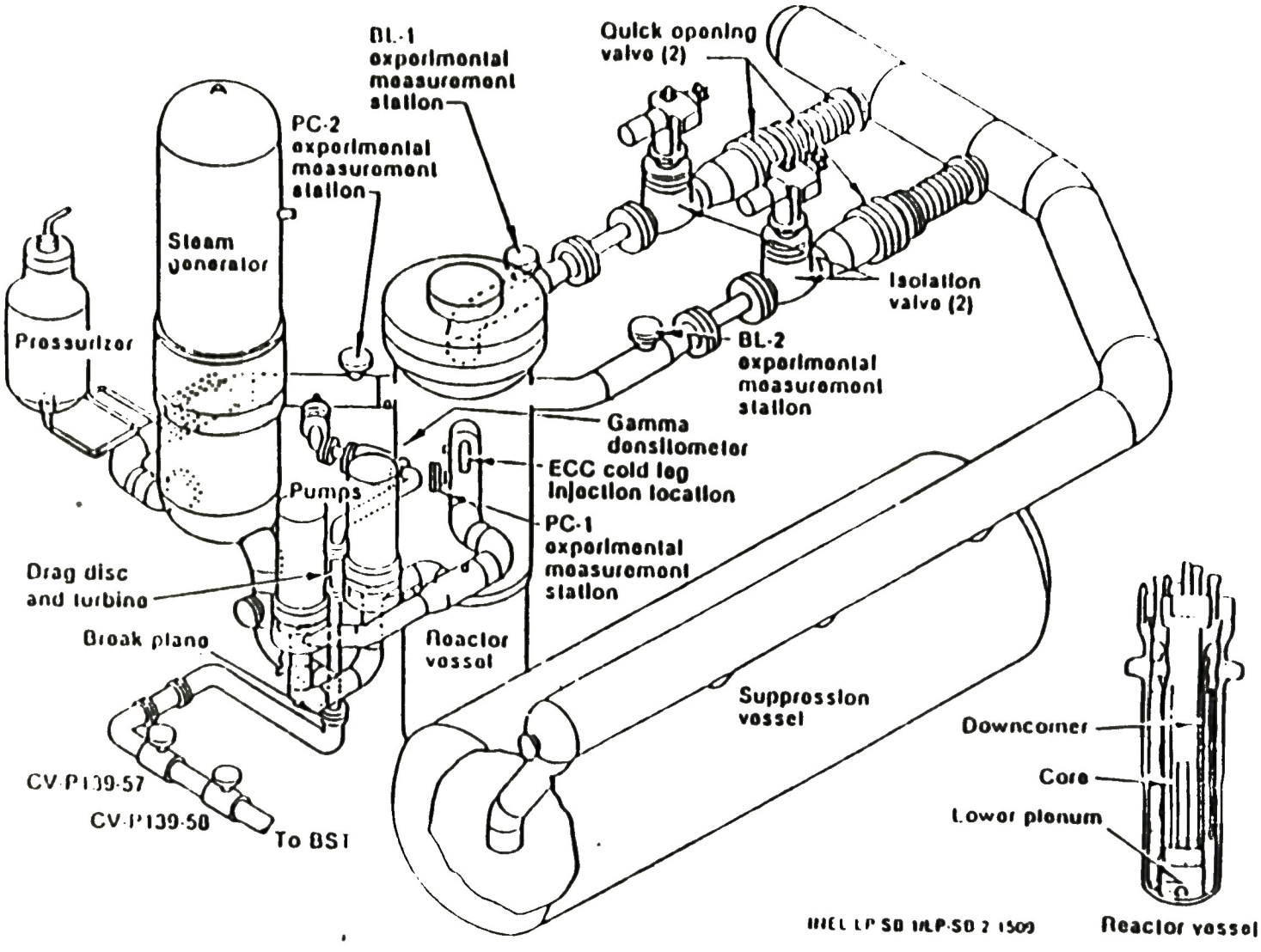

Figure 3.3. Configuration of the subsystems of the LOFT facility.

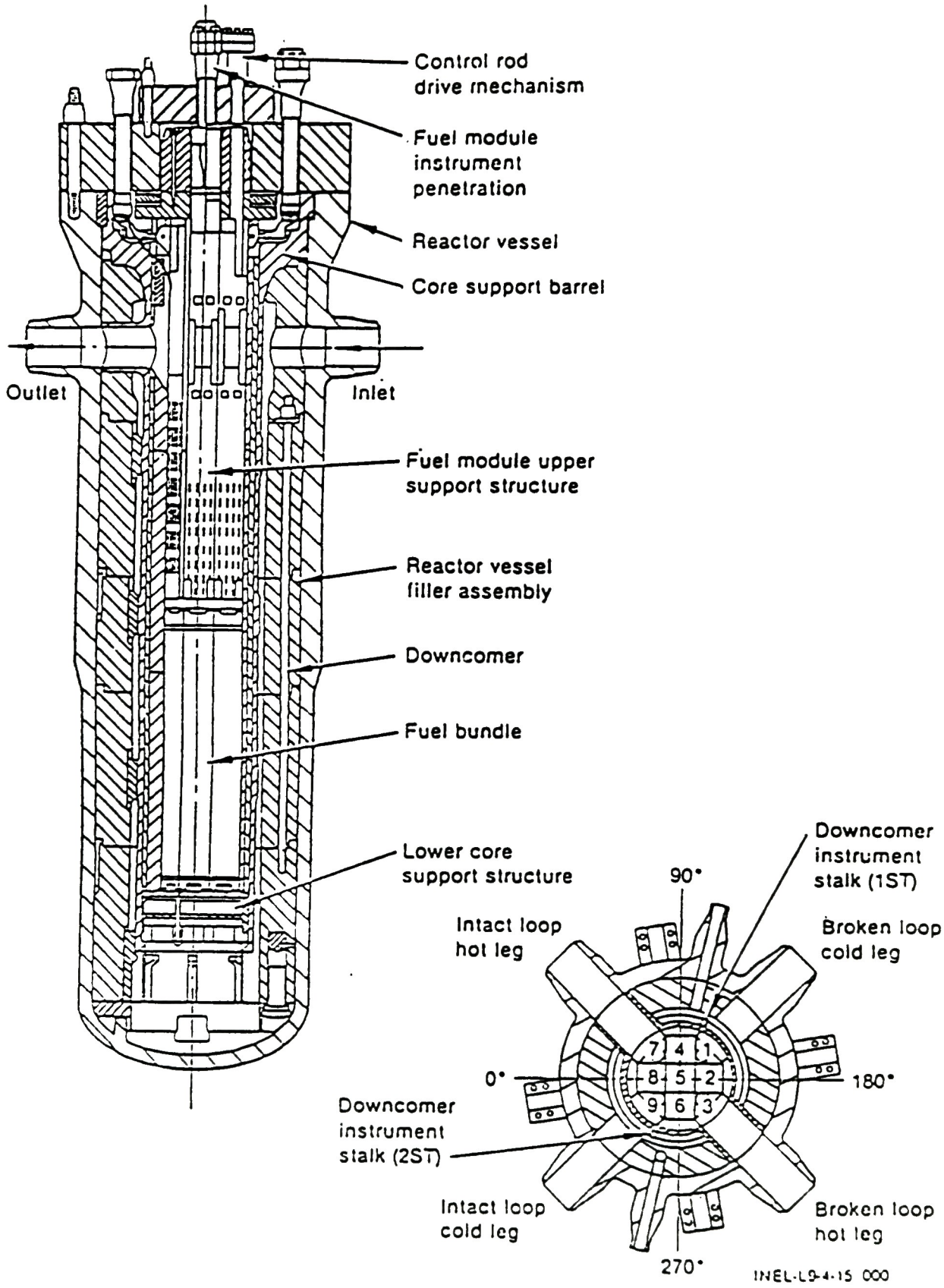

Figure 3.4. LOFT reactor vessel and internals.

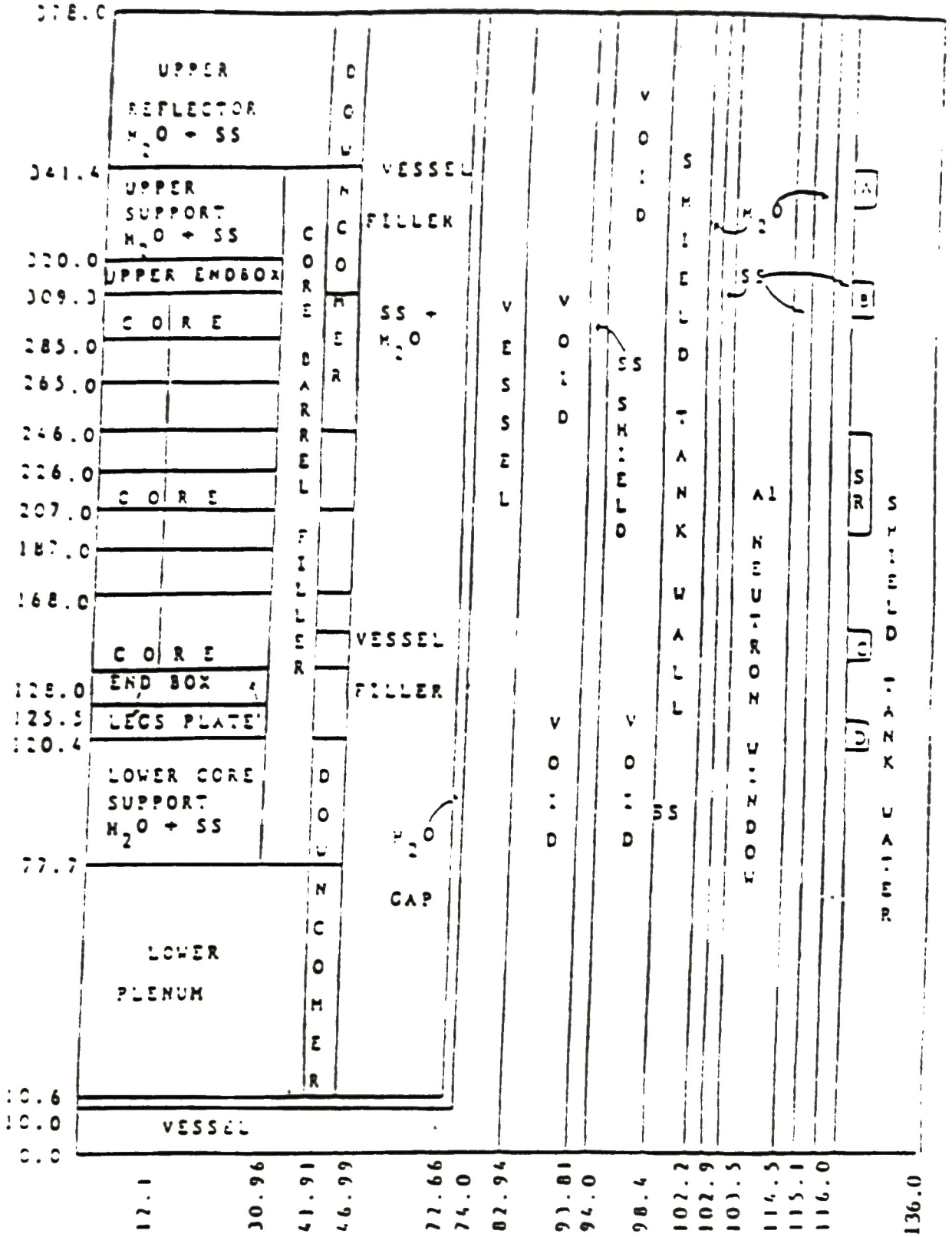

Figure 3.5. LOFT reactor R-Z model for DOT calculation. (Dimensions in cm)

simulates the core, downcomer, vessel, air gap, and the shield tank beyond the detector location, including the aluminum neutron windows, which are plates of aluminum in front of the detector tube locations. The aluminum neutron windows displace the water in the shield tank in front of the detectors resulting in less neutron absorption and a stronger detector response.[25] Boundary conditions used were vacuum top, bottom and right side and reflected on the left.

The model includes radial and axial core regions. The LOFT core consists of five full-fuel assemblies and four partial-fuel assemblies in order to simulate an approximate cylinder (Figure 3.4). The first radial boundary of the model corresponds to the boundary of the central fuel assembly. The axial regions are modeled according to the voiding data available from the LOFT facility. Voiding data available from the LOFT facility are in the form of a so called 'bubble plot', which is generated from conductivity probe data.[22] The conductivity probes are located at different elevations in the core and downcomer. The axial regions were modeled in such a way that every axial region covers two sections of the bubble plot data. Table 3.2 gives the axial and radial mesh spacing used in the LOFT reactor Model. The spacing used was found to be sufficient to prevent inaccuracies or negative fluxes in the discrete ordinates "diamond difference" model.

3.2.2 Cross Section Preparation

A five group cross section set was used in the LOFT small-break LOCA analysis. The five-group cross section set was collapsed from a 123-neutron-group library. The group structure used in this analysis

Table 3.2A LOFT Radial Mesh Distribution

1	0.0	2	1.539	3	3.078	4	4.617	5	6.156
6	7.695	7	9.234	8	1.066E+1	9	1.210E+1	10	1.360E+1
11	1.504E+1	12	1.649E+1	13	1.794E+1	14	1.938E+1	15	2.083E+1
16	2.228E+1	17	2.372E+1	18	2.517E+1	19	2.622E+1	20	2.806E+1
21	2.951E+1	22	3.096E+1	23	3.210E+1	24	3.308E+1	25	3.406E+1
26	3.504E+1	27	3.602E+1	28	3.700E+1	29	3.798E+1	30	3.896E+1
31	3.944E+1	32	4.092E+1	33	4.191E+1	34	4.291E+1	35	4.393E+1
36	4.495E+1	37	4.597E+1	38	4.699E+1	39	4.800E+1	40	4.902E+1
41	5.005E+1	42	5.108E+1	43	5.210E+1	44	5.313E+1	45	5.416E+1
46	5.518E+1	47	5.621E+1	48	5.724E+1	49	5.826E+1	50	5.929E+1
51	6.032E+1	52	6.134E+1	53	6.237E+1	54	6.340E+1	55	6.442E+1
56	6.545E+1	57	6.648E+1	58	6.750E+1	59	6.853E+1	60	6.956E+1
61	7.059E+1	62	7.161E+1	63	7.264E+1	64	7.327E+1	65	7.420E+1
66	7.517E+1	67	7.614E+1	68	7.711E+1	69	7.808E+1	70	7.905E+1
71	8.002E+1	72	8.100E+1	73	8.197E+1	74	8.294E+1	75	8.810E+1
76	9.381E+1	77	9.400E+1	78	9.842E+1	79	9.930E+1	80	1.002E+2
81	1.012E+2	82	1.022E+2	83	1.028E+2	84	1.035E+2	85	1.045E+2
86	1.054E+2	87	1.064E+2	88	1.074E+2	89	1.084E+2	90	1.094E+2
91	1.104E+2	92	1.114E+2	93	1.124E+2	94	1.134E+2	95	1.144E+2
96	1.150E+2	97	1.155E+2	98	1.160E+2	99	1.178E+2	100	1.193E+2
101	1.208E+2	102	1.223E+2	103	1.238E+2	104	1.253E+2	105	1.269E+2
106	1.284E+2	107	1.299E+2	108	1.314E+2	109	1.329E+2	110	1.344E+2
111	1.360E+2								

Table 3.2B LOFT Axial Mesh Distribution

1	0.0	2	2.500	3	5.000	4	7.500	5	1.000E+1
6	1.056E+1	7	1.306E+1	8	1.554E-1	9	1.803E-1	10	2.051E-1
11	2.300E+1	12	2.549E+1	13	2.549E+1	14	3.046E-1	15	3.295E-1
16	3.543E+1	17	3.792E+1	18	4.041E+1	19	4.289E+1	20	4.538E+1
21	4.787E+1	22	5.035E+1	23	5.284E+1	24	5.533E+1	25	5.781E-1
26	6.030E+1	27	6.729E+1	28	6.527E+1	29	6.776E+1	30	7.025E+1
31	7.273E+1	32	7.522E+1	33	7.771E-1	34	7.996E-1	35	8.248E+1
36	8.501E+1	37	8.754E+1	38	9.007E+1	39	9.260E-1	40	9.512E-1
41	9.765E+1	42	1.001E+2	43	1.027E+2	44	1.052E+2	45	1.077E+2
46	1.102E+2	47	1.128E+2	48	1.153E+2	49	1.178E+2	50	1.204E+2
51	1.229E+2	52	1.253E+2	53	1.280E+2	54	1.305E+2	55	1.330E-2
56	1.355E+2	57	1.380E+2	58	1.405E+2	59	1.430E+2	60	1.455E-2
61	1.480E+2	62	1.505E-2	63	1.530E+2	64	1.555E+2	65	1.580E+2
66	1.605E+2	67	1.630E+2	68	1.655E+2	69	1.680E+2	70	1.707E-2
71	1.734E+2	72	1.761E+2	73	1.788E-2	74	1.815E+2	75	1.842E-2
76	1.870E+2	77	1.895E+2	78	1.920E+2	79	1.945E+2	80	1.970E-2
81	1.995E+2	82	2.020E+2	83	2.045E+2	84	2.070E+2	85	2.094E+2
86	2.117E+2	87	2.141E+2	88	2.165E+2	89	2.188E+2	90	2.212E+2
91	2.236E+2	92	2.260E-2	93	2.285E-2	94	2.310E-2	95	2.335E-2
96	2.360E+2	97	2.385E+2	98	2.410E+2	99	2.435E-2	100	2.460E+2
101	2.485E+2	102	2.512E-2	103	2.540E-2	104	2.567E+2	105	2.595E-2
106	2.622E+2	107	2.650E-2	108	2.675E-2	109	2.700E-2	110	2.725E-2
111	2.750E+2	112	2.775E-2	113	2.800E+2	114	2.825E-2	115	2.850E-2
116	2.875E+2	117	2.899E-2	118	2.923E-2	119	2.947E+2	120	2.971E-2
121	2.996E-2	122	3.020E+2	123	3.044E+2	124	3.068E+2	125	3.093E-2
126	3.108E+2	127	3.121E-2	128	3.134E-2	129	3.147E-2	130	3.160E-2
131	3.173E-2	132	3.186E-2	133	3.199E-2	134	3.225E-2	135	3.252E-2
136	3.279E-2	137	3.306E-2	138	3.333E-2	139	3.360E+2	140	3.367E-2
141	3.414E-2	142	3.439E-2	143	3.465E-2	144	3.491E-2	145	3.517E-2
146	3.543E-2	147	3.570E-2	148	3.596E-2	149	3.622E-2	150	3.648E-2
151	3.675E-2	152	3.701E-2	153	3.727E-2	154	3.753E-2	155	3.780E+2

is shown in Table 3.3. The 123-neutron-group library has a fast group structure consisting of the GAM-II energy boundaries combined with a 30-group THERMOS structure below 1.86 ev. The 123-group neutron library is in AMPX master library format.[26] The AMPX code NITAWL[26] was used to make a resonance self-shielding calculation using the Nordheim Integral Method treatment.[27] The geometry, dimensions, and number densities for the various core regions and unit cells were taken from Reference 28. The core fuel rod unit cell, which is shown in Fig. 3.6, was a standard single-fuel-rod transport calculation with no control rod material present. The control rod super cell, shown in Fig. 3.7 consists of one control rod unit cell and four adjacent fuel cells. The fuel cells were homogenized at the outermost region of the super cell. To account for buckling, the height of both unit cells was chosen to be the core height. The radial reflector configuration shown in Fig. 3.8 extended out to the shield tank water in order to obtain cross sections for the radial reflectors, the reactor vessel, the stainless steel shields, the shield tank wall, the aluminum neutron window and the shield tank water. The number densities for all the compositions used in this model are given in Table 3.4. Cross sections for the fuel rod unit cell were generated for 0%, 20%, 40%, 60%, 80%, and 100% homogeneous void fraction. Cross sections for the control rod super cell were calculated for 0%, 50%, and 100% voiding.

The conventional few-group cross section generation procedure was used to create the five-group cross section library. The procedure is given in Fig. 3.9. The collapsing of the 123-neutron-group library was performed with the AMPX one-dimensional transport code XSDRNPM.[26] After the unit cell, the super cell and the reflector calculations

TABLE 3.3

LOFT Five Group Cross Section Energy Structure

Group	Upper Energy Bound (MEV)	Fission Spectrum
1	1.4918×10^{1}	0.68976
2	1.0026	0.31024
3	1.1706×10^{-2}	0.0
4	1.0130×10^{-4}	0.0
5	6.5000×10^{-7}	0.0

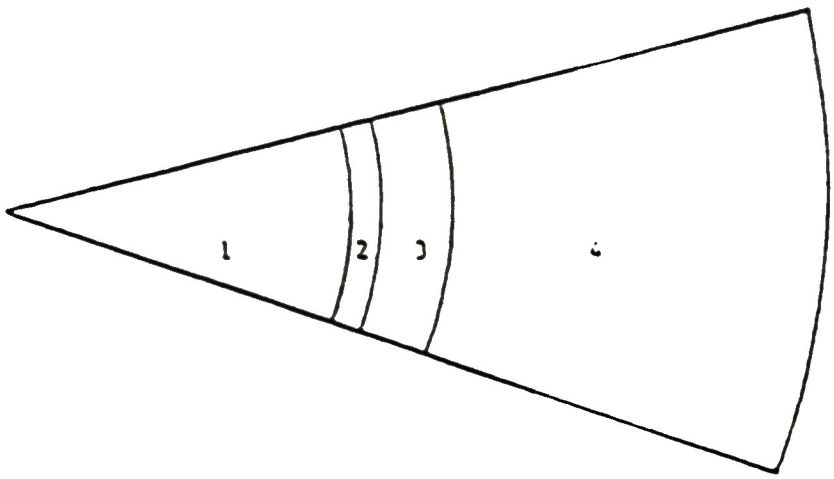

Region	Upper Radius (cm)	Material
1	0.46469	Uranium Dioxide
2	0.47428	Air Gap
3	0.53594	Zircaloy Cladding
4	0.80680	Borated Water

Figure 3.6. 1-D model for LOFT fuel unit cell.

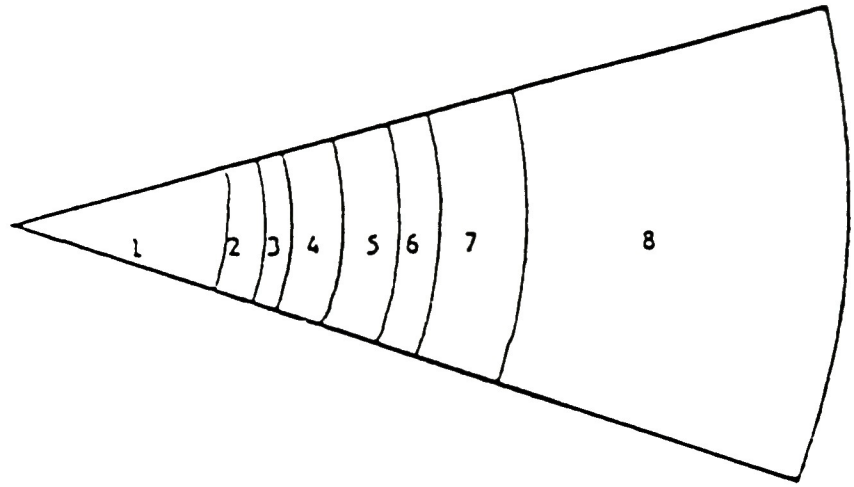

Region	Upper Radius (cm)	Material
1	0.45000	In-Cd-Ag Alloy
2	0.50546	In-Cd-Ag Alloy
3	0.51054	Air Gap
4	0.55880	S.S. 316
5	0.64896	Water
6	0.69219	S.S 316
7	0.80680	Water
8	1.80000	Homogenized Fuel

Figure 3.7. 1-D model for LOFT control rod super cell.

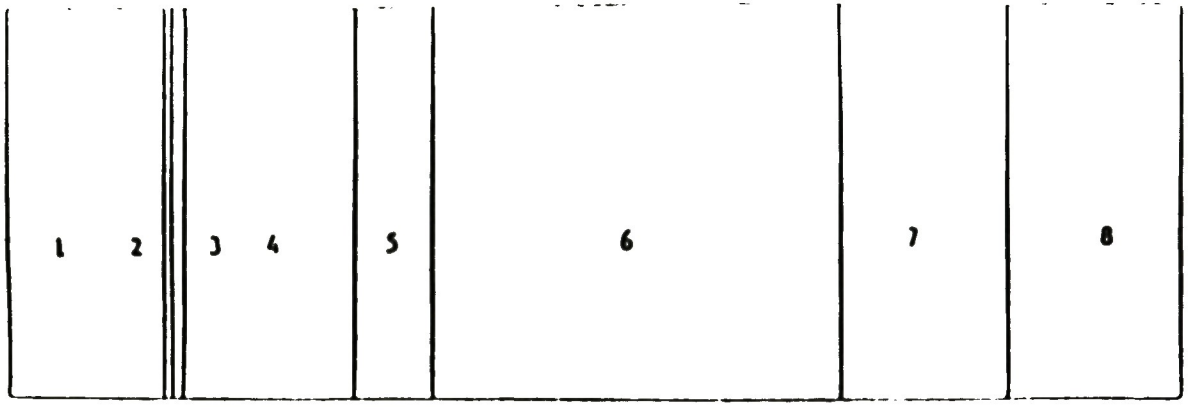

Region	Upper Radius (cm)	Material
1	10.000	Homogenized Fuel
2	10.100	Inconel-718
3	10.600	Homogenized Fuel
4	21.700	95% S.S 304 & 5% Water
5	26.797	Downcomer Water
6	52.446	Vessel Filler
7	64.500	Al Neutron Window
8	74.500	Shield Tank Water

Figure 3.8. 1-D model for LOFT radial reflector.

TABLE 3.4

LOFT Reactor Element Number Density

Zone	Element	Number Density (atom/barn-cm)
Fuel rod	H	2.55052E-02
	O	2.62132E-02
	B-10	9.46088E-07
	B-11	3.83670E-06
	Zr	3.70424E-03
	U-235	2.71168E-04
	U-238	6.45917E-03
Control rod	H	1.18430E-03
	O	5.92172E-04
	B-10	4.39320E-08
	B-11	1.78163E-07
	Mn	2.75850E-05
	Ni	1.06488E-04
	Fe	7.72415E-04
	Cr	2.28364E-04
	Ag	8.88704E-04
	In	1.69834E-04
	Cd	5.33106E-05
Downcomer water	H	5.01480E-02
	O	2.50740E-02
	B-10	1.86019E-06
	B-11	7.54369E-06
Core barrel	Mn	1.75400E-03
	Ni	8.20700E-03
	Fe	5.95300E-02
	Cr	1.76600E-02
Vessel	Fe	8.47500E-02
Shield tank water	H	6.68640E-02
	O	3.34320E-02
Window	Al	6.02420E-02

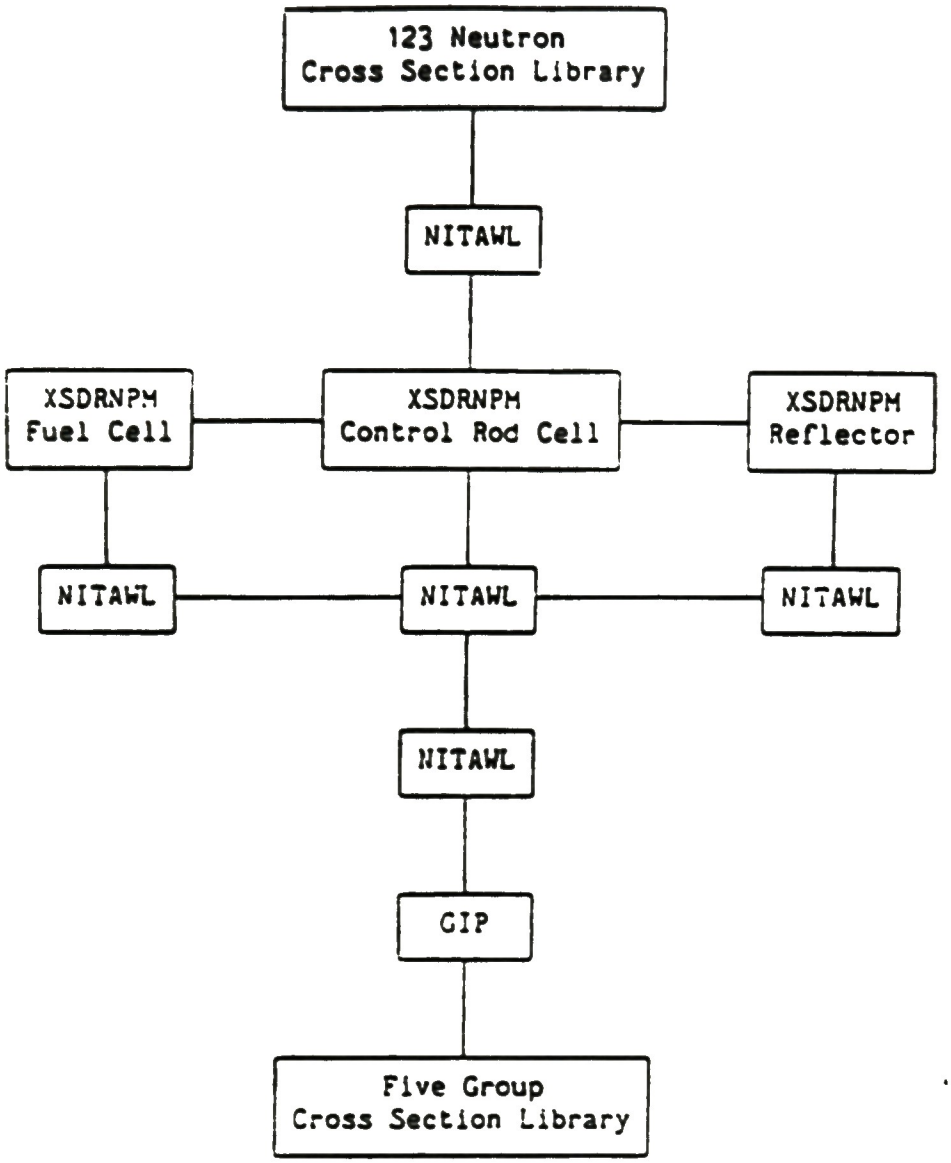

Figure 3.9. Five group cross section library preparation procedure for the LOFT neutronics analysis.

were made for each void fraction, the individual few-group cross section sets were combined two at a time using the code NITAWL to create a five-group microscopic cross section library. The code GIP[29] was then used to produce a five-group macroscopic cross section library in DOT library format (binary format).

3.3 TMI-2 Reactor Model and Cross Section Generation

3.3.1 Reactor Model

The configuration of the TMI-2 core is shown schematically in Fig. 3.10. The core, along with its pressure vessel and concrete biological shield was simplified to a form which could be handled by the DOT code. The reactor model of TMI-2, shown in Fig. 3.11, was based on the model reported in NSAC-28.[3] The core is separated into two radial regions. It is modeled in this way because there existed an approximately one-fuel-assembly thick band of undamaged, normal fuel around the core at its outer periphery. The presence of this fuel was determined by video and sonar readings taken of the damaged core.[10] Axial divisions in the core region are sized and spaced to provide more detail in regions of major core slumping and lowest core water level.

The spacer region is a homogenized representation of the core liner and the water between the liner and the barrel. This region is treated as part of the core, i.e., the void profile in this region is the same as that in the core region during the boil-off. The downcomer region consists of the core barrel, water gap, thermal shield and downcomer.

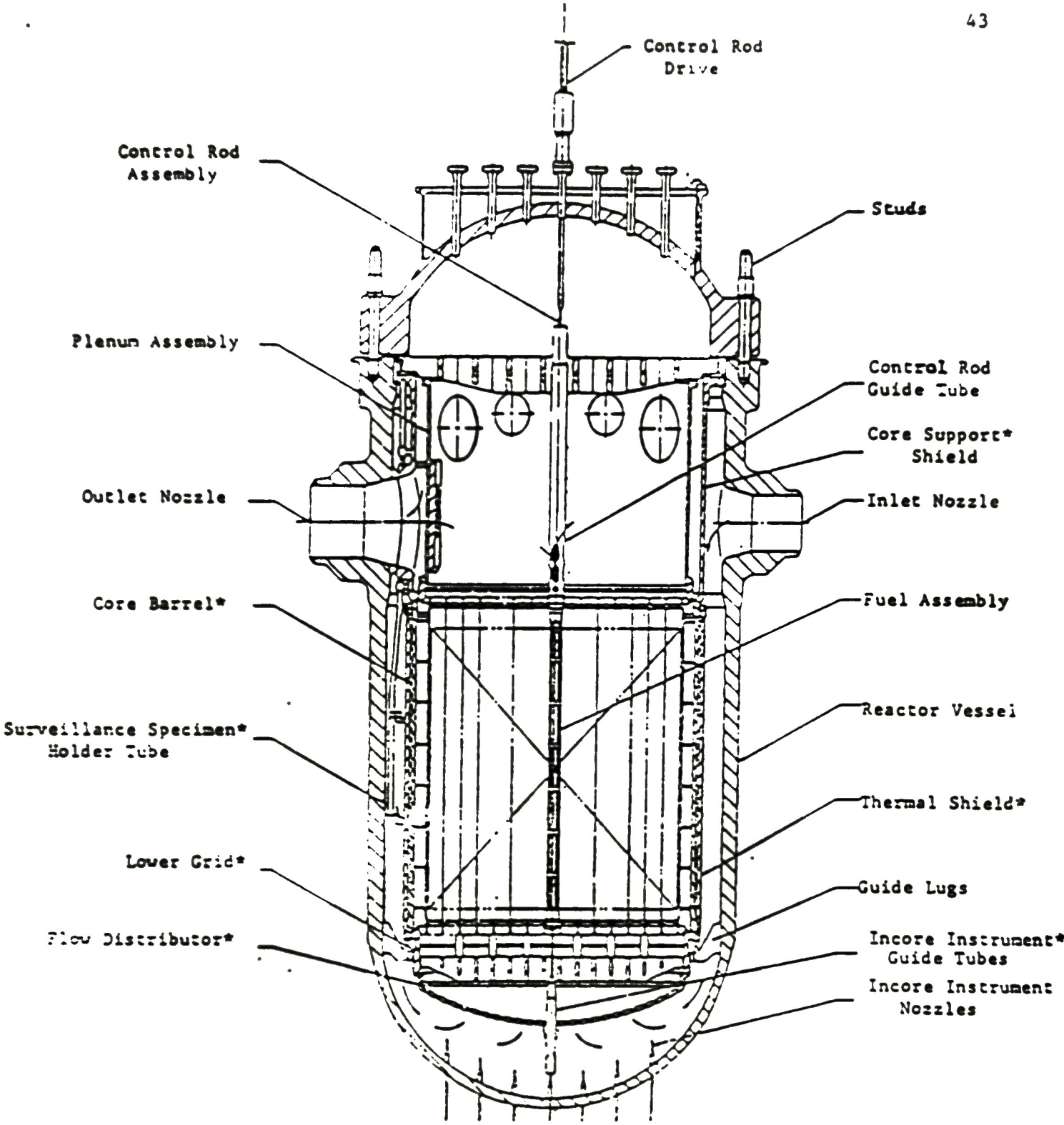

Figure 3.10. TMI-2 reactor vessel assembly.

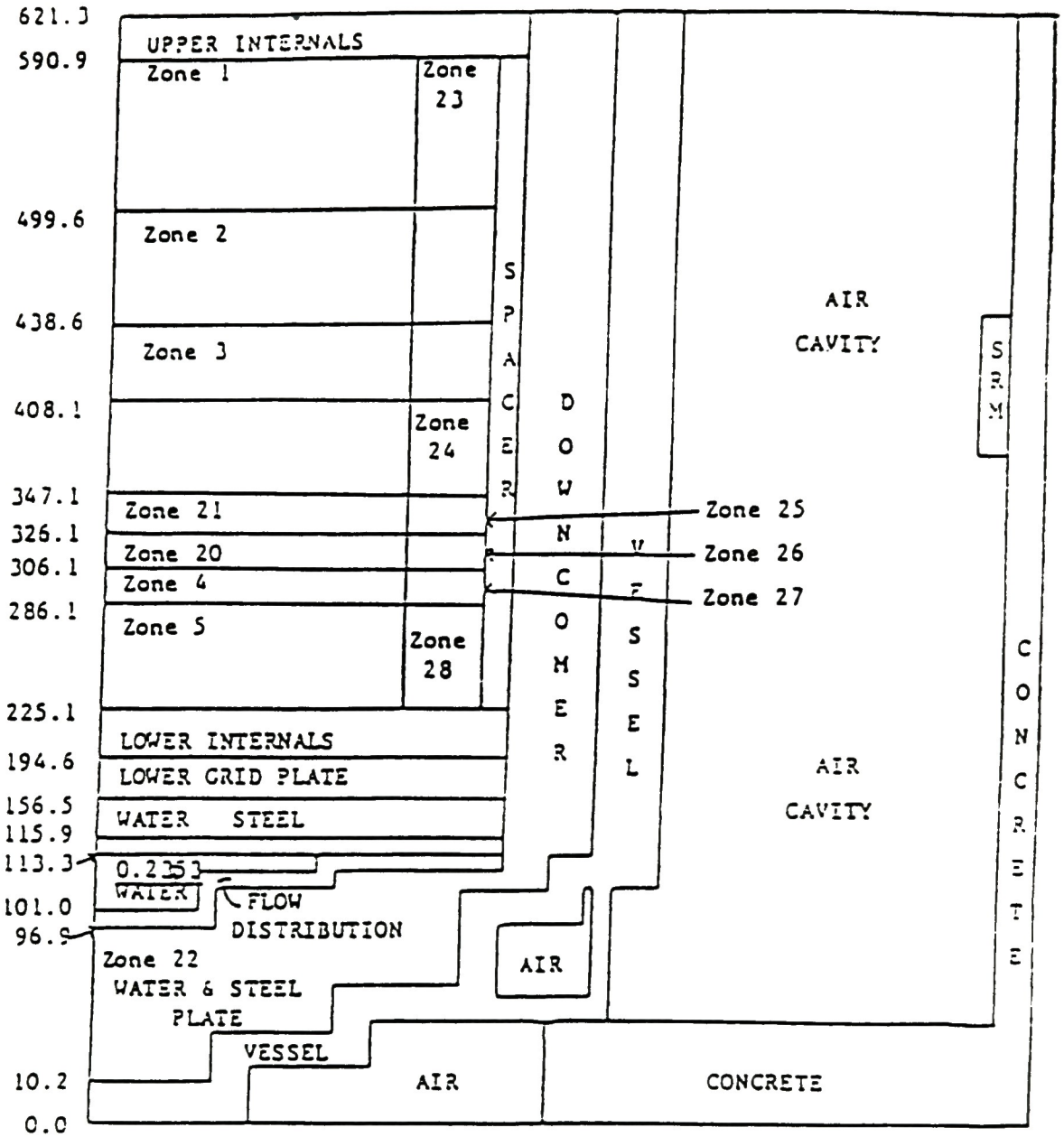

Figure 3.11. TMI-2 reactor R-Z model for DOT calculation. (Dimensions in cm)

The lower head portion of the model was not included in the original NSAC-28 model because the final status of the core was not completely known at that time. Video scans and sonar readings[10-12] have subsequently shown that the core was severely damaged and significant amounts of core material relocated to the lower head. The air gap near the lower head provides the neutron streaming path for the neutrons in the lower head to reach the detector. Analysis has shown that the fuel in the lower head provides the dominant neutron source to the ex-core detector response for the damaged core.[19,30] Hence, it is necessary to model the lower head portion to understand the SRM response during the accident. Table 3.5 gives the detailed axial and radial mesh into which the TMI-2 was divided. The model uses 24336 mesh cells, a number found to be sufficient to avoid inaccuracies or negative fluxes in the discrete ordinates "diamond difference" model.

Boundary conditions used were vacuum on top, bottom and right side of the model and reflected on the left boundary.

3.3.2 Cross Section Preparation

The DOT code calculations for the TMI-2 accident analysis were made using a five-group cross section set. The five-group energy structure, shown in Table 3.6 was used by Argonne National Laboratory for their TMI-2 neutronics study.[9] The intact core element number densities are given in Table 3.7. These number densities include control material and a soluble boron concentration of 1260 ppmB.

Table 3.5A TMI-2 Radial Mesh Distribution

1	0.0	2	2.730	3	5.460	4	8.190	5	1.092E+1
6	1.365E+1	7	1.638E+1	8	1.911E+1	9	2.184E+1	10	2.457E+1
11	2.730E+1	12	3.003E+1	13	3.276E+1	14	3.549E+1	15	3.822E+1
16	4.095E+1	17	4.368E+1	18	4.641E+1	19	4.914E+1	20	5.187E+1
21	5.460E+1	22	5.714E+1	23	5.968E+1	24	6.222E+1	25	6.476E+1
26	6.730E+1	27	7.009E+1	28	7.288E+1	29	7.567E+1	30	7.847E+1
31	8.126E+1	32	8.405E+1	33	8.684E+1	34	8.964E+1	35	9.243E+1
36	9.522E+1	37	9.801E+1	38	1.008E+2	39	1.036E+2	40	1.063E+2
41	1.091E+2	42	1.117E+2	43	1.142E+2	44	1.167E+2	45	1.192E+2
46	1.218E+2	47	1.246E+2	48	1.274E+2	49	1.302E+2	50	1.330E+2
51	1.358E+2	52	1.386E+2	53	1.414E+2	54	1.441E+2	55	1.469E+2
56	1.497E+2	57	1.525E+2	58	1.533E+2	59	1.581E+2	60	1.609E+2
61	1.637E+2	62	1.668E+2	63	1.699E+2	64	1.729E+2	65	1.760E+2
66	1.790E+2	67	1.817E+2	68	1.845E+2	69	1.872E+2	70	1.899E+2
71	1.926E+2	72	1.953E+2	73	1.981E+2	74	2.012E+2	75	2.044E+2
76	2.076E+2	77	2.108E+2	78	2.139E+2	79	2.171E+2	80	2.197E+2
81	2.222E+2	82	2.255E+2	83	2.287E+2	84	2.391E+2	85	2.352E+2
86	2.384E+2	87	2.435E+2	88	2.486E+2	89	2.537E+2	90	2.588E+2
91	2.639E+2	92	2.690E+2	93	2.741E+2	94	2.791E+2	95	2.842E+2
96	2.893E+2	97	2.944E+2	98	2.995E+2	99	3.046E+2	100	3.097E+2
101	3.148E+2	102	3.199E+2	103	3.250E+2	104	3.301E+2	105	3.352E+2
106	3.403E+2	107	3.454E+2	108	3.505E+2	109	3.534E+2	110	3.564E+2
111	3.593E+2	112	3.623E+2	113	3.652E+2	114	3.682E+2	115	3.711E+2
116	3.741E+2	117	3.770E+2	118	3.800E+2				

Table 3.5B TMI-2 Axial Mesh Distribution

1	0.0	2	3.386	3	6.773	4	1.016E-1	5	1.317E-1
6	1.618E-1	7	1.920E-1	8	2.237E-1	9	2.555E-1	10	2.872E-1
11	3.190E-1	12	3.487E-1	13	3.784E-1	14	4.082E-1	15	4.463E-1
16	4.844E-1	17	5.350E-1	18	5.656E-1	19	5.963E-1	20	6.270E-1
21	6.577E-1	22	6.884E-1	23	7.191E-1	24	7.498E-1	25	7.805E-1
26	8.111E-1	27	8.418E-1	28	8.736E-1	29	9.053E-1	30	9.371E-1
31	9.686E-1	32	9.942E-1	33	1.019E-2	34	1.031E-2	35	1.057E-2
36	1.082E-2	37	1.108E-2	38	1.133E-2	39	1.158E-2	40	1.187E-2
41	1.216E-2	42	1.245E-2	43	1.274E-2	44	1.304E-2	45	1.333E-2
46	1.362E-2	47	1.391E-2	48	1.420E-2	49	1.449E-2	50	1.478E-2
51	1.507E-2	52	1.536E-2	53	1.565E-2	54	1.594E-2	55	1.623E-2
56	1.653E-2	57	1.682E-2	58	1.711E-2	59	1.741E-2	60	1.770E-2
61	1.799E-2	62	1.829E-2	63	1.858E-2	64	1.887E-2	65	1.916E-2
66	1.946E-2	67	1.976E-2	68	2.007E-2	69	2.037E-2	70	2.068E-2
71	2.098E-2	72	2.129E-2	73	2.159E-2	74	2.190E-2	75	2.220E-2
76	2.251E-2	77	2.281E-2	78	2.312E-2	79	2.342E-2	80	2.373E-2
81	2.403E-2	82	2.434E-2	83	2.464E-2	84	2.495E-2	85	2.525E-2
86	2.556E-2	87	2.586E-2	88	2.617E-2	89	2.647E-2	90	2.678E-2
91	2.708E-2	92	2.739E-2	93	2.769E-2	94	2.800E-2	95	2.830E-2
96	2.861E-2	97	2.889E-2	98	2.918E-2	99	2.946E-2	100	2.975E-2
101	3.003E-2	102	3.032E-2	103	3.061E-2	104	3.089E-2	105	3.117E-2
106	3.146E-2	107	3.175E-2	108	3.203E-2	109	3.232E-2	110	3.261E-2
111	3.291E-2	112	3.321E-2	113	3.351E-2	114	3.381E-2	115	3.411E-2
116	3.441E-2	117	3.471E-2	118	3.501E-2	119	3.532E-2	120	3.562E-2
121	3.593E-2	122	3.623E-2	123	3.654E-2	124	3.684E-2	125	3.715E-2
126	3.745E-2	127	3.776E-2	128	3.806E-2	129	3.837E-2	130	3.867E-2
131	3.898E-2	132	3.928E-2	133	3.959E-2	134	3.989E-2	135	4.020E-2
136	4.050E-2	137	4.081E-2	138	4.111E-2	139	4.142E-2	140	4.172E-2
141	4.202E-2	142	4.233E-2	143	4.263E-2	144	4.294E-2	145	4.324E-2
146	4.355E-2	147	4.385E-2	148	4.416E-2	149	4.446E-2	150	4.477E-2
151	4.507E-2	152	4.538E-2	153	4.568E-2	154	4.599E-2	155	4.629E-2
156	4.660E-2	157	4.690E-2	158	4.721E-2	159	4.751E-2	160	4.782E-2
161	4.812E-2	162	4.843E-2	163	4.873E-2	164	4.904E-2	165	4.934E-2
166	4.965E-2	167	4.995E-2	168	5.014E-2	169	5.033E-2	170	5.081E-2

Table 3.5B (continued)

171	5.109E+2	172	5.138E+2	173	5.167E+2	174	5.195E+2	175	5.224E+2
176	5.252E+2	177	5.281E+2	178	5.309E+2	179	5.338E+2	180	5.366E+2
181	5.395E+2	182	5.423E+2	183	5.452E+2	184	5.480E+2	185	5.509E+2
186	5.537E+2	187	5.566E+2	188	5.594E+2	189	5.623E+2	190	5.651E+2
191	5.680E+2	192	5.708E+2	193	5.737E+2	194	5.766E+2	195	5.794E+2
196	5.823E+2	197	5.851E+2	198	5.880E+2	199	5.908E+2	200	5.939E+2
201	5.969E+2	202	6.000E+2	203	6.030E+2	204	6.061E+2	205	6.091E+2
206	6.122E+2	207	6.152E+2	208	6.182E+2	209	6.213E+2		

TABLE 3.6

TMI Five Group Cross Section Energy Structure[9]

Group	Upper Energy Bound (Mev)	Fission Spectrum
1	1.0000×10^{1}	0.760544
2	8.2085×10^{-1}	0.239295
3	5.5308×10^{-3}	1.80408×10^{-4}
4	1.8554×10^{-6}	0.0
5	6.2493×10^{-7}	0.0

TABLE 3.7

TMI-2 Reactor Element Number Densities

Zone	Element	Number Density (atom/barn-cm)
Upper internals	H	4.6684E-02
	O	2.3328E-02
	Si	1.1139E-04
	Cr	1.9820E-03
	Mn	1.7227E-04
	Fe	6.6202E-03
	Ni	9.7004E-04
	B-10	9.8641E-06
Core	H	3.1296E-02
	O	1.2952E-02
	Zr	4.1537E-03
	U-235	1.6902E-04
	U-238	6.3069E-03
	Cd	2.0069E-05
	In	4.9802E-05
	Ag	4.0576E-04
	B	1.2760E-05
Lower internals	H	4.2330E-02
	O	2.1143E-02
	Si	1.7520E-04
	Cr	3.4250E-03
	Mn	2.9856E-04
	Fe	1.1440E-02
	Ni	1.6763E-03
	B	8.9400E-05
Spacer	H	3.7138E-02
	O	1.8534E-02
	Si	2.6334E-04
	Cr	5.1749E-03
	Mn	4.4875E-04
	Fe	1.7195E-02
	Ni	2.5195E-03
	B	7.8364E-06
Downcomer	H	3.9595E-02
	O	1.9766E-02
	Si	2.2172E-04
	Mn	4.3342E-03
	Fe	3.7783E-04
	Ni	1.4477E-02
	B	8.3600E-02
Vessel	Mo	2.7137E-04
	Si	4.2641E-04
	Cr	1.2746E-04
	Mn	1.1201E-03
	Ni	8.1979E-02

Zone	Element	Number Density (atom/barn-cm)
Air	N	7.3462E-05
	O	2.9378E-05
Lead	Pb	3.2960E-02
Poly	H	5.6350E-03
	C	2.7880E-03
Concrete	Al	1.7410E-03
	Mg	1.2386E-04
	Fe	3.4509E-04
	Ca	1.5026E-04
	H	8.6039E-02
	O	4.3289E-02
	C	1.1534E-04
	K	4.6052E-04
	Na	9.6403E-04
Lower grid plate	H	2.3910E-02
	O	1.1127E-02
	Si	5.1353E-04
	Cr	1.0552E-02
	Mn	8.7253E-04
	Fe	3.3531E-02
	Ni	4.9132E-03
	B	4.7048E-06
Lower grid distribution plate	H	2.0040E-02
	O	9.9448E-03
	Si	5.5347E-04
	Cr	1.0819E-02
	Mn	9.4038E-04
	Fe	3.6138E-02
	Ni	5.2952E-03
	B	4.2161E-06
Lower flow distribution plate	H	2.5479E-02
	O	1.2678E-02
	Si	4.6115E-04
	Cr	9.0146E-03
	Mn	7.8353E-04
	Fe	3.0110E-02
	Ni	4.4120E-03
	B	5.3605E-06
Lower plenum	H	5.0437E-02
	O	2.5214E-02
	Si	3.7710E-05
	Cr	7.3717E-04
	Mn	6.4072E-05
	Fe	2.4623E-03
	Ni	3.6079E-04
	B	1.0661E-05

The cross sections were generated from the VITAMIN-E[31] 174-group neutron cross section library and collapsed by using the codes in the AMPX system. The original 174-group library was in AMPX master library format. This library has separate resonance information for several elements, including Uranium-238. The code BONAMI[26] was used to make a Bondarenko resonance self-shielding calculation to combine the resonance and non-resonance data. In these resonance self-shielding calculations, the damaged fuel was modelled as a sphere whose radius is the same as that of an intact pellet. This fuel was in turn surrounded by shells of cladding and coolant such that the fuel occupies 63% of the total cell volume.

The five-group cross section preparation procedure for TMI-2 neutronics analysis is slightly different from that of the LOFT analysis. The procedure is shown in Fig. 3.12. The code BONAMI was used to make resonance calculations because the VITAMIN-E cross section library can only be handled by the BONAMI code. Unit cell calculations were performed to homogenize the materials in the unit cell with void fractions of 0%, 20%, 40%, 60%, 80%, and 100%. No group collapsing was performed during the cell calculations. Cell weighting was used in the cell calculations to generate cross sections consistent with the mockup of a cell configuration as a homogenized region. One-dimensional radial full reactor model calculations were performed by XSDRNPM[26] code to collapse the 174-group cross section library to a five-group cross section set with void fractions of 0%, 20%, 40%, 60%, 80%, and 100%.

To justify the adequacy of the cross section preparation used in this work, a series of calculations were carried out using the

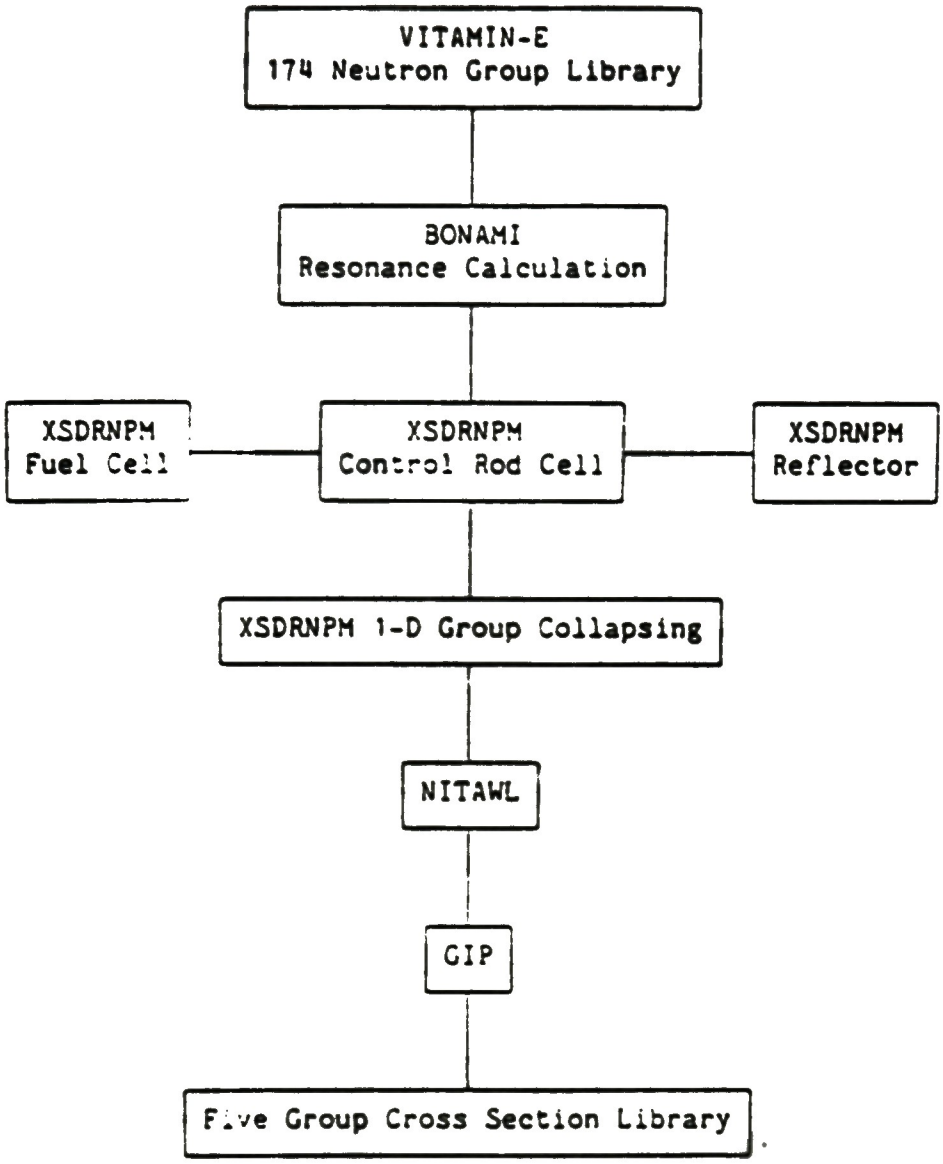

Figure 3.12. Five group cross section library preparation procedure for the TMI-2 neutronics analysis.

one-dimensional ANISN code.[32] All calculations were performed using an S_8-quadrature set with P_3 scattering. The calculated results showed that the total flux at the detector location increased by a factor of 122 with void fraction of 100% in the vessel using the 174-group cross section library. There was an increase by a factor of 140 using the five-group cross section library. These results satisfactorily benchmarked the mesh and group structure, thus indicating that the five-group cross section sets were adequate for this analysis but provide an uncertainty of about 15% in the flux. A detailed analysis of this uncertainty as well as that originating from other factors is included in Section 4.

3.4 LOFT Experiment LP-SB-2

In the above, we have described how the source term was calculated, how the DOT models were constructed, and how the neutron cross sections were prepared. Having done these, we can now calculate the SRM response. To justify the adequacy of the method, we first applied it to LOFT experiments LP-SB-2 and LP-SB-3. A series of computer simulations were conducted and the LOFT SRM response calculated. This calculated response was compared with the observed detector response in these experiments. Sensitivity studies on these simulations were also performed in order to understand the general behavior of the detector response. The resulting agreement between the calculated response and the measured response showed that the method described above was adequate for the SRM analysis.

The LOFT experiment LP-SB-2 was a small-break LOCA experiment. It simulated a three-inch-diameter pipe break in the primary system hot leg.[33] In this experiment the primary coolant pumps were kept operating. This resulted in a homogenized and uniform distribution of the coolant for the first 1050 seconds. After that point, flow degradation set in and forced circulation ceased at about 1300 seconds. Therefore, to evaluate the response of the detectors, particularly the source range monitor, a simulation of such conditions was performed using the method outlined previously for various void fractions. The results of these calculations are given in Table 3.8, where A, B, C and D are the detectors of Penn State Non-Invasive Liquid Level/Density Gauge System, and SRM is the source range monitor. The locations of these detectors are shown in Fig. 3.5. This table was constructed using both the startup source and the photoneutron source detailed earlier. Figure 3.13 is a plot of the data for the SRM response based on Table 3.8.

To account for the effect of density changes on the photoneutron source, the effective source S_{eff} was expressed as

$$S_{eff} = (1 - \alpha)S_{\gamma n} + S_s,$$

where $S_{\gamma n}$ is the photoneutron source for a non-voided core, α the void fraction, and S_s the startup source. The term $(1-\alpha)$ is included in the photoneutron source to account for the reduction of coolant density through core voiding. It should be noted that this expression neglects the photoneutron source in the steam. Sensitivity analysis showed this to be negligible even in a highly voided core.

TABLE 3.8

Effect of LOFT Homogeneous Voiding on Detector Response*

Void Fraction	Normalized Detector Response*				
	A	B	SRM	C	D
0%	1.0	1.0	1.0	1.0	1.0
20%	2.19	2.91	2.21	2.21	2.20
40%	3.46	4.48	3.42	3.41	3.41
60%	4.45	5.64	4.29	4.26	4.30
80%	4.72	6.03	4.81	4.57	4.61
100%	4.84	6.24	5.04	4.83	4.76

* Detectors A, B, C, and D are part of The Penn State Non-Invasive Level Gauge. The source range monitor (SRM) is part of the normal LOFT nuclear instrumentation.

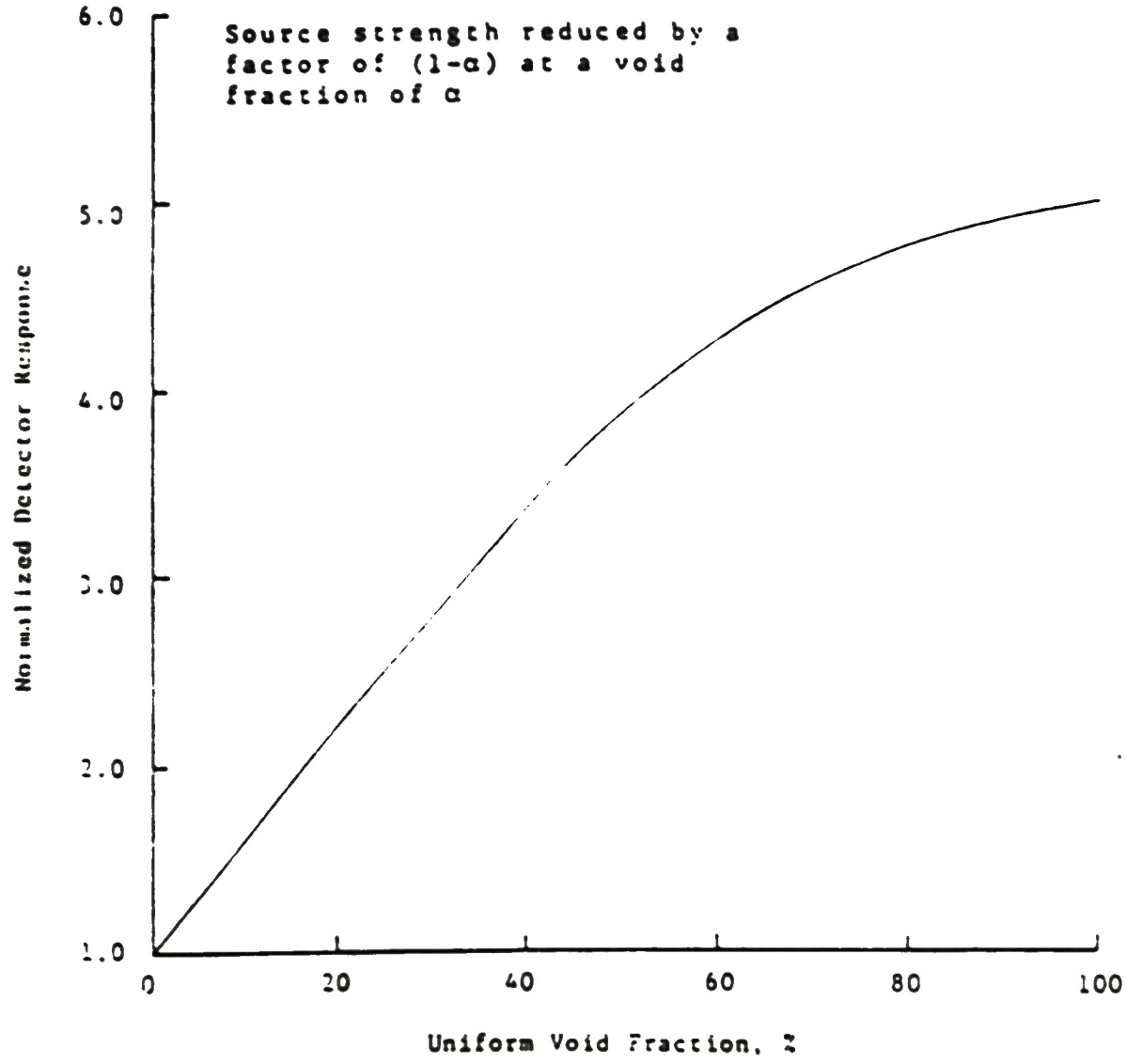

Figure 3.13. Calculated normalized response of installed LOFT SRM versus homogeneous void fraction.

Figure 3.14 shows the response of the installed LOFT SRM during the experiment LP-SB-2. The experiment began with a reactor scram at 500 sec. The SRM response started to deviate from the normal shutdown curve at about 900 seconds and reached a maximum deviation at about 1500 seconds. The ratio of the observed count rate to the normal shutdown curve at this time is about a factor of 2.7. According to the results of the neutronics analysis shown in Fig. 3.13, the core void fraction at this point is estimated to be approximately 30%. Cold-leg densitometer readings reported in Reference 33 yield a void fraction of 33%, in good agreement with the neutronics analysis. A comparison of cold-leg void fraction obtained from the densitometer readings and those obtained from the neutronics analysis from 900 to 1500 seconds is shown in Fig. 3.15. Again, the agreement between the measured data and that obtained from the neutronics analysis is good.

In summary, the results of the analysis of the LP-SB-2 experiment show that the variation in neutron level can be used to obtain information on void fraction in the core during the forced circulation phase of a small-break LOCA.

3.5 LOFT Experiment LP-SB-3

Experiment LP-SB-3 was conducted to simulate a cold-leg small-break LOCA, with a scaled break size corresponding to a 1.84-inch pipe diameter in a reference commercial pressurized water reactor.[33,34] The experiment was specially designed to achieve conditions that would allow an assessment of the phenomena associated with slow coolant boil-off leading to an uncovered core at high system

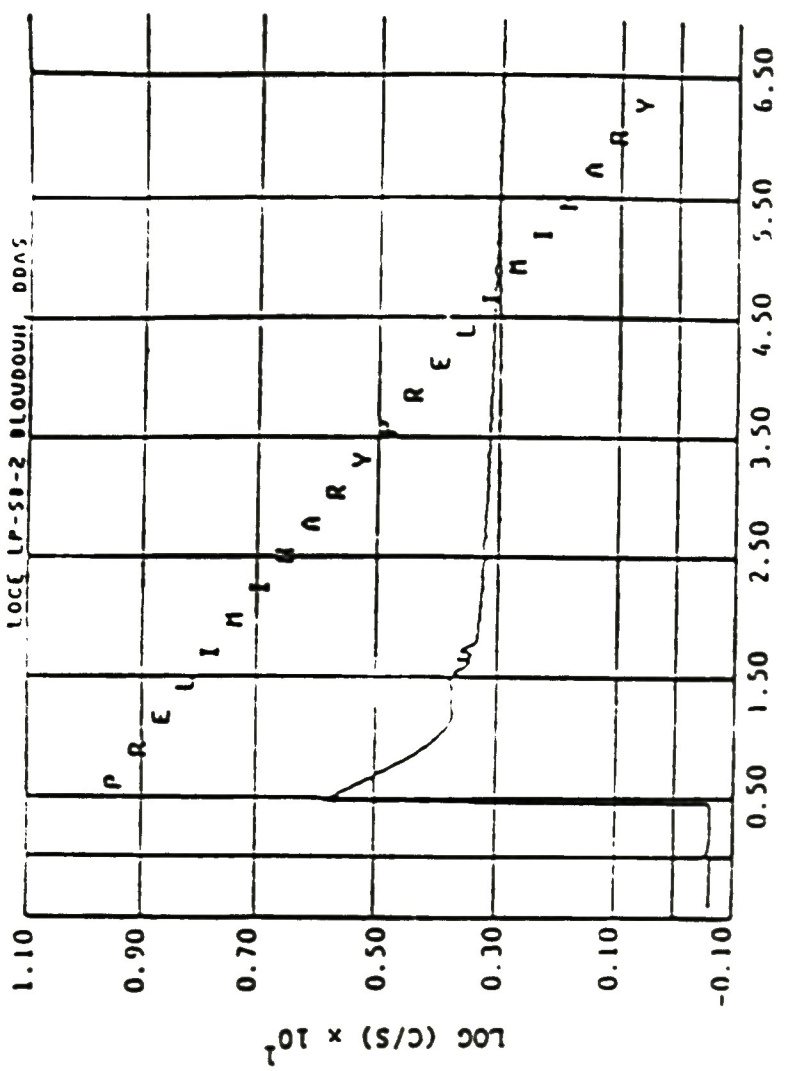

Figure 3.14. Source range monitor response during experiment LP-SB-2.

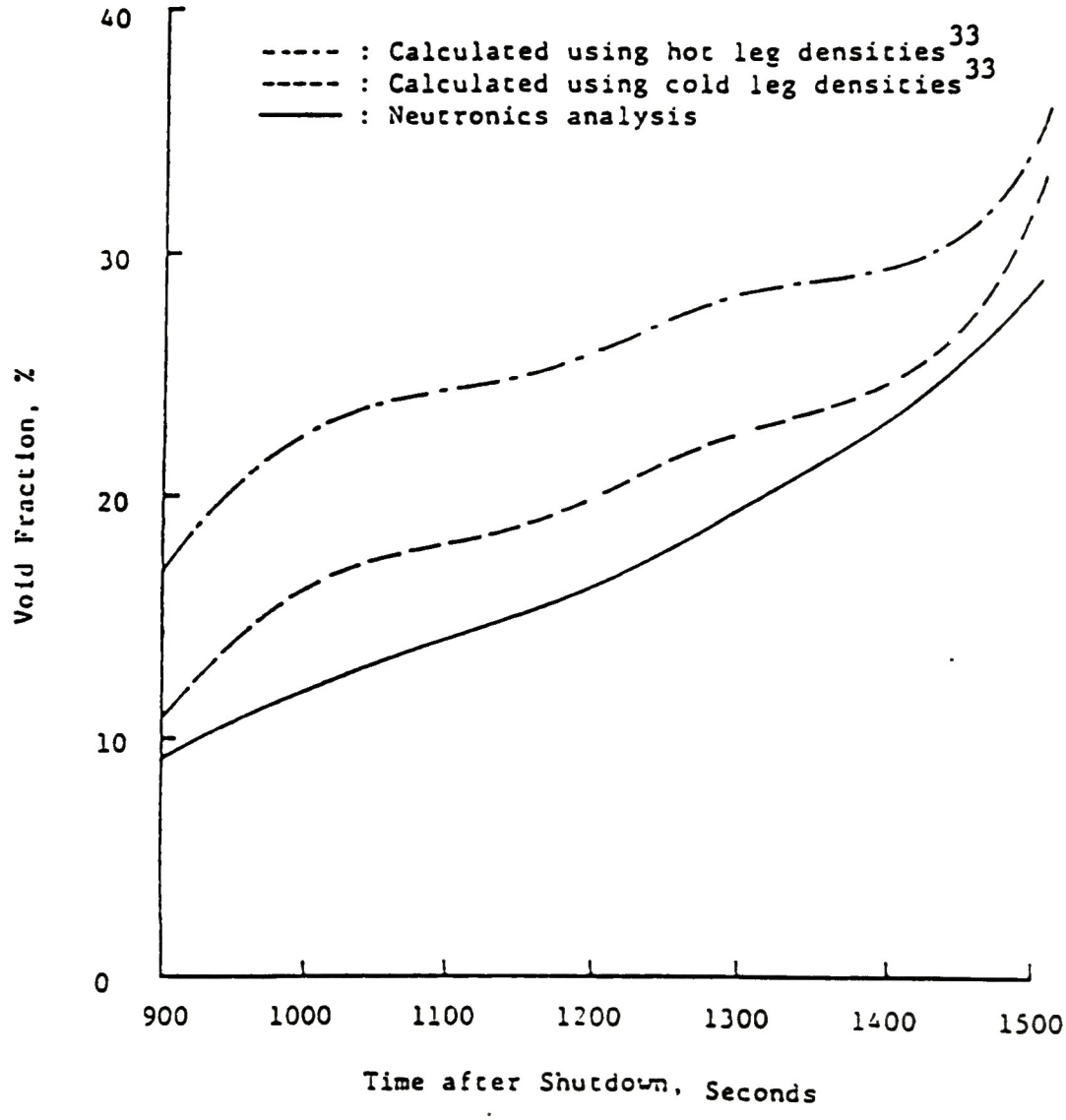

Figure 3.15. Comparison of calculated cold leg void fraction from gamma densitometer with that obtained from neutronic analysis of LP-SB-2.

pressures and the usefulness of steam generator feed-and-bleed as a means of plant recovery from degraded-core cooling conditions.

Figure 3.16 gives the actual SRM response during the experiment. As shown in the figure, the SRM response started to deviate from the normal shutdown curve at about 1100 seconds. The steady increase in the count rate indicated an increase in void fraction in the vessel during operation of the primary coolant pump. The cold-leg densities measured in the experiment also indicated that the homogenized two-phase mixture was pumped by the operating primary coolant pumps throughout the system until the pumps were tripped at 1600 seconds. The sharp decrease in the SRM response at 1600 seconds was due to the shutoff of the primary coolant pumps resulting in phase separation with the voids rising to the upper region of the vessel. The core and downcomer regions were filled with liquid resulting in a shielding effect on the ex-core detector. This effect was also observed in the responses of the other detectors (A, B, C and D).

As pointed out earlier, the SRM response deviated at around 1000 seconds from the normal shutdown curve. The deviation continued until 1600 seconds when the pumps were tripped. Fig. 3.17 compares the calculated void fraction obtained from the SRM data with that calculated from cold-leg densitometer readings reported in Reference 34. The resulting void fraction obtained from the neutronics analysis agrees well with that obtained from the cold-leg densitometer measurements.

At 3650 seconds, the SRM response again deviated from the normal shutdown response. The deviation was due to boil-off of the coolant causing the liquid level to decrease in both the core and downcomer

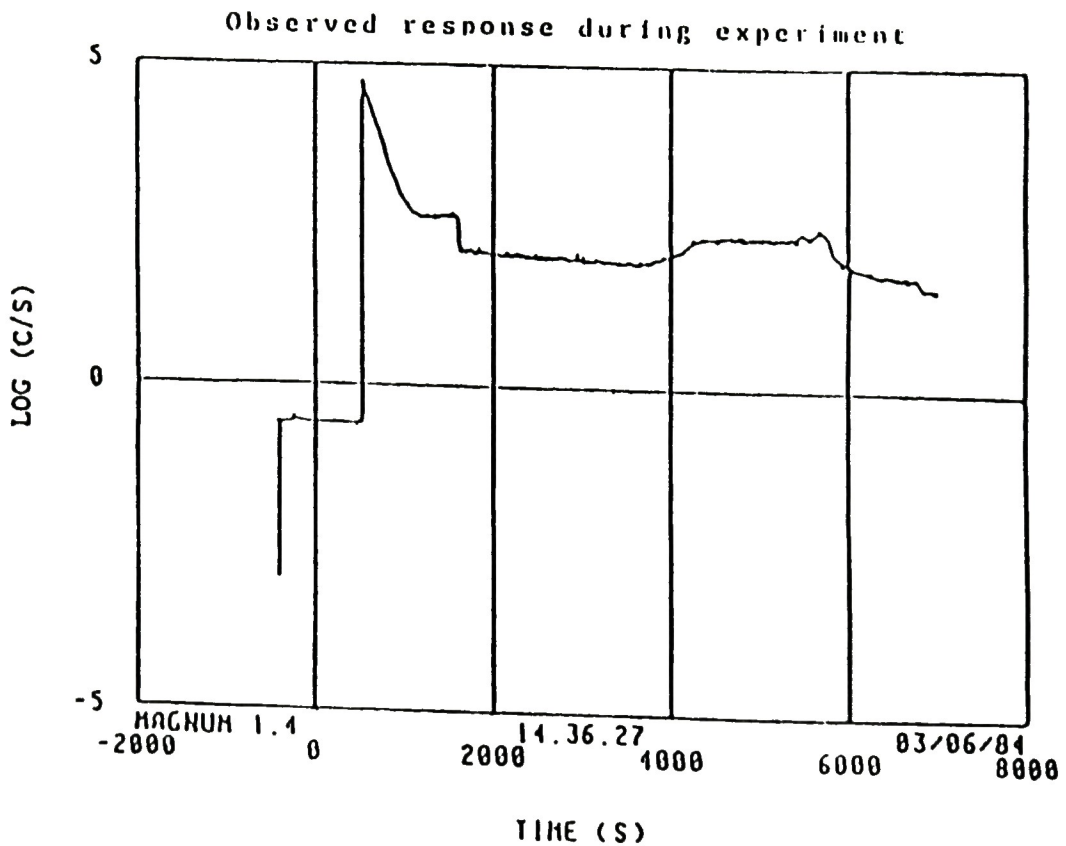

Figure 3.16. Source range monitor response during experiment LP-SB-3.

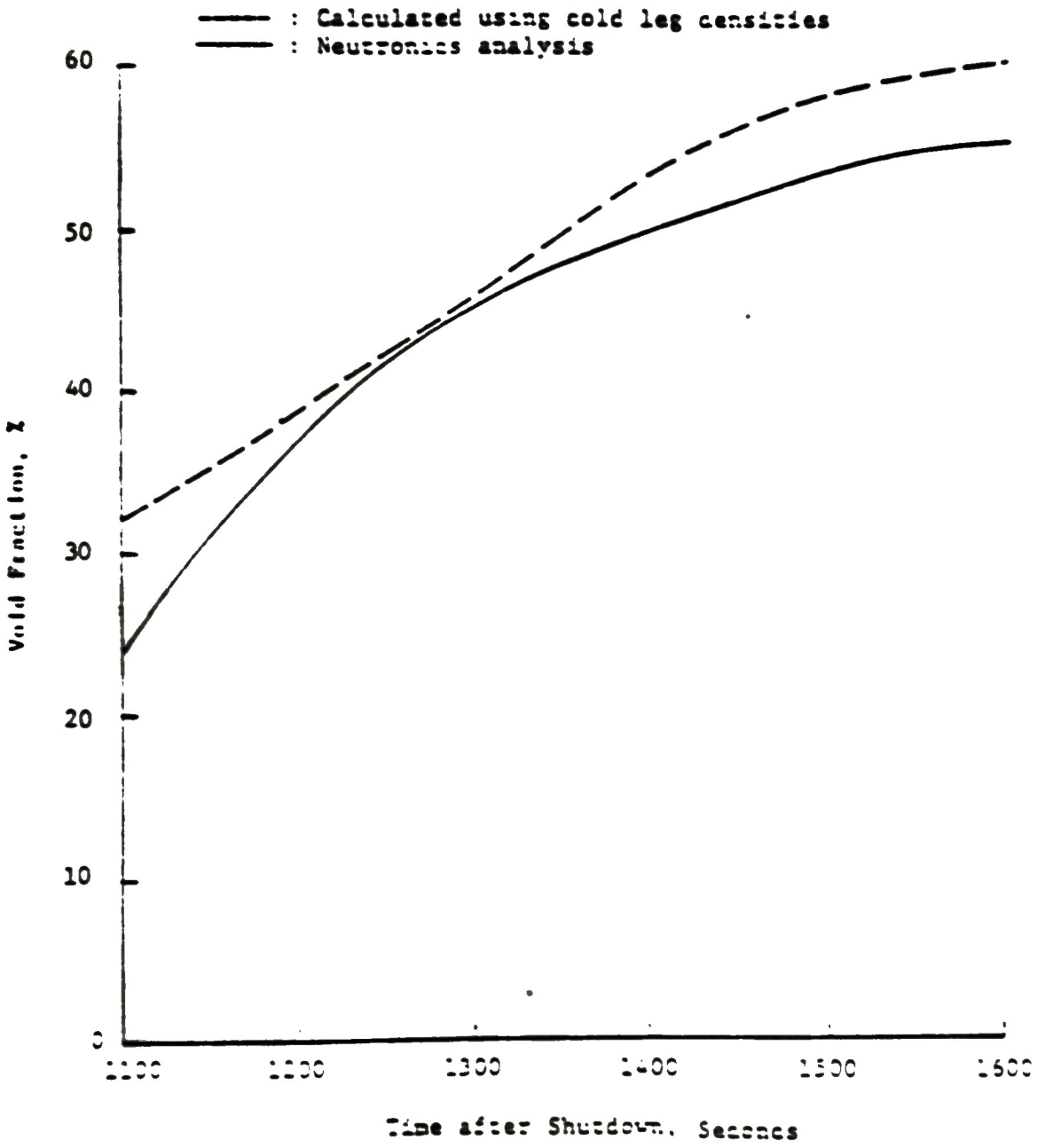

Figure 3.17. Comparison of calculated cold leg densities obtained from gamma densitometer with that obtained from neutronic analysis of LP-SB-3.

regions. The level above the bottom of the core during LP-SB-3 was estimated using the neutronic analysis during the coolant boil off period from 3600 seconds to 5400 seconds using LOFT SRM response. The neutronic analysis showed that the SRM response increases as water level decreases. Fig. 3.18 shows the relationship between normalized SRM response and downcomer water level. Here the downcomer is assumed to be in hydraulic equilibrium with the core, thus, the core mixture level is greater than the downcomer level due to the steam voids generated in the core.

The data shown in Fig. 3.14 was used to estimate the core water level above the bottom of the core during LP-SB-3 was estimated. Fig. 3.19 shows the water level obtained from the neutronics analysis and compares it with that estimated from the bubble plot data and thermocouple data. Excellent agreement was obtained with the thermocouple data. The comparison with the bubble plot data is also good except for the period between 4700 to 5400 seconds where it is poor. The disagreement between the bubble plot data and neutronics analysis for times greater than 4700 seconds is believed to be due to uncertainties in the bubble plot data rather than neutronics study.

Nonetheless, the analysis of the LOFT source range monitor response shows that the SRM response can be explained in terms of level and density changes in the core. To further demonstrate this, the SRM response for LP-SB-3 was simulated using the estimated void fractions obtained from cold-leg densities and the estimated core water level obtained from the core thermocouples. The resulting response obtained from this simulation and the actual SRM response are compared and shown in Fig. 3.20.

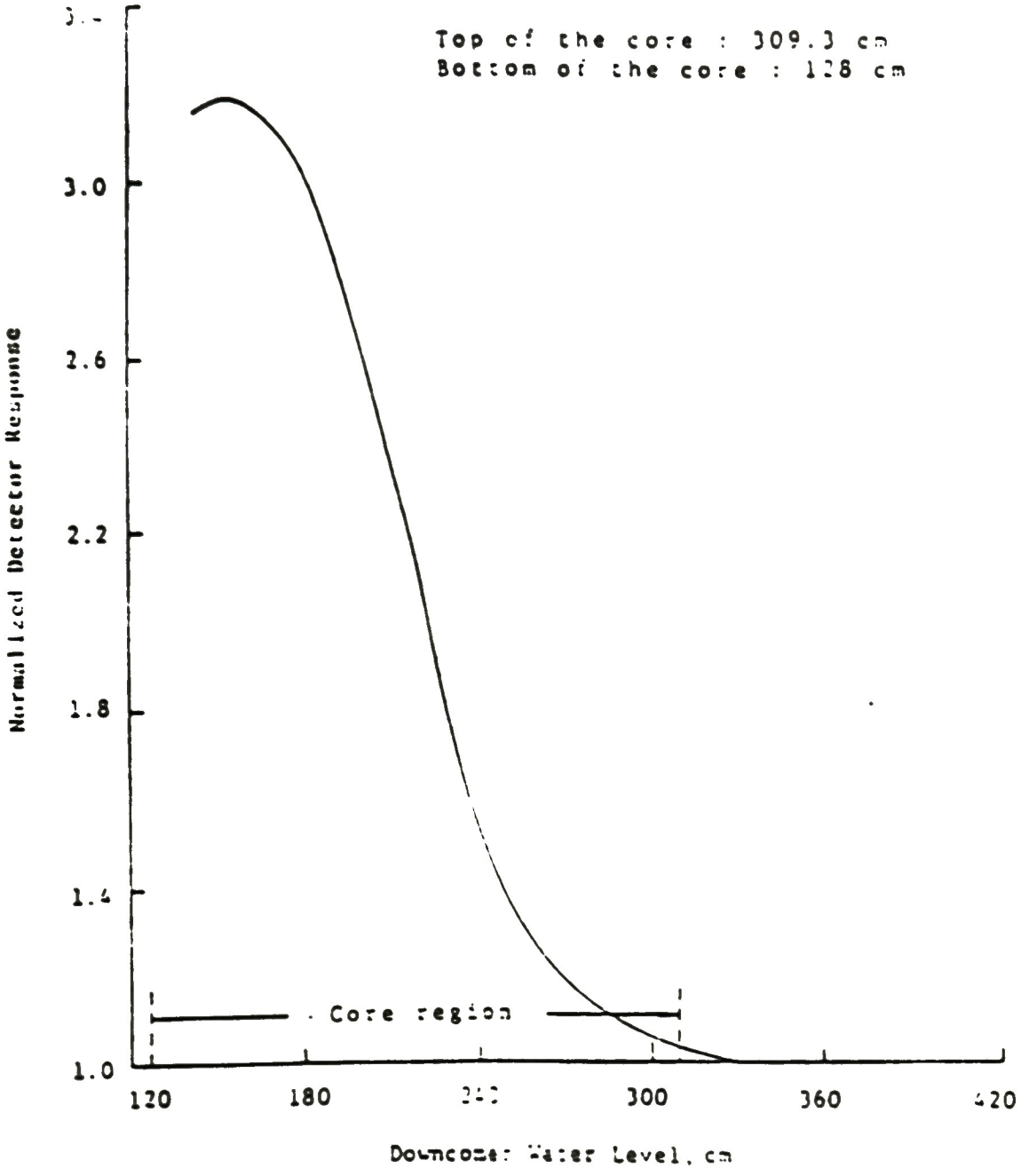

Figure 3.18. Source range detector response versus downcomer water level during core uncovery.

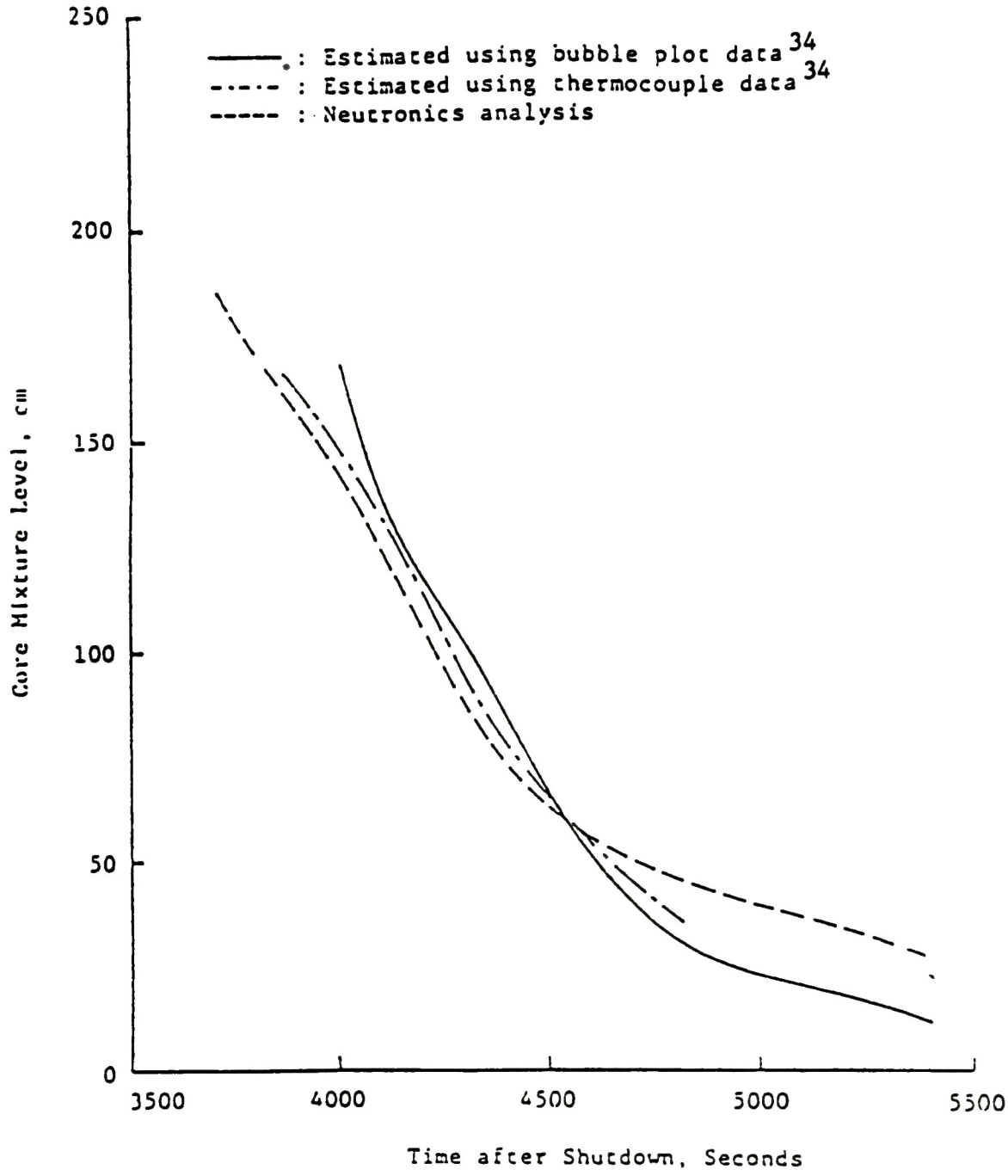

Figure 3.19. Estimated water level above the bottom of the core during experiment LP-SB-3.

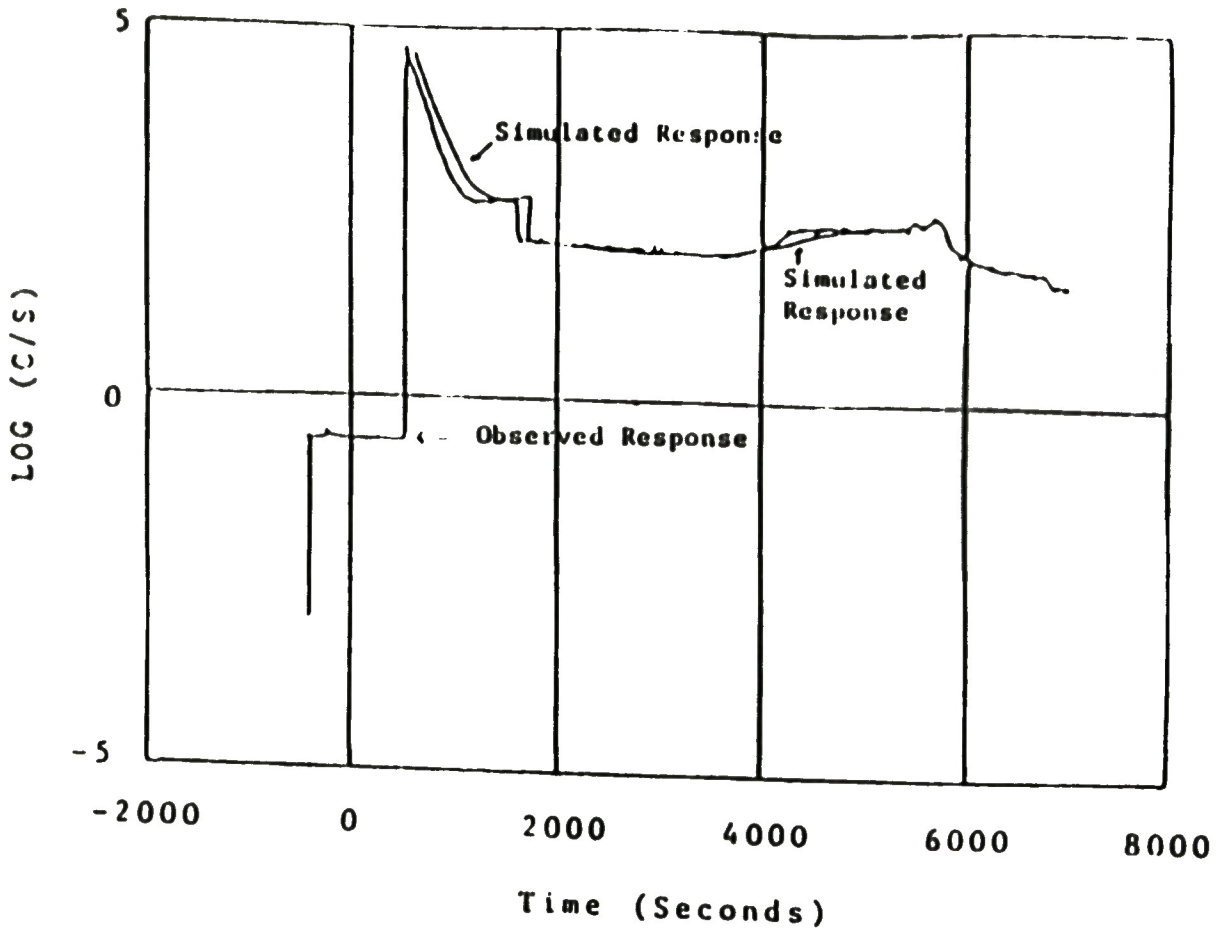

Figure 3.20. Comparison of LOFT installed source range monitor response to simulated response for experiment LP-SB-3.

In conclusion, the application of the present calculational method to LOFT experiments, LP-SB-2 and LP-SB-3, shows that the method gives satisfactory simulations of the actual detector response, and lends credence to the calculational method that is further used to analyze the SRM response during the TMI-2 accident.

4. RESULTS OF ANALYSIS

As described in section 2, the SRM response during the TMI-2 accident has been analyzed by a number of researchers.[1-3,7,9] Using the actual SRM response data, these analyses interpret the core status during the accident. For example, water levels during the first 174 minutes into the accident have been estimated by use of this information.[3] The SRM response from 174 to 225 minutes and beyond have not, however, been neutronically analyzed in detail. It is believed that a core reconfiguration could have occurred during this time period.[6] Therefore, the SRM response from 174 to 225 minutes is likely to contain information relative to the core reconfiguration during the accident. Since previous work has shown the count rate to be very sensitive to the presence of fuel in the lower head, such a reconfiguration should manifest itself in the SRM count rate.

A series of neutronics calculations using the calculational method described in section 3 were made to estimate core water levels and to evaluate the hypothesis of the fuel relocation during the accident. Calculations were performed in an effort to describe the changes of the count rate in the SRM response for the period from 30 to 225 minutes after shutdown. From these results, a possible explanation for the observed response of the detector and the conditions of the core were then inferred. This analysis used as input the scenario described in Section 1. It thus serves to benchmark and amplify this scenario.

The dominant neutron sources that were present in the TMI-2 core during the first 3 hours of the accident were photoneutrons and the

Americium-Beryllium-Curium (ABAC) start-up sources.[9] Originally, there were two start-up sources in the TMI-2 core, each with an estimated strength of 1.4×10^9 n/sec. The photoneutron source was obtained for different times during the accident by the calculational procedure described in subsection 3.1. A five-group cross section library was collapsed from the VITAMIN-E 174-group cross section library. The DOT model and cross section preparation procedures were described in subsection 3.3. The transport calculations utilized the P_3/S_8 approximation.

To make maximum utilization of the knowledge learned about the accident, the SRM response was not analyzed chronologically. Since the SRM response showed normal readings at the beginning of the accident, the response before the attempted restart of a B-loop pump (i.e., for $t < 174$ minutes, where t is the time after the reactor shutdown) was analyzed first. Then, the knowledge about the end state of the reactor learned from recent defueling work and analytical studies was used to analyze the SRM response from $t = 225$ minutes backward to $t = 174$ minutes. The procedures of the present analysis are summarized in Fig. 4.1, where the calculational sequence of the observed SRM response, the reactor conditions and/or system event on which the calculations were based, and the parameters/quantities determined from each calculation are given sequentially. This figure also outlines the rationale for the present analysis. In the following subsections, the details of these calculations and their results are described.

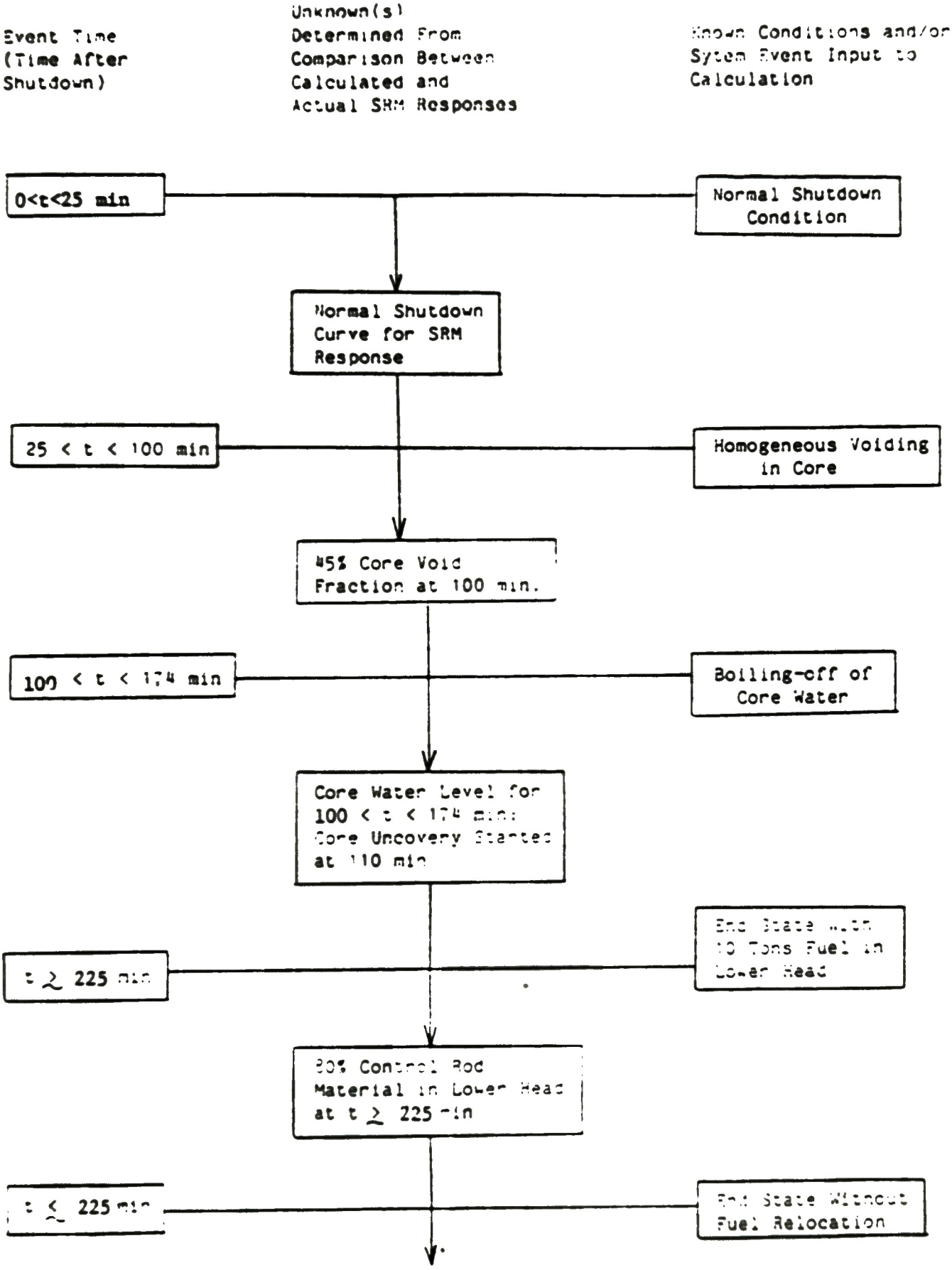

Figure 4.1. Calculational sequence of the present analysis.
(Continued on next page)

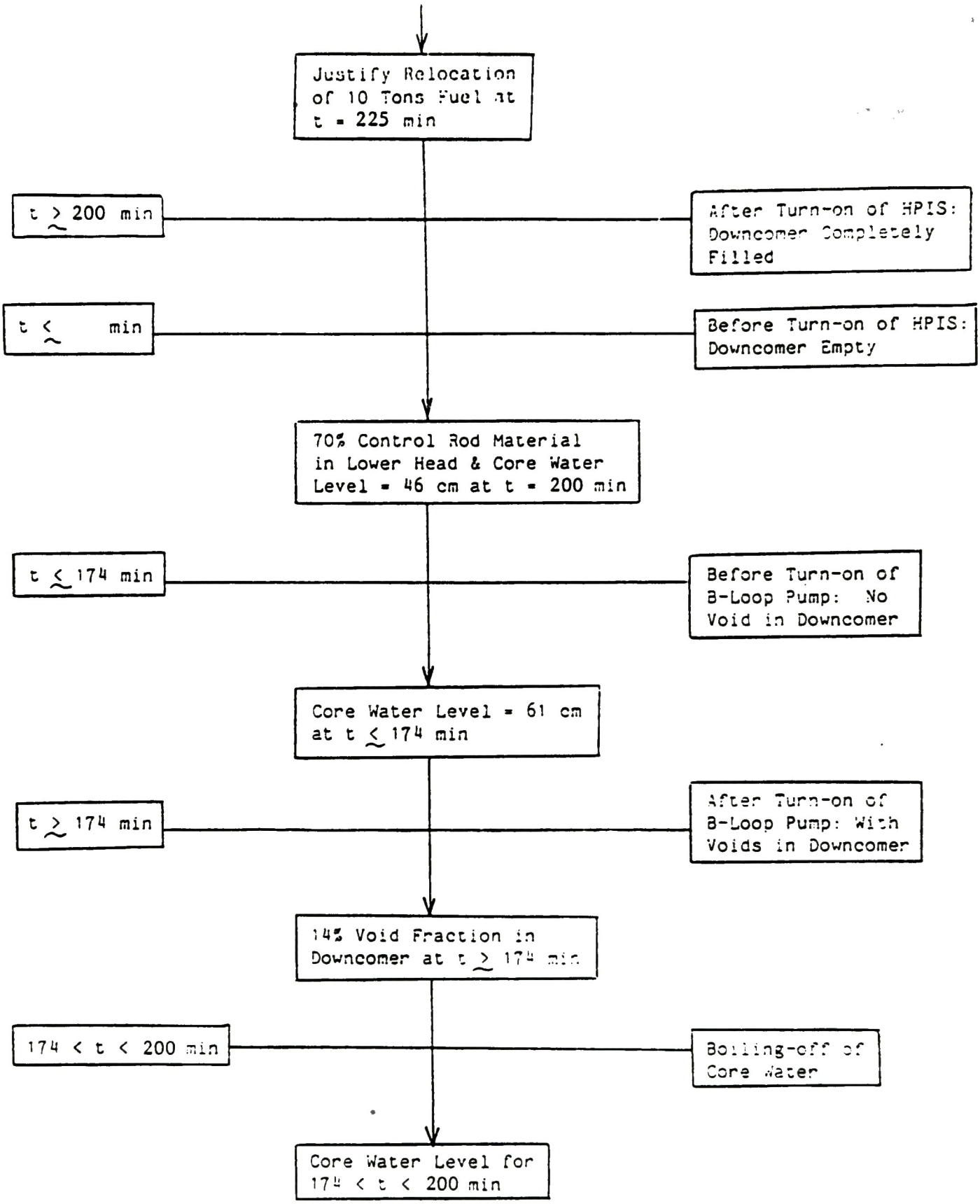

Figure 4.1 Calculational Sequence of the Present Analysis
(Continued from previous page)

4.1 Homogeneous Voiding Model 25 (<t < 100 Minutes)

One-dimensional (1-D) ANISN[32] calculations were used to determine the effect of homogeneous voiding on the source range monitor in the time period from 30 to 100 minutes into the accident while the primary coolant pumps were operating. The one-dimensional ANISN model is given in Fig. 4.2.

The percent voided coolant number density used in this and all later calculations is that of saturated liquid at the prevailing primary system pressure. The boron concentration was kept fixed at 1260 ppmB.

Figure 4.3 shows the TMI-2 SRM response and the calculated normal shutdown curve for the first 240 minutes into the accident.[1] The calculated normal shutdown curve was normalized to the observed response as follows. A normal shutdown curve was generated using the power history and shutdown data for TMI-2 and the ORIGEN computer code. In order to verify the accuracy of the calculated curve, this curve was first compared with the data from a shutdown of TMI which occurred a week earlier. The calculated curve was then compared with the TMI-2 accident data as extracted from the strip chart data.[33,34] It was found that aside from a constant multiplication factor, the theoretical shutdown curve tracked the accident data up until about 20-25 minutes into the accident. Furthermore, the point at 100 minutes was found to agree with the calculated curve when numerical uncertainties in the calculation were accounted for. These comparisons provided a calibration or normalization factor for use in comparing the actual and calculated or predicted SRM response

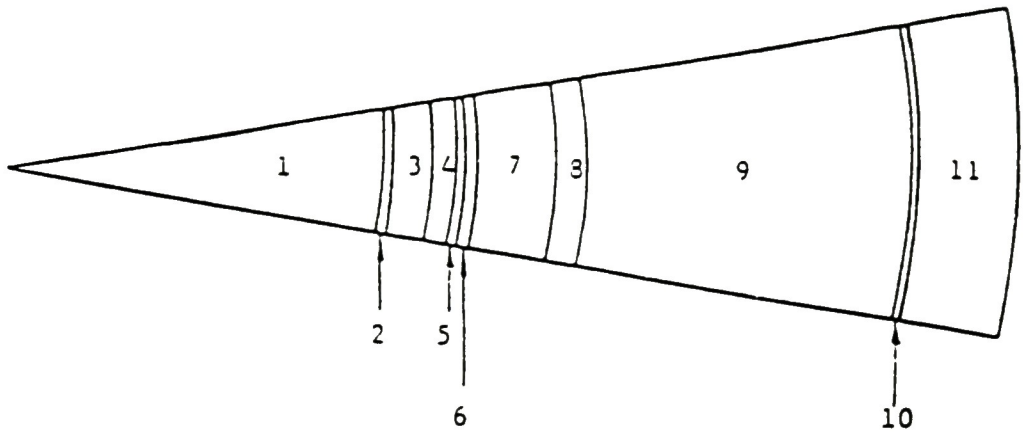

1 : Core
2 : Core Linear
3 : Water
4 : Core Barrel
5 : Water
6 : Thermal Shield
7 : Downcomer
8 : Reactor Vessel
9 : Air Gap
10 : Detector
11 : Concrete

Figure 4.2. One-dimensional ANISN model for TMI-2 reactor.

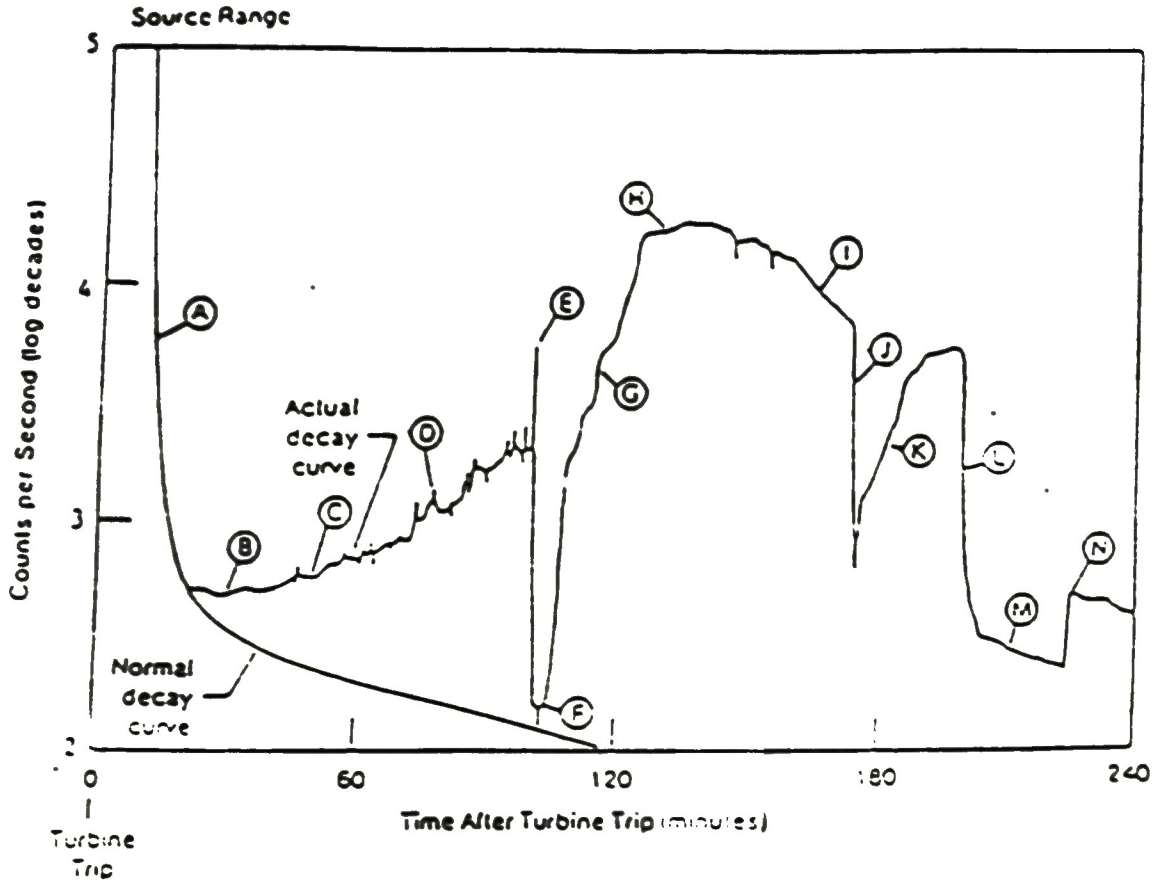

Figure 4.3. TMI-2 source range monitor response and calculated normal shutdown curve.[1]

throughout the accident. The agreement between the calculated curve and the accident curve at 103 minutes confirmed the assumption that when all the primary coolant pumps were tripped at 100 minutes, essentially complete phase separation occurred. The phase separation caused the core and downcomer to be temporarily filled with water of very low or no void fraction. The SRM sensed the normal hydraulic condition in the vessel at this moment.

Prior to the time the primary coolant pumps were tripped after the reactor shutdown, the SRM response began to deviate from the normal shutdown response at between 20 and 25 minutes. This was apparently caused by flushing of water containing voids into the reactor vessel. For the purpose of this study, the voiding during this time is assumed to have a homogeneous void distribution in the vessel.

A summary of the one-dimensional calculations performed to examine the effect of homogeneous voiding on the SRM response is shown in Fig. 4.4. Two types of neutron sources, namely photoneutrons and the start-up source were used in these calculations. The strength of the start-up source was kept constant throughout the calculations, because the half lives of the radionuclides are much greater than the time period involved. The strength of the photoneutron source was time dependent and was decreased by a factor of $(1-\alpha)$ as the void fraction α increased. The energy spectra, as shown in Table 4.1, of these two sources are quite different. Most of the neutrons from the start-up source are born in Group 1, whereas most of the photoneutrons are born in Group 2. The importance of the start-up source to the SRM response then depends on the relative strength of the start-up source

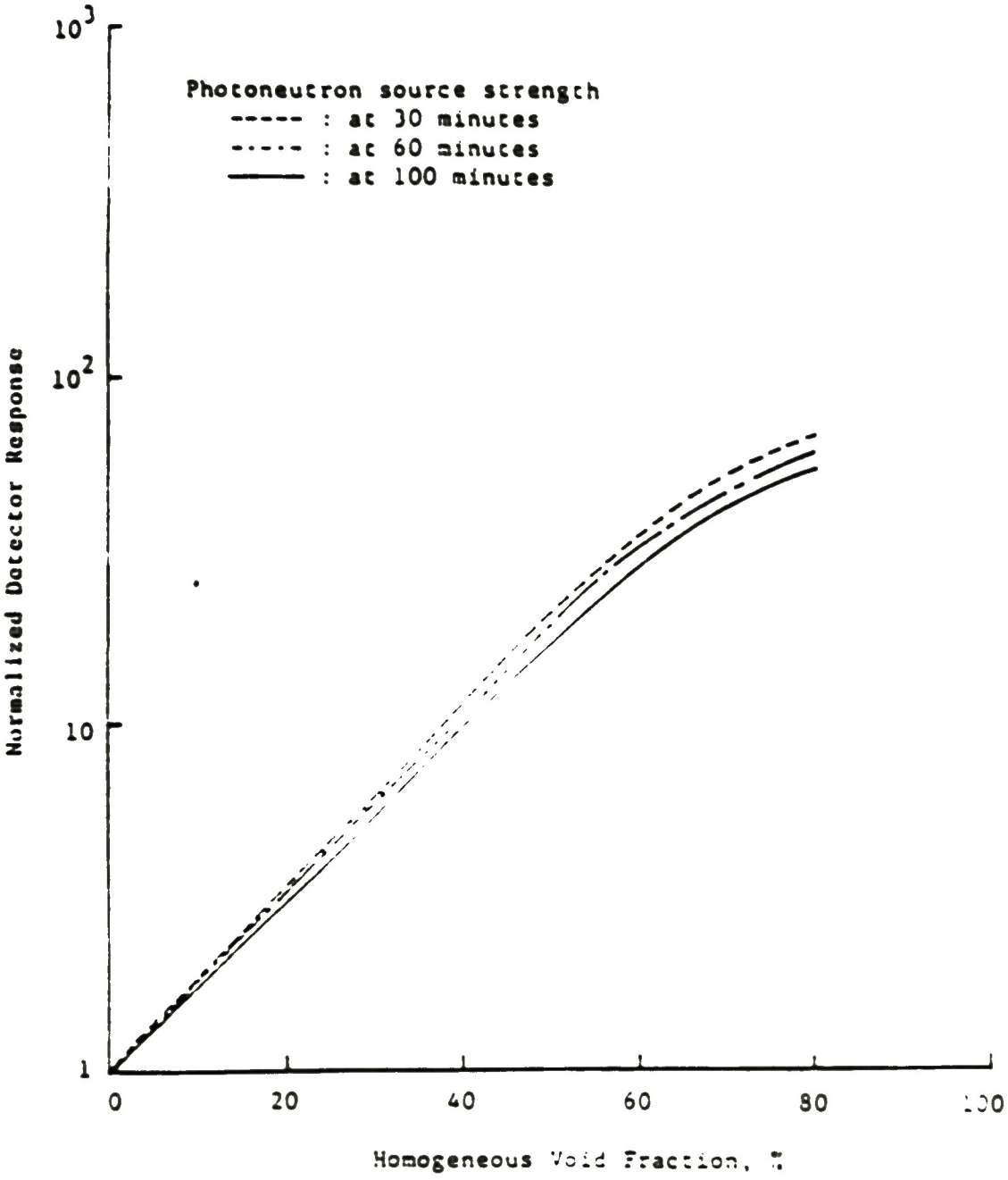

Figure 4.4. Source range monitor response versus homogeneous void fraction for the TMI-2 reactor.

TABLE 4.1

Energy Spectra of Photoneutron Source and Start-up Source

Group	Upper Energy Bound (MeV)	Photoneutron	Start-up Source
1	1.0000×10^{1}	4.66×10^{-6}	0.97442
2	8.2085×10^{-1}	0.999534	0.02558
3	5.5308×10^{-3}	0.0	0.0
4	1.8554×10^{-6}	0.0	0.0
5	6.2493×10^{-7}	0.0	0.0

as compared with the photoneutron source. Hence, the homogeneous voiding calculations were performed with the start-up source strength kept constant and the photoneutron source strength at 30, 60 and 100 minutes into the accident, respectively.

Based on comparison with actual SRM data,[35,36] the observed response was about 14 times higher than the normal shutdown response just before the loop-A pumps were tripped at about 100 minutes into the accident. From the neutronics analysis using the homogeneous model, it is estimated from Fig. 4.4 that the core was approximately 45% voided at this time.

4.2 Initial Core Heat-Up Response (100 < t < 174 min)

The homogeneous voiding calculations are applicable to approximately the first 100 minutes into the accident when the primary coolant pumps remained in operation. After the pumps were stopped, the coolant in the core continued to boil, resulting in a loss of the coolant and thereby reducing the water levels in the core and downcomer. Since boiling is assumed not to occur in the downcomer region, the downcomer water level is lower than the core water level when the core is uncovered (see Figure 4.5). Thus, the partially emptied downcomer provides an unshielded streaming path of varying size for the neutrons to leak out of the core.

A series of two-dimensional calculations were performed to determine the effect of water level changes in the core and downcomer on the SRV response. The two-dimensional (2-D), R-Z cylindrical model shown in Fig. 3.11 was used for core uncovery and fuel relocation analyses.

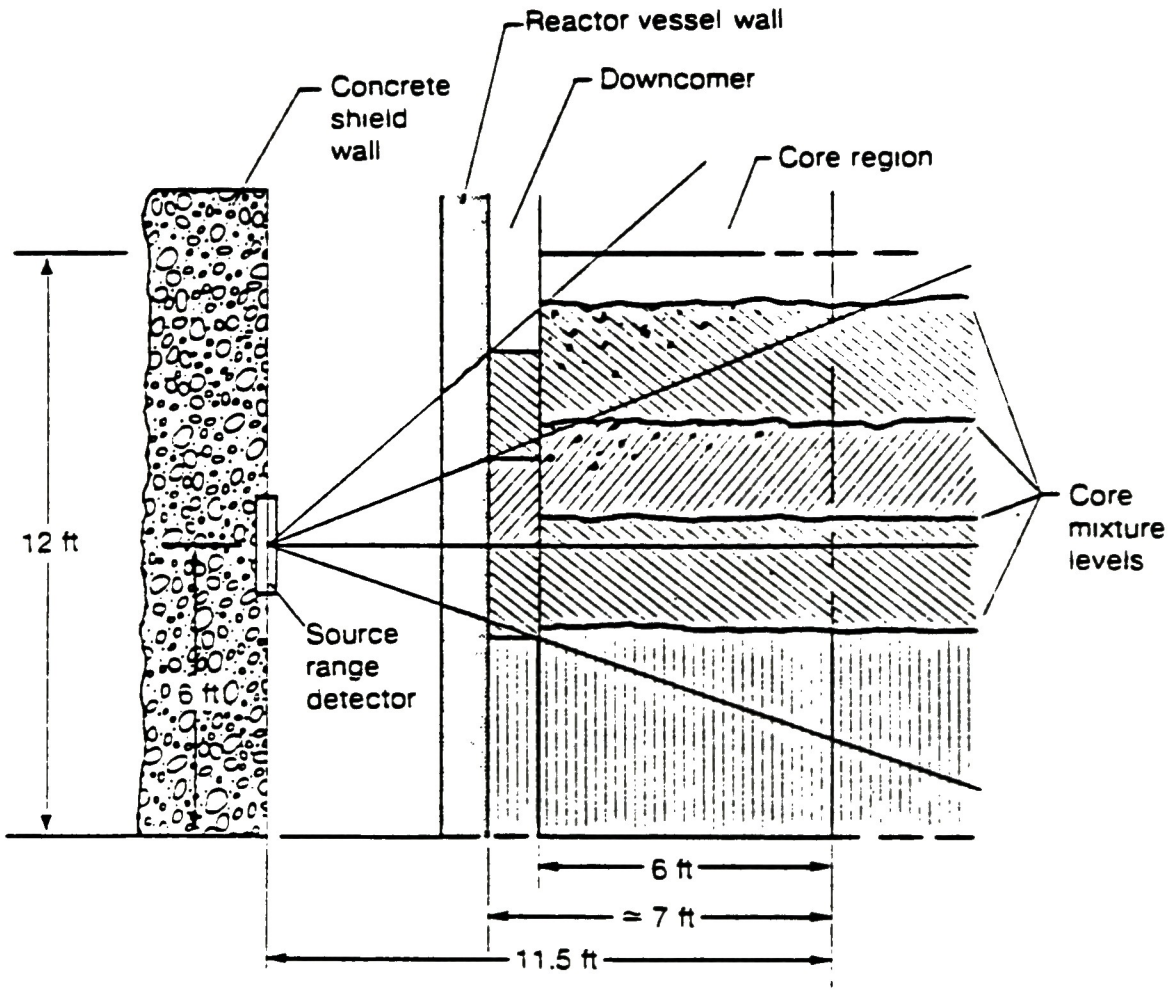

Figure 4.5 Source range neutron detector field of view versus core mixture level.[1]

A model of the core void fraction distribution as a function of axial position was obtained from NSAC-28.[9] This model expressed the core void fraction in terms of the height Z, above the bottom of the core, as

$$\alpha(Z) = 0.045 + 0.024\ Z + 0.066 \exp[-(Z-0.9)/1.3] \quad \text{for } Z>2 \text{ ft}, \qquad (4.1)$$
$$= 0 \quad \text{for } Z \leq 2 \text{ ft},$$

where α is the core void fraction and z is in feet. The average void fraction in each core region was calculated by integrating Eq. (4.1) over the height of each region and then dividing by the height of the region.

If the core void fraction obtained by the above procedure and no voids are assumed in the downcomer, the hydrostatic pressure balance between the core liquid and the downcomer liquid requires a one-to-one correspondence between the two water levels. The various core water levels and the corresponding downcomer water levels are given in Table 4.2. The calculated core multiplication factor for each core water level is also given in the table.

Two-dimensional calculations were performed for various core water levels from full (365.76 cm) to 30.48 cm (1 foot) above the core bottom with the photoneutron source strength at 100, 140 and 174 minutes, respectively. The calculated results are shown in Fig. 4.6.

The results shown in Fig. 4.6 indicate that the SRM response would increase by a factor of about 11 when the core is first uncovered. The observed SRM response during the TMI-2 accident, as shown in Fig. 4.3, increased by a factor of about 11 at about 110

TABLE 4.2

Relationship Between Water Level in the Core and Water Level in the Downcomer

Core Water Level Above Core Bottom (cm)	Downcomer Water Level Above Core Bottom (cm)	K_{eff}
365.76*	300.84	0.9180
304.88	257.59	0.8850
243.84	212.54	0.8842
182.88	164.59	0.8838
121.92	113.90	0.8758
91.44	87.63	0.8696
60.96	60.96	0.8247
30.48	30.48	0.7776

* Top of the Core

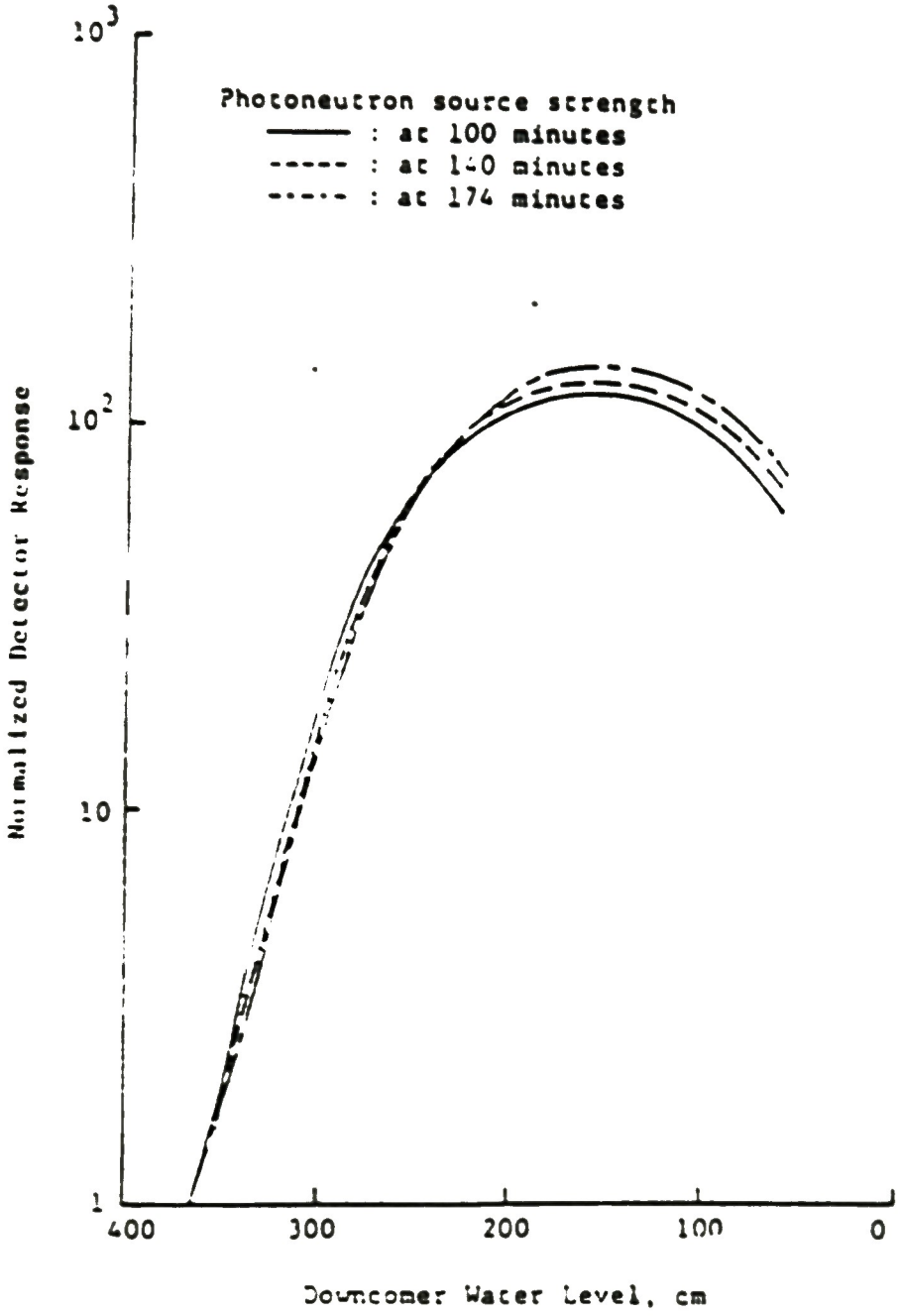

Figure 4.6. Source range monitor response versus downcomer water level for the TMI-2 reactor during core uncovery.

minutes into the accident. This observation suggests that core uncovery occurred at this time. Based on the previously mentioned assumption, this result agrees with the prediction of the thermal hydraulic analysis.[2]

The calculated results were used to estimate the water levels during the period of 100 through 174 minutes. The estimated core water levels are compared with predictions of the thermal hydraulic analysis in NSAC-24[2] and the previous SRM analysis in NSAC-28[3] in Fig. 4.7.

The water level estimated in this work was about 91 cm (3.0 feet) above the bottom of the core at 174 minutes just before the B loop pump was turned on. However, it is believed that the actual water level was probably lower. The above analyses were based on an intact core geometry and no core damage was assumed. According to a thermal hydraulic analysis, control rod materials could have begun to melt and flow downward at about 145 minutes into the accident.[16] Based on a sensitivity analysis performed as part of this work, a partial absence of control rod material in the core region would cause the neutron multiplication to increase and the SRM response to correspondingly increase. Hence, the water level should be lower in order to compensate for the increase in the SRM response due to a decrease in control rod materials. A more detailed discussion will be presented in the next subsections.

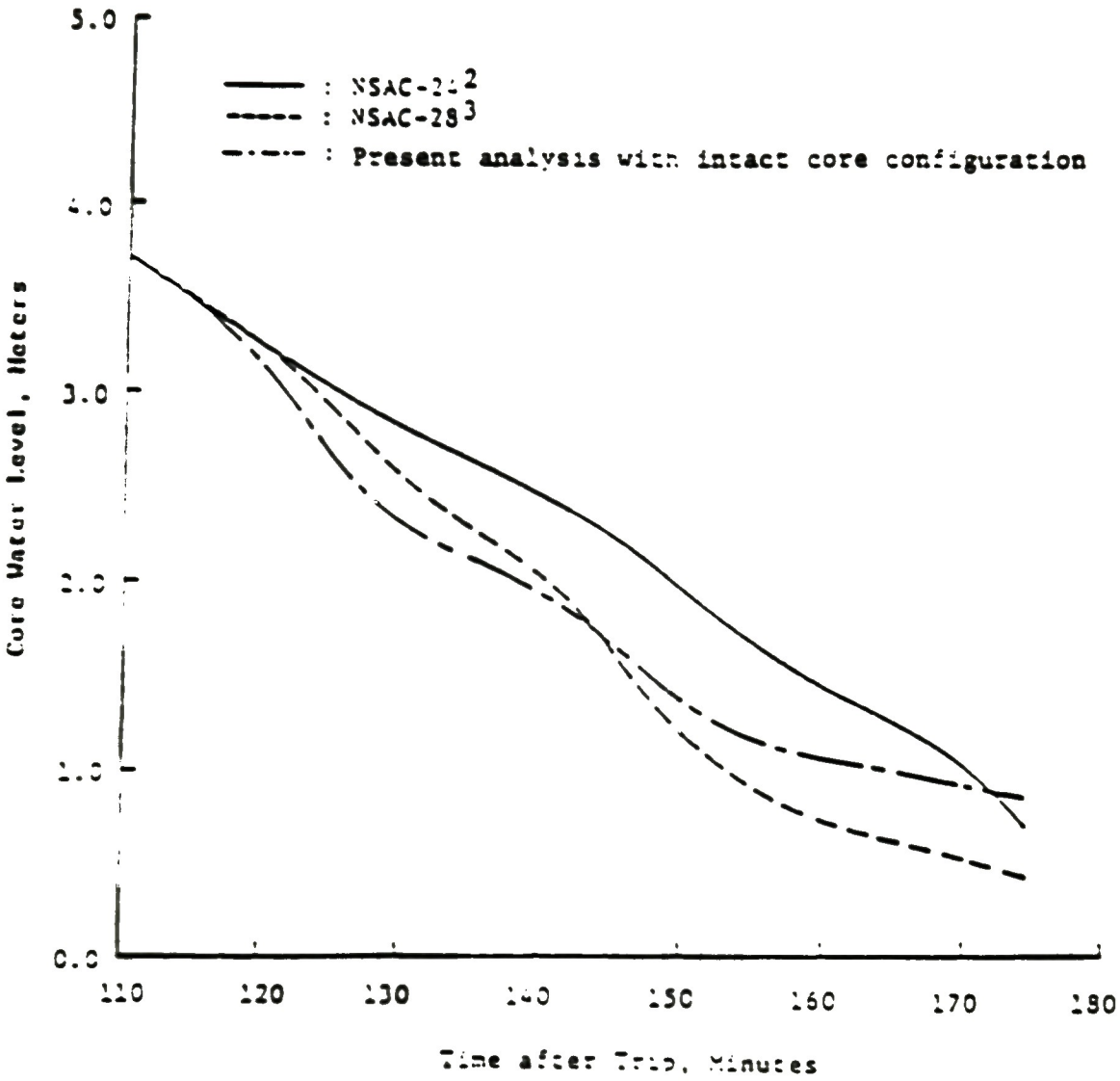

Figure 4.7. Estimated water level above the bottom of the core for TMI-2 during core uncover[y].

4.3 Core Relocation Analysis (t = 225 minutes)

The increase in the SRM response at 225 minutes into the accident is believed to be due to the relocation of the damaged core while reaching its final status. The end-state conditions of the damaged core are known and have been modeled appropriately.[30] Hence, performing the analysis backwards from 225 to 174 minutes should be the better approach to analyze the SRM response in this time period.

The known post-accident end-state of the damaged core is shown in Fig. 4.8. About one-third of the original fuel in the upper core region is no longer there; a voided cavity was formed in this region. A rubble bed is resting on top of the existing core with about 10 to 20 tonnes of fuel residing on the vessel bottom.[6]

In earlier work, the end-state conditions of the damaged core were modeled to analyze solid-state track recorder measurements of neutron levels in the air gap of the TMI-2 reactor.[19,30] This analysis predicted the presence of fuel in the lower head with the best estimate of 10 tonnes.[30] The prediction was in fact subsequently confirmed by video inspection of the lower head. The model used is given in Fig. 4.9. The underlined numbers denote the fuel volume fraction in the region. The normal fuel volume fraction in the TMI core is 0.31. The ratio of the volume of clad, structure, control rod material, etc. to the volume of fuel in all damaged fuel zones is always set equal to that of the intact core. Coolant at 90°F and atmospheric pressure with 3300 ppm Boron was placed in the volume of the fuel containing zones not containing solid material. This model was used as the first step to analyze the SRM response at 225 minutes.

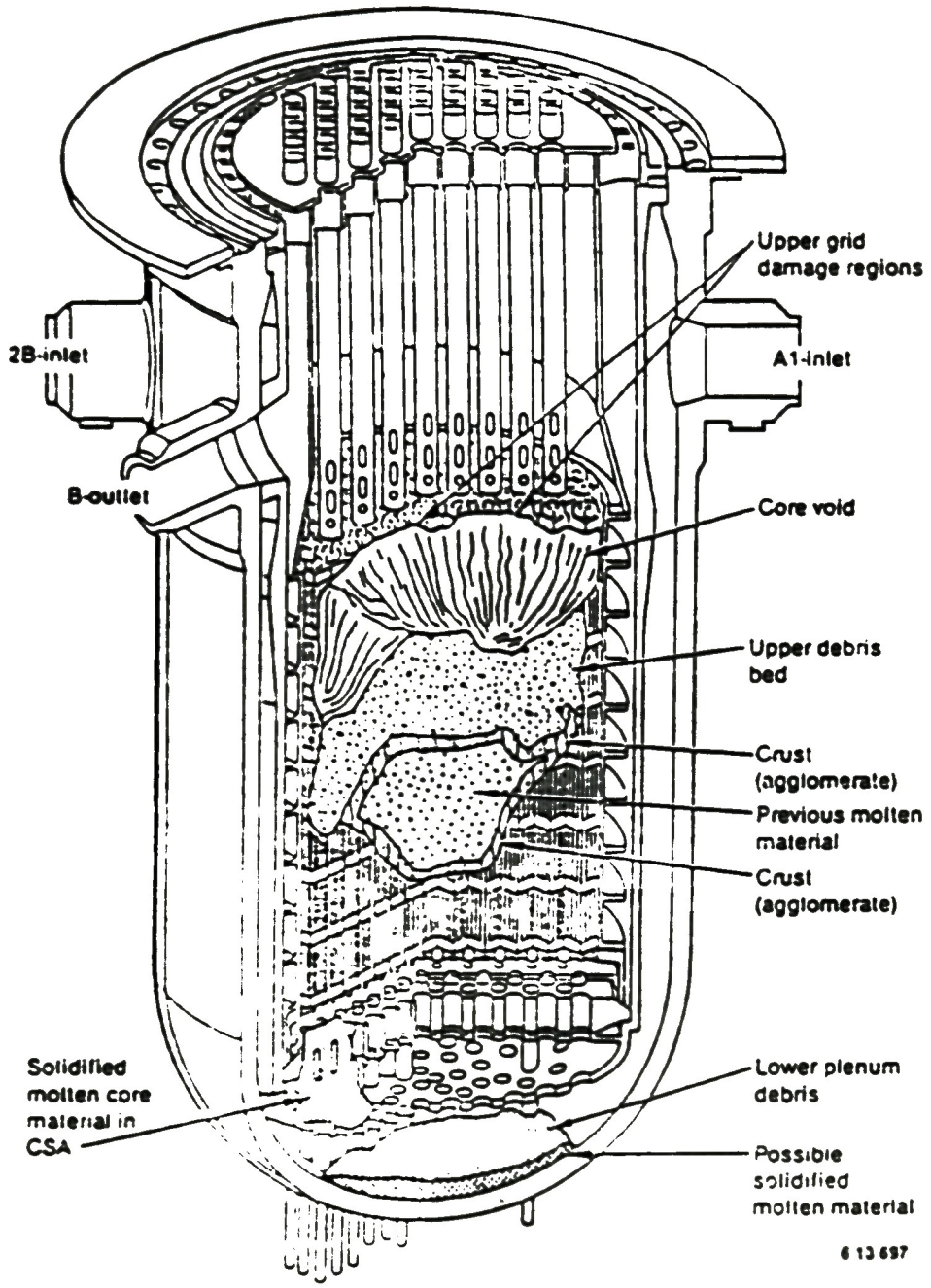

Figure 4.8. TMI-2 known post-accident end-state core configuration.[6]

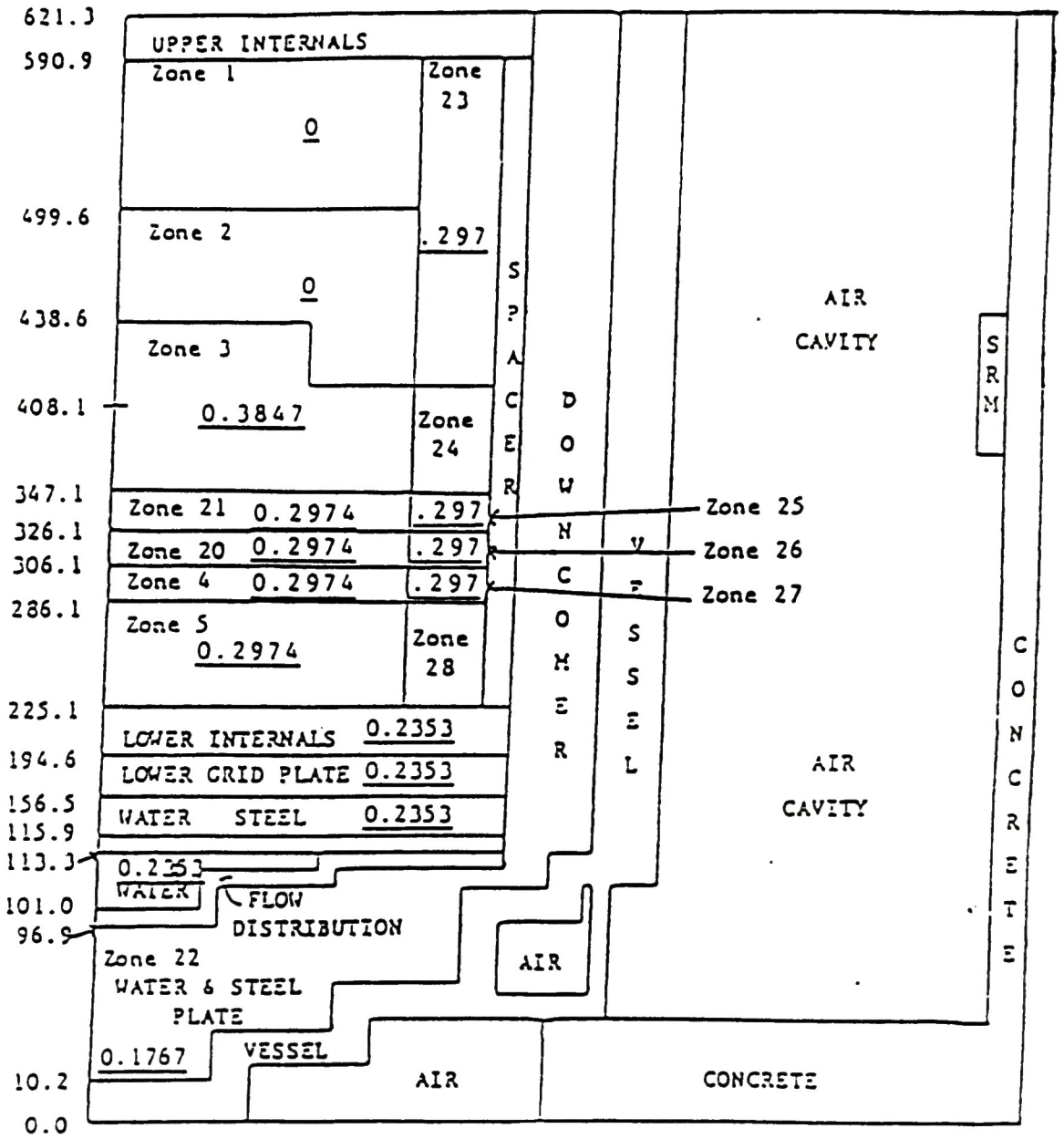

Figure 4.9. End-state of TMI-2 DOT model. (Dimensions in cm)

However, the calculated SRM response based on this model was too high, compared with the actual response at 225 minutes.

Using this 2-D end-state DOT model which had about 10 tonnes of fuel in the lower head and noting that both the core and the downcomer were completely filled with water (with no voids) at this time, the only variable in calculating SRM response was the amount of control rod materials in the lower head. It was also noted from our previous study[30] that the neutron source existing in the lower head makes the dominant contribution to the SRM response at that time, and that an increase in the control rod materials in the lower head could reduce the SRM response. Hence, a series of calculations were then performed that used the model shown in Fig. 4.9 with different quantities of control rod materials in the lower head. When the calculated SRM response was compared with the actual reading at $t > 227$ minutes (point N in Fig. 4.3), it was determined that about 80% of the control rod material would have relocated to the lower head. The calculated results also showed that the jump in the SRM response at 227 minutes could be explained by this relocation of 10 tonnes of fuel at that time.[30]

As discussed in the following section, the control rod material migrated slowly from the core. This migration began early on in the accident (at about 120 minutes) as soon as the temperatures reached the melting point of the eutectic Ag-In-Cd control rod material.

4.4 Pump Transient and HPIS Injection ($174 < t < 200$ Minutes)

The next step was to determine the core status at 200 minutes

into the accident when the High Pressure Injection System (HPIS) was initiated. Since the TMI-2 ex-core detectors showed nearly the same behavior during the time period of 174 to 200 minutes as during the period of 100 to 174 minutes, further fuel relocation probably did not occur during this period. Hence, the physical configuration of the fuel and core structural material at 200 minutes is believed[37] to be the same as that at 174 minutes just after B-loop pump was turned on.

The zircaloy cladding in the upper region of the core is believed to have become highly oxidized and embrittled by 174 minutes just prior to start-up of the B-loop pump.[16] Turning on the B-loop pump is thought to have thermal-shocked and embrittled the fuel rods. This shock could shatter the oxidized fuel rods in the upper core region and result in a debris region. Fig. 4.10 shows the core configuration as it is thought to have existed after 174 minutes. The corresponding DOT model is shown in Fig. 4.11. The underlined numbers in each core region give the fuel volume fraction in that region.

At 200 minutes, initiation of the HPIS pumped water into the vessel and shortly thereafter filled the downcomer region. The effect of this filling can be seen as region L of Fig. 4.3. Several core water levels and different amounts of the control rod materials lost from the core region were assumed to determine the possible status at this point. In this analysis, the control rod materials were arbitrarily placed in the lower head. This was done to properly account for observed SRM response at 225 minutes. The calculated results are given in Fig. 4.12. Here, the vertical axis is the ratio of the SRM response to that of a full core with the geometry in Figure 4.11. As shown in Fig. 4.3, the observed SRM response just after the

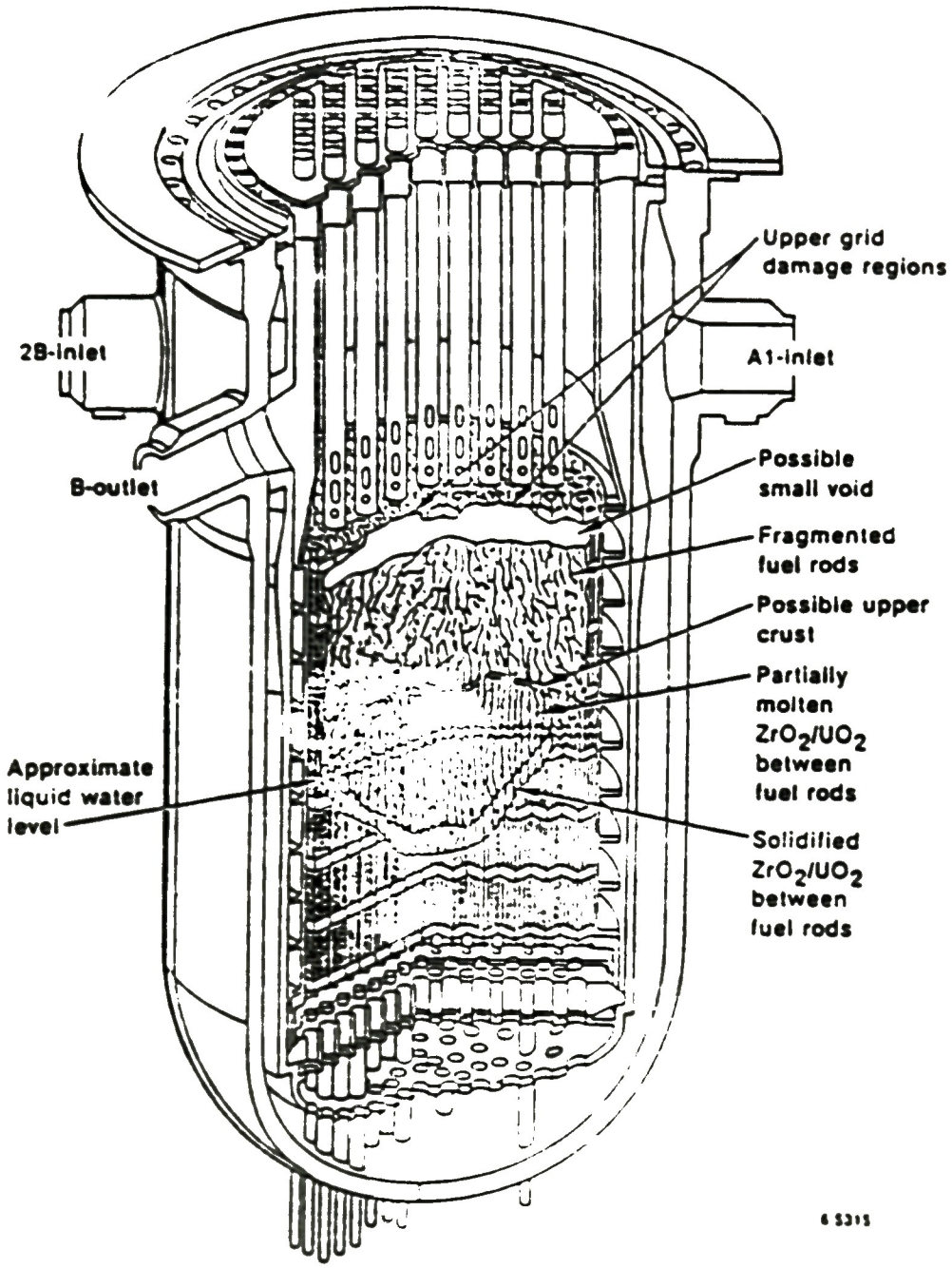

Figure 4.10. Estimated TMI-2 core configuration at 175 to 180 min, after the pump transient, showing the upper debris bed formation.[6]

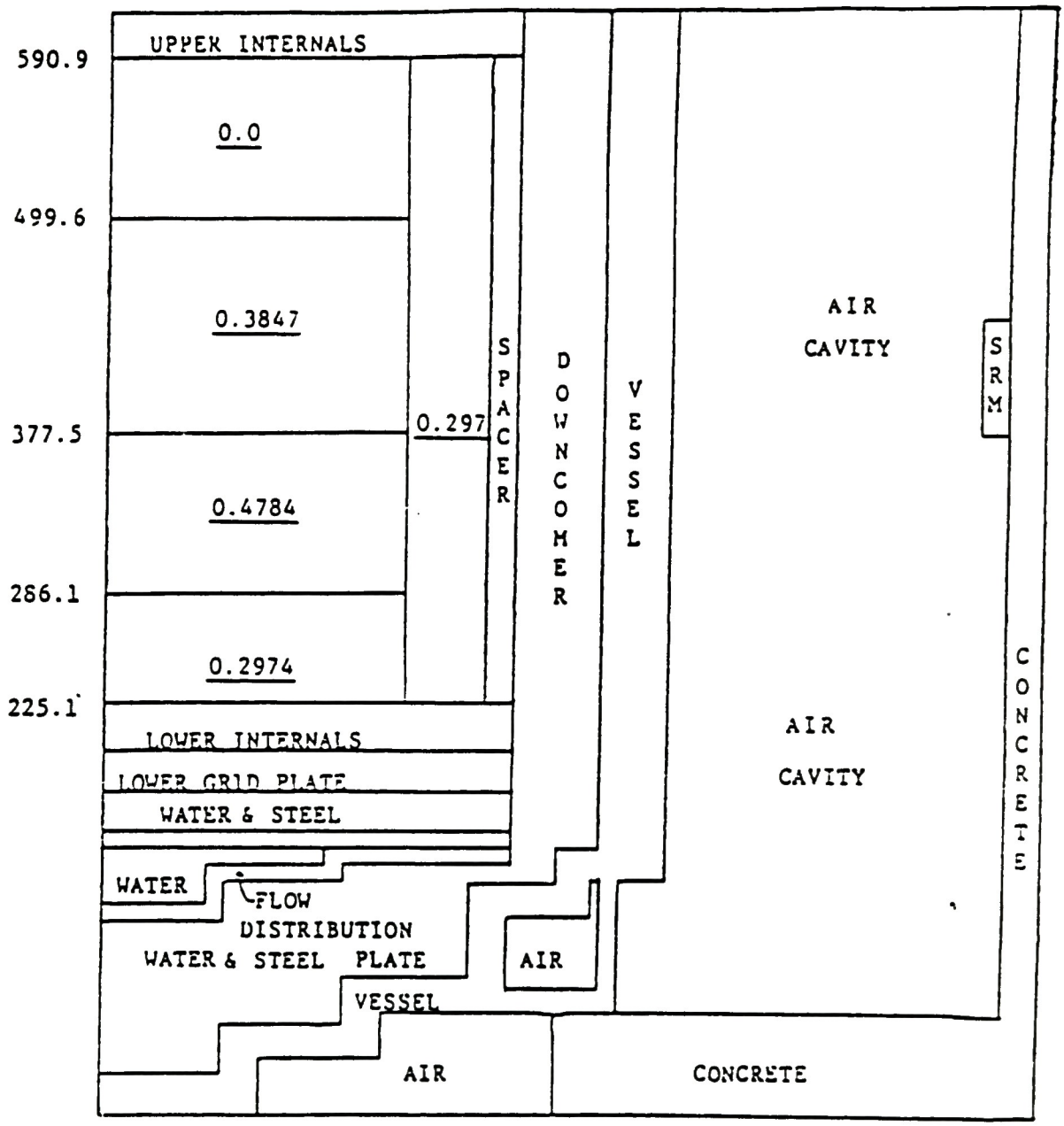

Figure 4.11. DOT core model at 174 minutes after turning on the B-loop pump. (Dimensions in cm)

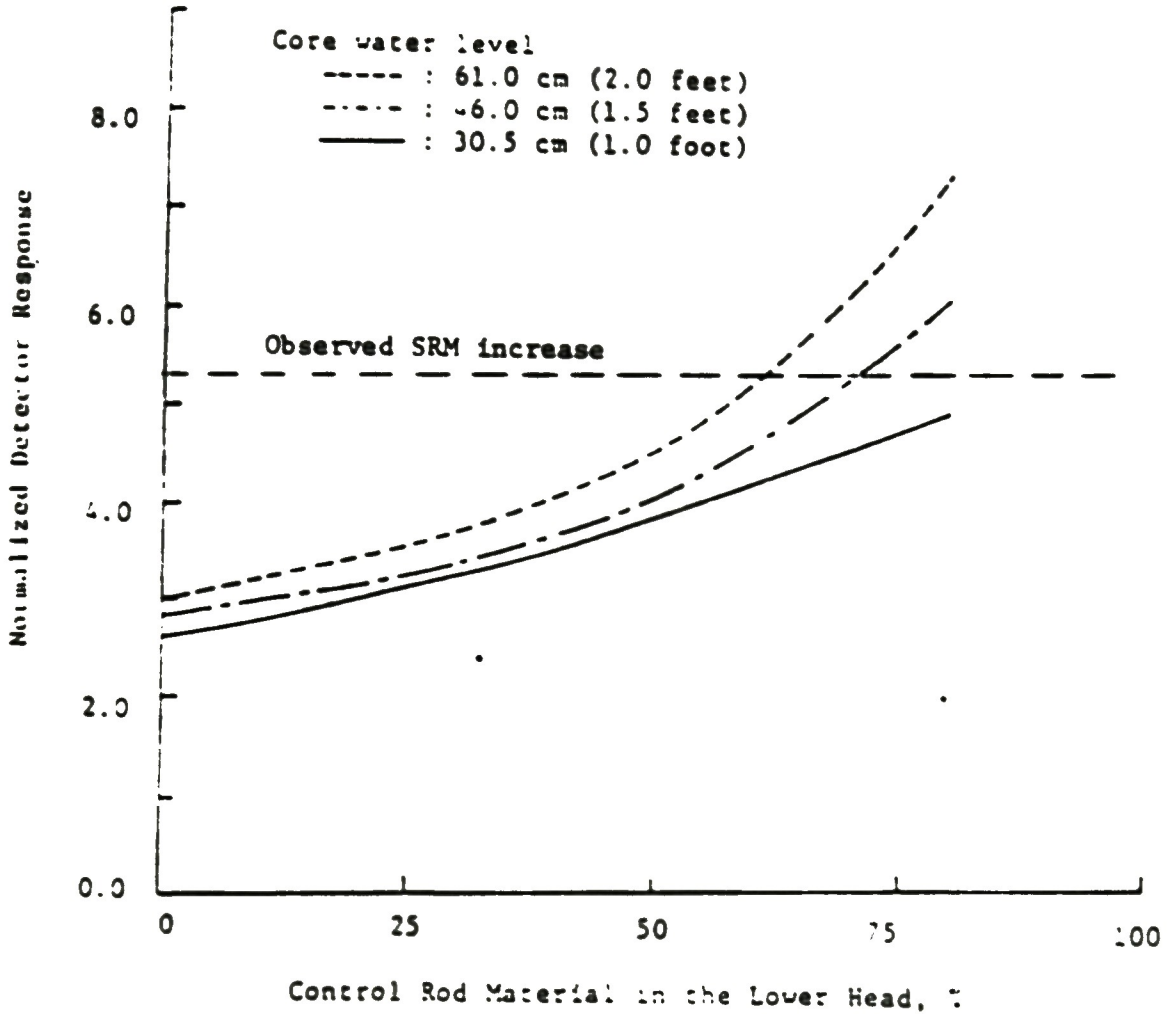

Figure 4.12. Normalized detector response versus control rod material located in the lower head with downcomer filled with water at 210 minutes after initiation of the HPIS.

HPIS refilled the downcomer (i.e., the point at the beginning of the labelled region M in Fig. 4.3) was a factor of about 5.3 larger than that of the normal shutdown value for a core as given in Figure 4.11. Figure 4.12 shows that the water level could be in the range of 38 to 61 cm above the bottom of the core with 60 to 80% of the control rod materials in the lower head just after initiation of the HPIS.

Since initiation of the HPIS pumped water into the downcomer, the physical geometries and water levels in the core should be the same just before and after the HPIS was turned on. Since there could not be an instantaneous change in core water level, the only difference between those two points would be the downcomer water level. The downcomer was assumed full and the water level in the core was assumed to be the same as that in the core before the HPIS was turned on. These calculations were then repeated with an emptied downcomer to simulate the status just before the HPIS was initiated. The results of the calculations are shown in Fig. 4.13. As shown in Fig. 4.3, the observed SRM response just before the HPIS was turned on (i.e., the point at the beginning of the labelled L region) was larger by a factor of about 70 than the normal shutdown value for a core as configured in Figure 4.10. Figure 4.13 shows the possible status at this moment. The core water level could be between 42 to 61 cm with 30 to 80% of the control rod materials absent from the core.

For the reasons stated in the preceding paragraph, in order to have consistent count rates both before and after the HPIS was turned on, the core water level and amount of control rod material in the lower head must satisfy both the curves in Figure 4.12 and the curves in Figure 4.13. Namely, the observed SRM count rates at both the

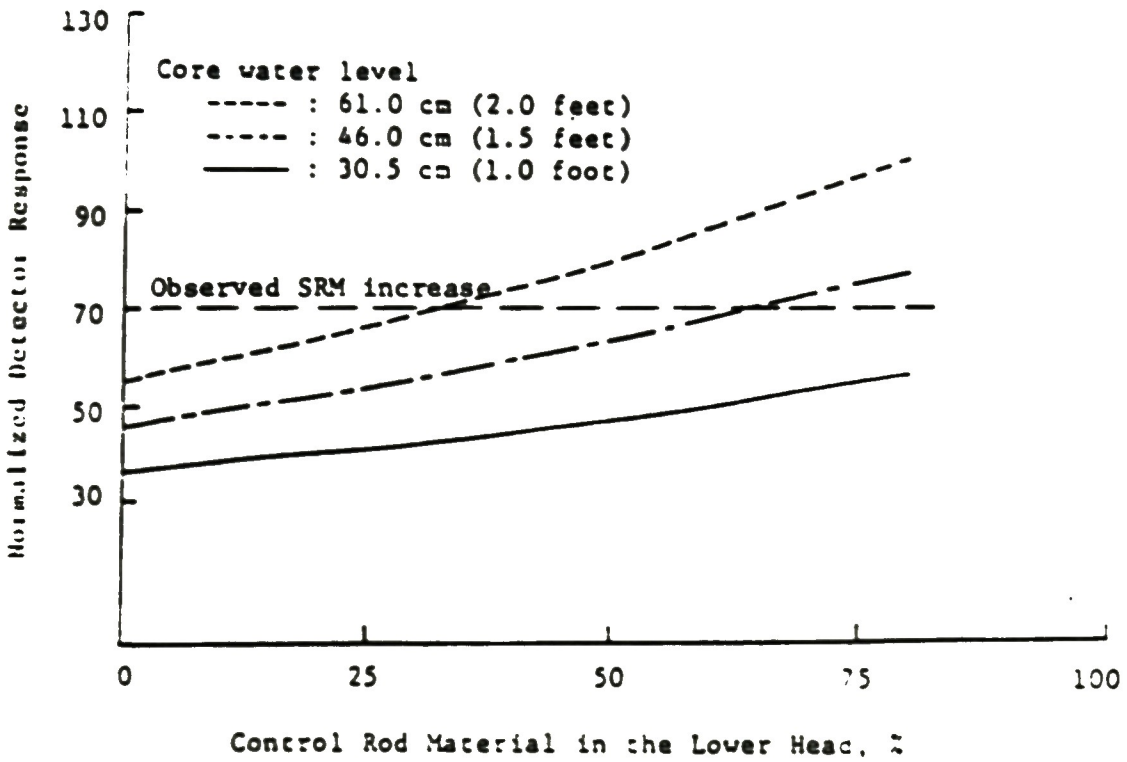

Figure 4.13. Normalized detector response versus control rod material located in the lower head with emptied downcomer at 200 minutes before initiation of the HPIS.

beginning of region L and the beginning point of region M in Figure 4.3 provide two conditions for uniquely determining the two variables, i.e., the core water level and the amount of control rod material in the lower head.

A comparison of the curves in Figs. 4.12 and 4.13 shows that an intersection occurs at the water level 46 cm (1.5 feet) with 70% of the control rod materials in the lower head, as shown in Fig. 4.14. These calculations suggest that at 200 minutes into the accident the core configuration would look similar to the model shown in Fig. 4.11 with the water level at the height of about 46 cm above the bottom of the core and with about 70% of the control rod materials in the lower head.

The last step was to analyze the core status at 174 minutes just before and after the B-loop pump was turned on. Since it is believed that the zircaloy cladding began to melt at about 150 minutes into the accident,[16] the molten zircaloy would react with the UO_2 and dissolve some of the UO_2 in the liquid zircaloy. Molten zircaloy and liquefied fuel would then flow downwards, freezing near the coolant surface in the lower portion of the core. Fig. 4.15 shows the estimated core configuration at 174 minutes just before turning on the B-loop pump. The corresponding DOT model is shown in Fig. 4.16. Again, the underlined numbers denote the fuel volume fraction in the region.

A series of calculations that used the model shown in Fig. 4.16 were made to determine the water level just before the B-loop pump was turned on. These calculations assumed 70% of the control rod materials in the lower head, which was the number obtained from the analysis of SRM response at 200 minutes, with different water levels

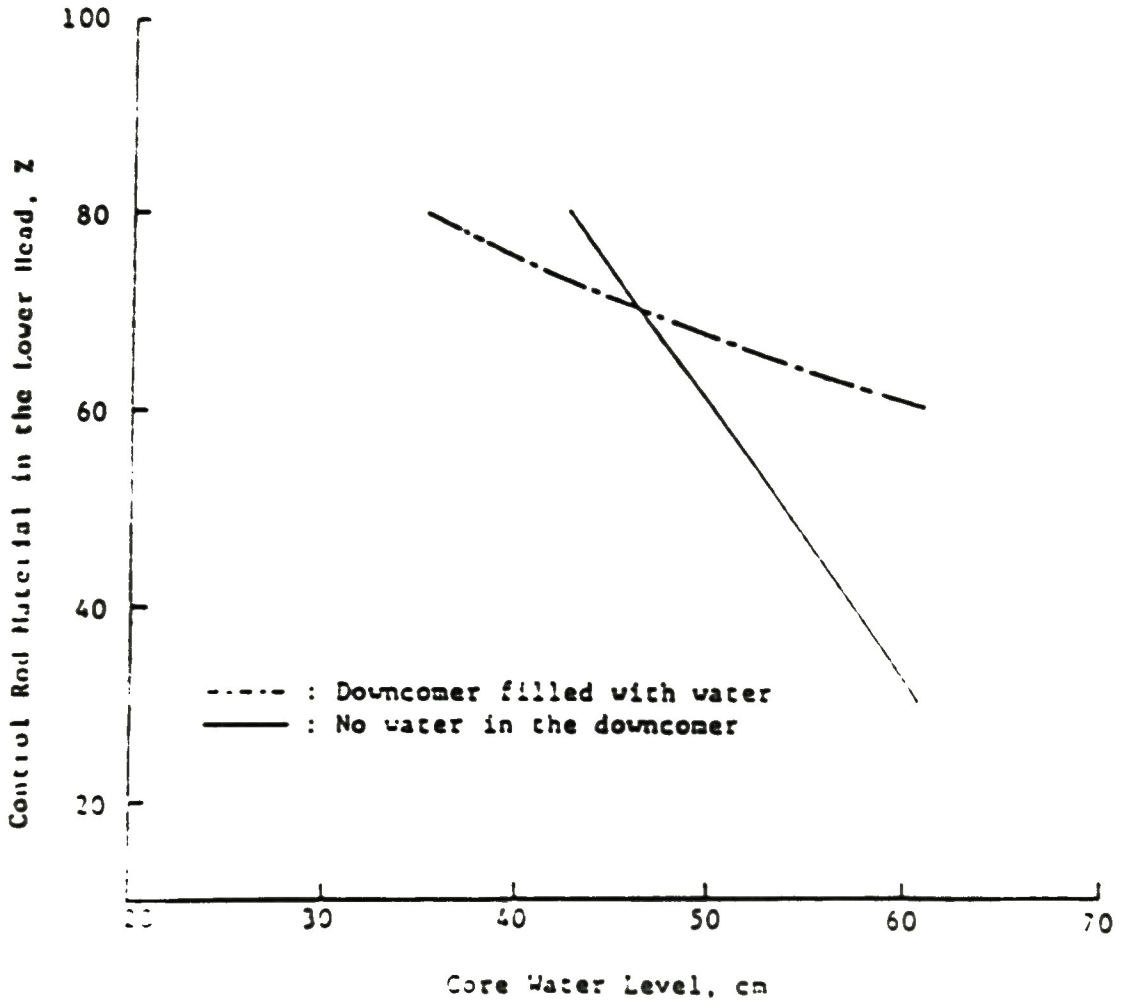

Figure 4.14. Control rod material in the lower head versus core water level for the possible status in the vessel at 200 minutes.

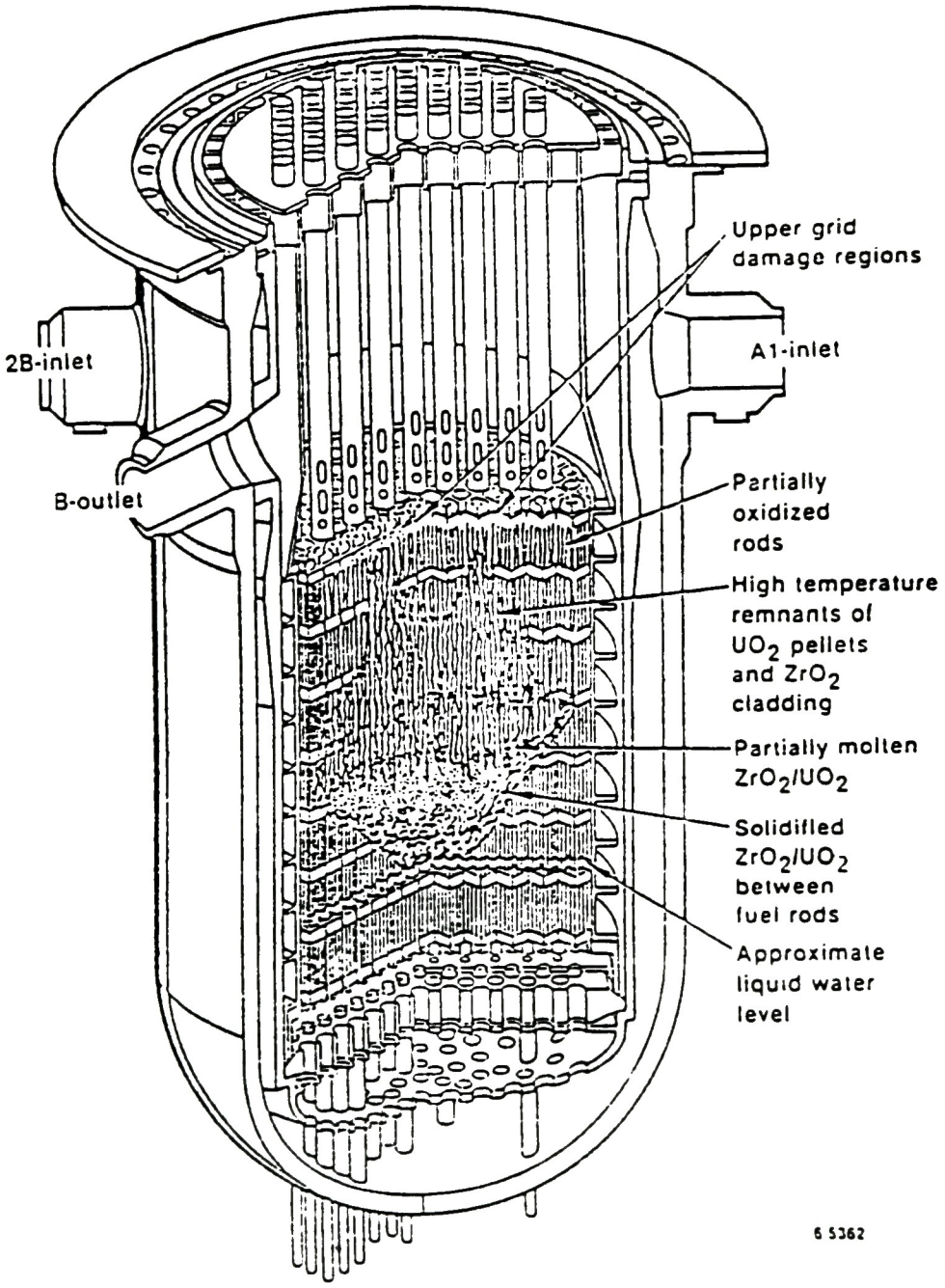

Figure 4.15. Estimated TMI-2 core damage configuration at 174 min, just prior to the pump transient, showing extensive relocation of core materials into the lower core regions.[6]

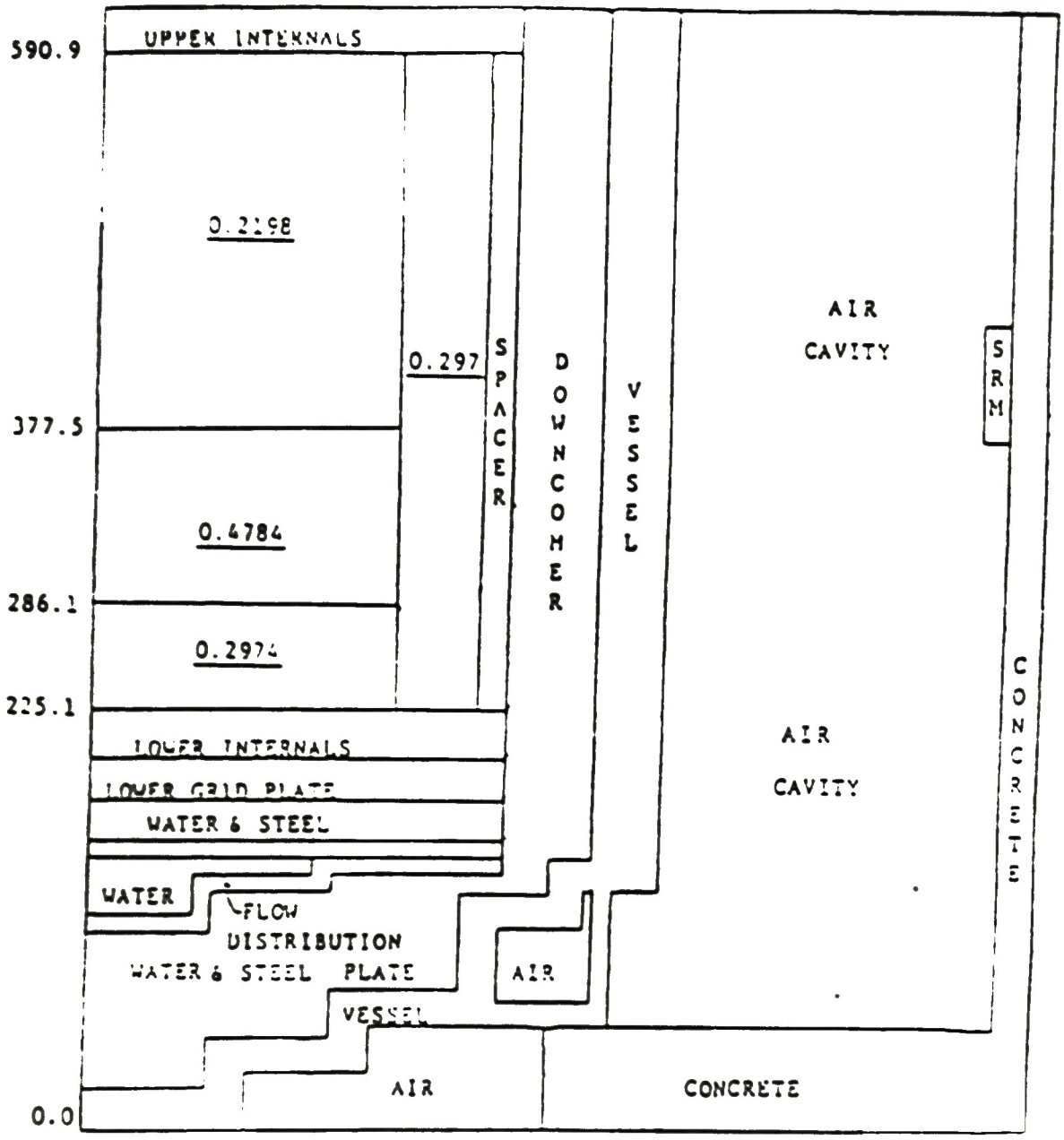

Figure 4.16. DOT core model at 174 minutes before turning on the B loop pump. (Dimensions in cm)

in the core region. The calculated results showed that the water level at this moment was about 61 cm (2 feet) above the bottom of the core.

After the B-loop pump was turned on, slugs of water were pumped into the vessel. It was estimated that about 1,000 cubic feet of water could have been pumped into the vessel.[2] This volume of water would be sufficient to fill the downcomer. However, the flowmeter in the hot leg showed that the pump operated efficiently for only about 9 seconds and then began to pump steam voids into the vessel. Hence, it is believed that the downcomer at this moment was not completely filled with the fluid, and in fact should contain some voids.

The model shown in Fig. 4.10 (with core water level at the height of 61 cm (2 feet) above the bottom of the core) was used at this point. Calculations were then performed by the authors to determine the coolant status, i.e., the void fraction, in the downcomer. The calculated results show that about 14% of voids existed in the downcomer just after the B-loop pump was turned on.

Fig. 4.17 summarizes the water level as determined by this study and compares it with those given in NSAC-24 and NSAC-28. This figure shows that the NSAC-24 results tended to overestimate the water inventory during much of the accident when compared with the neutronics studies. The reason for the discrepancy is not known, but it may be due to assumptions made in the NSAC-24 analysis on make-up flow during the accident.

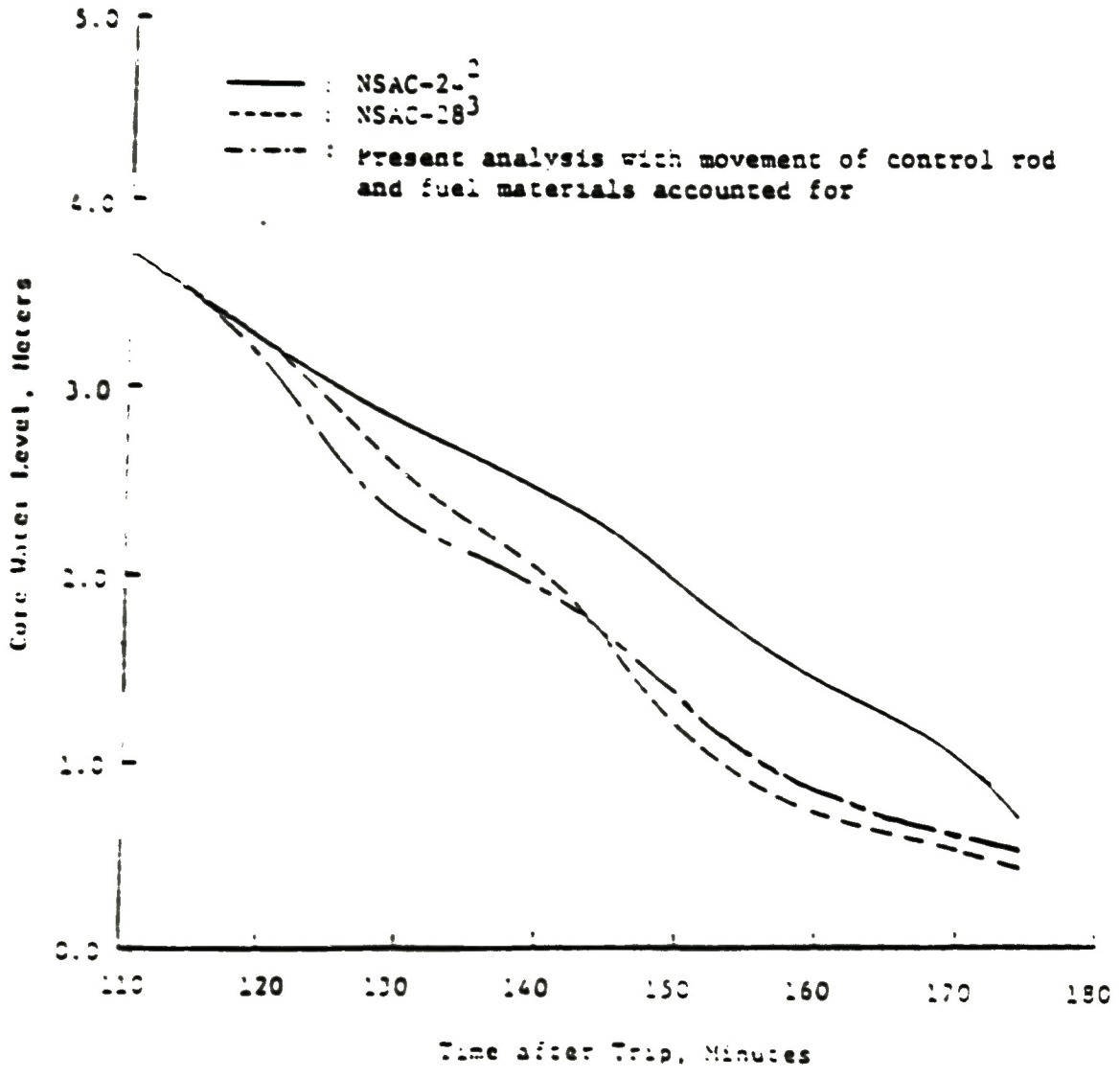

Figure 4.17. Estimated Water level above the bottom of the core for TMI-2 during core uncovery.

4.5 Uncertainties

A key point remaining to be addressed is what is the uncertainty associated with each of the parameters determined from this study. To quantify these uncertainties requires that the adequacy of the methodology and the validity of the assumptions be addressed. In this section, estimates of the uncertainties relating to void fraction, level, and time of fuel relocation are developed and examined.

4.5.1 Void Fraction Uncertainty During $0 < t < 100$ Minutes

To assess the uncertainty in the homogeneous void fraction estimates during the first 100 minutes, a comparison with LOFT data was conducted. Experiment LP-SB-3 essentially duplicates the TMI accident, including both the pumped homogeneous void formation period ($t \leq 100$ min) and the core uncovery period ($100 < t \leq 174$ min) but on a somewhat different time scale.[33-34] Since both density and level data are available as well as a transport analysis of the LOFT SRM response, this comparison allows for experimental verification of the method and assumptions and an estimation of the uncertainties.

Fig. 3.17 shows a comparison of the calculated cold leg densities obtained during LOFT experiment LP-SB-3 from gamma densitometer data with that obtained from analysis of the LOFT SRM response. Examination of the data in Fig. 3.17 shows that the neutronics analysis tends to underestimate the void fraction by varying amounts. For the periods around 1100 seconds and 1600 seconds, the neutronics

analysis underestimates the measured void fraction by about 15%. For the period around 1300 seconds, there is very little discrepancy between the measured and calculated densities. This suggests that the neutronics analysis introduces an error of between 0 to 15% in the void fraction estimates.

To understand the origin of the error, the 1-D Standard Light Water Reactor Problem[38] was used to calculate the response of a hypothetical TMI detector (the standard problem does not include such a detector). The problem was first run using the very fine neutron energy group structure of VITAMIN-C.[39] This group structure consists of 171 neutron energy groups. Cross sections for the problem were also generated using the VITAMIN-C library.

The same calculation was then performed using the five neutron energy groups described in Section 3.3.2. Both the five group response and the five group problem were done with 0% voiding in the core and downcomer. The calculations were then repeated for void fractions of 20%, 50% and 80%. Each of these results were normalized to the 0% void fraction case for both the 5-group and the 171-group cases. Since it was thought that the most likely cause of the uncertainty was in the use of only five groups, the (γ,n) source in the water was omitted. The results are shown in Table 4.3.

Examination of the results in Table 4.3 reveals that the 5 group calculations overestimate the count rate for a given void fraction compared with the 171 group calculation. The effect of this overestimate on the estimated void fraction would be to underestimate the void fraction. A review of the radial flux profiles calculated using the 5 group flux shows that the 5 group calculations

TABLE 4.3
Relative SRM Count Rate vs. Void Fraction
for Standard Light Water Reactor Problem

Void Fraction (%)	Relative Count Rate 171 Group	5 Group	Difference
0	1	1	--
20	2.89	3.44	19%
50	17.9	26.7	49%
80	202	329	63%

underestimate the total flux at the detector for 0% void fraction when compared to the 171 group calculation. At progressively higher void fractions, the underestimate decreases. Thus the relative change in SRM response for a given change in void fraction is larger in the 5 group case than in the 171 group case. It appears then that the major source of uncertainty in the void fraction estimates is due to the use of a coarse 5 group energy structure.

Based strictly on the results of these 1-D calculations, the underestimate at 50% void fraction could be as much as 50%. The LOFT results from experiments LP-SB-3 and LP-SB-2, however, do not support this large an uncertainty.

A more reasonable approach to estimate the uncertainty is to compare LOFT data with estimates of the void fraction during the experiments as determined from the SRM response. If one examines Fig. 3.17, one finds that the predicted void fraction at 1600 seconds just prior to tripping of the LOFT coolant pumps is about 59%. The neutronics analysis yielded a value of 54% which is about 9% lower than the measured value. Since the same assumptions and methods were applied to analyze the LOFT data as in the TMI analysis, the uncertainties should be of the same order. At a comparable point during the TMI accident (100 min), it was stated in Section 4.1 that the maximum homogeneous void fraction in the TMI core was ~5%. Using the estimated uncertainty developed from LOFT, the TMI void fraction could have been as high as 53% at two sigma (i.e., 95% confidence level). Based on this approach, the maximum void fraction during the accident would then be 45% plus 8% and minus 0%.

4.5.2 Level Uncertainty

Fig. 4.16 shows the water level as determined by this study compared to that quoted in NSAC-28[3] from analysis of the SRM response and that determined from a thermal hydraulic analysis described in NSAC-24.[2] To estimate the uncertainty in this analysis, the results of calculations to estimate core water level during the LOFT experiment LP-SB-3 were compared with the measured LOFT vessel water level as determined from in-core thermocouples and conductivity probe data. Fig. 3.19 compares the vessel water level determined from the neutronic analysis with the measured values.

The largest disagreement occurs at 4000 seconds, shortly after the core begins to uncover. At that point, the neutronics analysis suggests a water level of 170 cm, compared with a measured level of 150 cm, about 13% too high. Once the water level has dropped to the core midplane, there is very little (< 5%) disagreement between calculated water level and the measured level determined using the thermocouple data. The bubble plot data suggests a somewhat larger uncertainty, particularly near the end of the transient. For example, at 5000 seconds, the level based on the bubble plot data is about 40 cm compared with 20 cm as determined from the neutronics analysis. It should be pointed out, however, that the conductivity probes are thought to be considerably less precise than the thermocouples.[40] As a result, a better indication of the error is obtained by comparison with the thermocouple data. Based on this comparison, the error in the water level is most likely no greater than about plus 15% and minus 0%.

Referring to Fig. 4.17, one finds that including an uncertainty of 15% in the water level determined by this study brackets both the NSAC 28 and NSAC 24 estimated water level at 174 minutes. When the water level is near the core midplane, the NSAC 24 falls outside this uncertainty. There the NSAC 24 thermal hydraulic analysis yields a water level considerably higher than either the NSAC 28 results or the findings of this work. The source of this disagreement is unknown. Since the LOFT results are reproduced very well at a comparable point in the LP-SB-3 experiment, one might suspect an error in the thermal hydraulic analysis of NSAC 24.

4.5.3 Fuel Relocation Analysis

In Section 4.3, it was stated that the core relocated to the lower head at 225 min, producing the sudden abrupt increase in the SRM response recorded at that time. This hypothesis was based on several factors. The first involved the nature of the change in SRM response, the second involved the nature of the reactor system pressure and incore instrumentation response, and lastly, the results of the degraded core thermal analysis suggesting the degraded core to have occurred by 224 minutes as well as neutronics calculations assuming a damaged core.

The SRM response increased by a factor of at least two at 224-225 min. This abrupt shift in SRM response coincided with a sudden increase in the primary system temperature and pressures. A variety of causes have been postulated for this event, including loss of one or more control rods from the core, massive fuel/clad damage resulting in

fuel compaction, and movement of fuel material into other regions of the reactor vessel.[3]

NSAC in NSAC-28[3] discounted the first of these hypotheses since their analysis showed that the loss of all control rods would produce only a 60% rise in SRM response. They also discounted the second of these possible causes based on 1-D ANISN calculation of the core multiplication. Their results showed a decreasing multiplication factor with increased fuel volume fraction. These results are in conflict with those found by B&W.[4,1] The B&W analysis found that k_{eff} would increase with increasing fuel volume fraction until a volume fraction of about 0.45 was obtained (nominal fuel volume fraction is approximately 0.3).

To resolve the discrepancy between the B&W and NSAC results, a series of models were constructed in which the core was compacted to varying degrees. The results of these calculations did not indicate a doubling of the SRM response. Only when the fuel was relocated to the lower head were increases of that order obtained. The only similar changes in SRM response were those produced when the core or downcomer were suddenly flooded. In those cases, the SRM response dropped abruptly. To obtain the sudden upward jump in SRM response as observed would require nearly the entire downcomer to suddenly empty and remain empty. Since such an event is extremely unlikely and inconsistent with the observed hydraulic data, it can be readily discounted.

Based on these results and those of NSAC, the only plausible cause of the SRM jump is in fact fuel relocation between 224-225 min.

5. CONCLUSIONS AND RECOMMENDATIONS

5.1 Conclusions

The source range monitor response during the TMI-2 accident was analyzed by incorporating the knowledge learned about the end state of the damaged reactor from recent studies and correlating the known system events during the accident to the SRM response. Many crucial parameters relative to the core conditions and coolant status were quantified in the present neutronic analysis providing benchmarks for the development and verification of a best-estimate accident progression scenario.

Based on the present analysis, the interpretation of the SRM response during the first 4 hours of the accident is as follows.

The observed SRM response began to deviate from the normal shutdown response at about 25 minutes after shutdown. This is due to buildup of the voids in the core and downcomer regions. As time elapsed, continued loss of the primary coolant through the failed block valve led to the increased void fraction and increased SRM response. At 100 minutes, just before the A-loop primary coolant pumps were turned off, the void fraction is estimated to be about 45% + 8 and -0% in the vessel based on the neutronics analysis.

Turning off the A-loop pumps caused a separation of voids to the upper regions of the vessel. Since the coolant mass inventory was sufficient to cover the core and downcomer at this point, the core and downcomer were filled with water. Therefore, the SRM sensed a normal thermal hydraulic condition and its response dropped to a normal shutdown response.

As the water continued to boil off, the downcomer water level dropped to a level lower than the corresponding two-phase mixture level in the core due to static pressure equilibrium. The emptied downcomer region then provided an unshielded streaming path for the neutrons to leak out of the core and caused the SRM response to increase. The core probably began to uncover at about 110 minutes into the accident when the SRM response showed an increase by a factor of about 11.

The leveling off of the SRM response at about 140 minutes was due to the shielding effect being counter-balanced by a decrease in the neutron source caused by a reduction in neutron multiplication as the core uncovered further. At 174 minutes just before the B-loop pump was turned on, the zircaloy cladding in the upper region of the core should be highly oxidized, setting the stage for subsequent embrittlement when cooled. A molten zone of zircaloy and liquefied fuel would exist in the central region of the core. The water level was about 61 cm (2 feet) above the bottom of the core and about 70% of the control rod materials should have been removed from the core.

Turning on the B-loop pump at 174 minutes shattered the oxidized, embrittled fuel rods in the upper core region and resulted in a debris region with a voided cavity overhead. The downcomer was filled with water containing about 14% of voids. The SRM response decreased by a factor of about 10 at this moment. Thereafter, the downcomer water flowed into the core region and was boiled off. The SRM sensed a decrease in the shielding effect and the response increased again.

At 200 minutes into the accident, initiation of the HPIS filled the downcomer and caused the SRM response to decrease by a factor of

about 13. At 225 minutes into the accident a portion of the molten zone in the center of the core apparently broke through the surrounding crust and about 10 tons of the molten fuel materials relocated to the lower head.

Based on the estimated progression of the accident, the SRM response for the first 225 minutes during the accident can then be reconstructed. The best estimate SRM response using the neutronics analysis is shown in Fig. 5.1. As can be seen by comparing Figure 5.1 with the observed SRM response shown in Fig. 4.3, all the major features of the response have been accounted for. It is noted that the above interpretation developed from an analysis of the SRM response is consistent with the accident scenario envisioned by the Accident Evaluation Program of the DOE. This study thus provides a semi-independent verification of the postulated scenario.

5.2 Recommendations

While the work reported here corrects a number of shortcomings in previous studies and includes knowledge only recently available, there still remain a number of unresolved questions. For example, what is the effect of a varying level in the core bypass region on SRM response? In this and all previous studies, this region was homogenized with the normal core region. Thomas[12] has suggested that the core bypass region will not have the same level as the core but rather will act more like the downcomer. Detailed hydraulic studies are required to resolve this discrepancy.

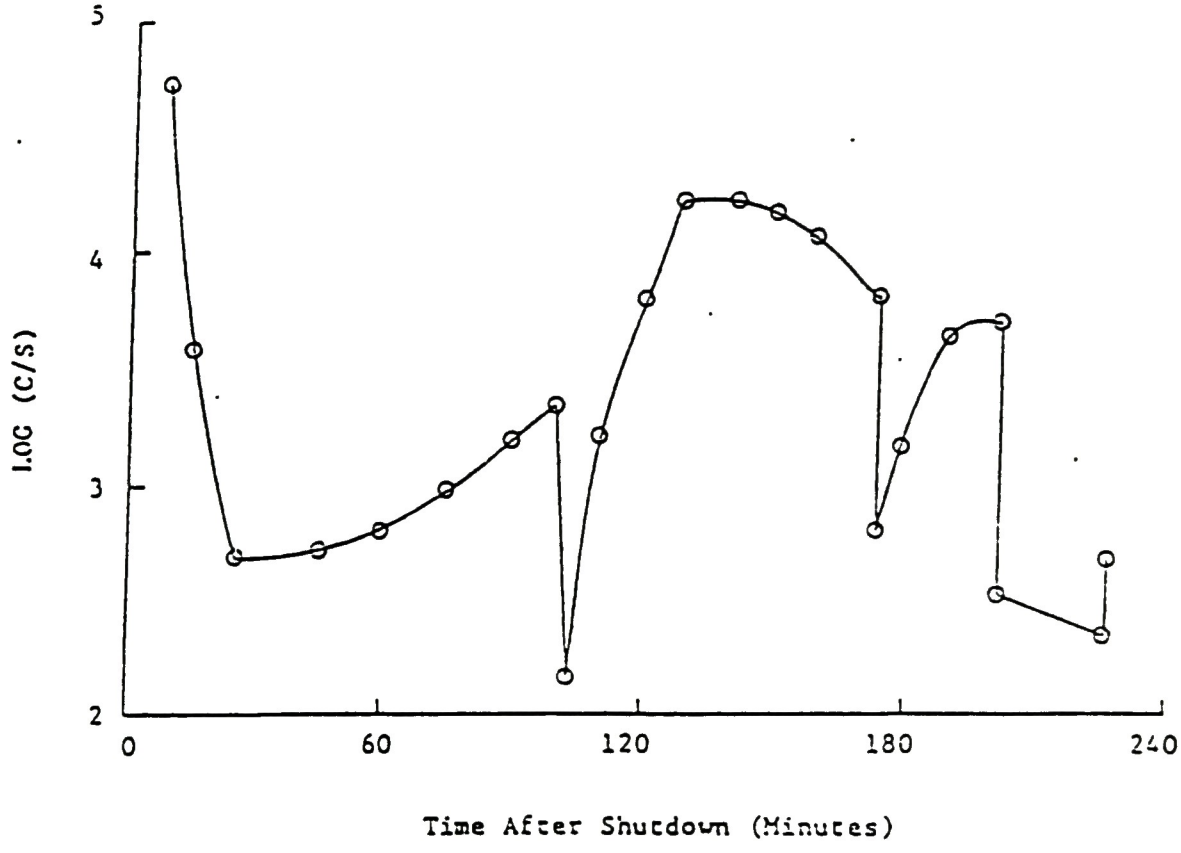

Figure 5.1. Estimated SRM response during the TMI-2 accident.

Furthermore, this study analyzed the SRM response for only the first 225 min. of the accident. A number of features occur in the SRM response beyond this time period and have as yet to be adequately explained. For example, the clearly increasing SRM count rate from 5-15 hours with the subsequent decrease over the next 15 to 30 hours (see Figure 1.2). This longer term response was initially thought to be due to release of fission products to the coolant. Recent inspection of the damaged core shows that considerable material relocated outwards from the core into the core former region. It is possible that the longer term SRM response might be explained by that migration. Another point concerns the coolability of the fuel in the lower head. This study assumed a homogenized fuel water mixture in the lower head. It is known, however, that the fuel is compacted into a roughly cylindrical volume. Attempts to incorporate this compacted lower plenum fuel material into the study produced anomalously low count rates. This suggests that further information may be available in the SRM response regarding the actual fuel configuration at this point in time.

Finally, this study concluded that the control rod material began migrating from the core near the beginning of the core uncovery phase. One question worthy of examination concerns the possibility of recriticality during reflood at that time. A reflood would involve the injection of highly borated water into a semirodless core. Tests have shown that the boron may precipitate out of the resulting steam water mixture in the core region, effectively lowering the boron content in the core region below that otherwise anticipated. Another question that should be addressed concerns the amount of control rod

material in the core as a function of time and its effect on recriticality under a postulated reflood.

Data is also available from the other nuclear instrumentation. For example, the intermediate range detector data reported in NSAC-1 shows definite structure. Some of the structure parallels that seen in the SRM data, whereas some does not. Previous work by the authors of this work has shown that the detectors are sensitive to azimuthal asymmetry in the source distribution. As a result, correlation and analysis of the intermediate range data as well as the limited data available from the other SRM may provide some information on the asymmetry of the core damage progression.

Future work should address these areas of uncertainties relative to the TMI-2 accident in order to improve our understanding of the core damage progression.

An improved understanding of the TMI-2 accident progression will allow the TMI-2 research results to be more fully integrated with other severe accident research towards resolving major technical issues relative to core damage progression, reactor system thermal hydraulic response and fission product transport during such accidents.

REFERENCES

1. Nuclear Safety Analysis Center, "Analysis of Three Mile Island Unit 2 Accident," NSAC-80-1, Revision 1 (1980).

2. K. H. Ardron and D. G. Cain, "TMI-2 Accident Core Heat-Up Analysis," NSAC-24 (1981).

3. H. Warren et al, "Interpretation of TMI-2 Instrument Data," NSAC-28 (1982).

4. E. L. Tolman, et al, "TMI-2 Accident Evaluation Program" EGG-TMI-7048 (1986).

5. E. L. Tolman et al, "TMI-2 Core Bore Acquisition Summary Report," EGG-TMI-7385 (1986).

6. E. L. Tolman, et al, "TMI-2 Accident Scenario Update," EGG-TMI-7489 (1986).

7. R. L. Childs et al, "Calculation of the TMI-2 Source Range Monitor Reading for Several Core Water Levels," Trans. Am. Nucl. Soc., 34, 558 (1980).

8. P. S. Pickard et al, "Neutronic Sensitivity Analysis of the SRM Response for the TMI-2 Accident," Trans. Am. Nucl. Soc., 34, 559 (1980).

9. D. J. Malloy and Y. I. Chang, "Neutronic Analysis of the Three Mile Island Unit-2 Ex-core Detector Response," ANL-81-75 (1981).

10. GPU Nuclear TMI-2 Division, "Quick Look Inspection Results," GPU Data Report TPO/TMI-026 (1982).

11. GPU Nuclear TMI-2 Division, "Fuel Conditions and Locations," TMI-2 Technical Planning Department, TPO/TMI-166 (1985).

12. Bechtel Northern Corporation, "Quick Look Inspection: Results," Vol. II, GEND-030 (1983).

13. M. W. Crump and J. C. Lee, "Calculation of Spatial Weighting Function for Ex-core Neutron Detectors," Nucl. Tech., 41 (1978).

14. E. W. Okyere, "A Non-Invasive Liquid Level/Density Measurement in Pressure Vessels," Ph.D. Thesis, Nuclear Engineering Department, The Pennsylvania State University (1985).

15. C. M. Allison., S. T. Polkinghorne and M. S. Sohal, "SCDAP/MOD1 Analysis of the Progression of Core Damage During the TMI-2 Accident," EGG-SAR-7104 (1985).

16. L. M. Gundy, "Application of the Adiabatic Spatially Dependent Reactor Kinetics Method to Voided Pressurized Water Reactors," Ph.D. Thesis, Nuclear Engineering Department, The Pennsylvania State University (1984).

17. Nuclear Safety Analysis Center, Appendix G NSAC-1, unpublished.

18. A. J. Baratta and B. R. Bandini, "Determination of Fuel Distribution in TMI-2 Based on Axial Neutron Flux Profile," Internal Report, Nuclear Engineering Department, The Pennsylvania State University (1985).

19. Gold et al, "Solid State Track Recorder Neutron Dosimetry in the Three Mile Island Unit-2 Reactor Cavity," Hanford Engineering Development Laboratory Report HEDL-7484 (1984).

20. W. A. Rhodes and R. L. Childs, "DOT 4.3, One- and Two-Dimensional Transport Code System," CCC-429, Radiation Shielding Information Center (1982).

21. M. Tanaka et al, "Quick-Look Report on OECD LOFT Experiment LP-SB-3," EG&G Idaho, Inc. (1984).

22. S. Nakamura, "Point Reactor Kinetics (PRK) Code," Nuclear Engineering Department, Ohio State University (1977).

23. M. J. Bell, "ORIGEN-The ORNL Isotope Generation and Depletion Code," Oak Ridge National Laboratory, CCC-217 (1977).

24. G. E. Putman, "LOFT-I Source, Intermediate, and Power Range Detector Fluxes," EG&G Idaho, Inc., LOFT Technical Report LTR-111-84 (1977).

25. N. M. Greene et al, "A Modular Code System for Generating Coupled Multigroup Neutron-Gamma Libraries from ENDF/B", ORNL/TM-3706, Revised (1978).

26. L. W. Nordheim, F. T. Adler and G. W. Hinman, "The Quantitative Evaluation of Resonance Integrals," Peaceful Use of Atomic Energy, P/1988 (1958).

27. E. Fast and F. J. Wheeler, "LOFT-I Shutdown Margin During Initial Fuel Load-An Independent Monte Carlo Analysis," EG&G Idaho, Inc., LOFT Technical Report LTR-111-89 (1978).

28. L. P. Ku and J. Kolibal, "GIP - A Cross Section Mixing Code for Group Independent Files," Princeton Plasma Physics Laboratory, Princeton University (1982).

29. A. J. Baratta et al, "Verification of the Fuel Distribution in TMI-2 Using Neutron Transport Theory," Internal Report, Nuclear Engineering Department, The Pennsylvania State University (1985).

30. R. W. Roussin, "VITAMIN-E: A Coupled 174-Neutron, 38-Gamma Ray Multigroup Cross Section Library for Deriving Application-Dependent Working Libraries for Radiation Transport Calculations," DLC-113, RSIC (1984).

31. W. W. Engle, Jr., "A Users Manual for ANISN-A One Dimensional Discrete Ordinates Transport Code with Anisotropic Scattering," CCC-254, Radiation Shielding Information Center (1973).

32. S. M. Modro et al, "Experiment Analysis and Summary Report on OECD LOFT Nuclear Experiments LP-SB-1 and LP-SB-2," EC&G Idaho, Inc. (1984).

33. E. L. Tolman et al, "Thermal Hydraulic Features of the TMI Accident," EG&G Idaho, Inc., (1985).

34. Specifications for One-D Light Water Reactor (LWR) Shielding Benchmark, prepared by American Nuclear Society Standard Committee 6.2.' (1979).

35. R. W. Roussin, et al, "VITAMIN-C: The CTR Processed Multigroup Cross Section Library for Neutronics Studies," ORNL/RSIC-37, 1978.

36. E. L. Taylor, EG&G Idaho, private communication.

37. J. R. Worsham, "Methods and Procedures of Analysis for TMI-2 Criticality Calculation to Support Recovery Activities Through Head Removal," B&W Technical Report BAW-1738, June 1982.